MASTERARBEIT | MASTER'S THESIS

Titel | Title

Unravelling sulfobacin biosynthesis in Bacteroidota: enzyme localization, gene expression, and comparative lipid profiling

verfasst von | submitted by

Lea Anna Donata Arneth BSc

angestrebter akademischer Grad | in partial fulfilment of the requirements for the degree of

Master of Science (MSc)

Wien | Vienna, 2026

Studienkennzahl lt. Studienblatt | Degree programme code as it appears on the student record sheet:	UA 066 838
Studienrichtung lt. Studienblatt | Degree programme as it appears on the student record sheet:	Masterstudium Ernährungswissenschaften
Betreut von | Supervisor:	Univ.-Prof. Dipl.-Biol. Dr. Alexander Loy

Contents

Acknowledgements

First and foremost, I would like to express my sincere gratitude to Univ.-Prof. Dipl.-Biol. Dr. Alexander Loy for granting me the opportunity to expand my research horizon by participating in this captivating project. His contribution to creating a stimulating environment for research is greatly valued.

In addition, gratitude is extended to Dr. Tomohisa Sebastian Tanabe for his exemplary mentorship and illuminating discourse on a plethora of research subjects. His initial bioinformatic analysis, specifically the BLAST searches of the *F. johnsoniae* genome against sphingolipid biosynthetic enzymes, was essential in identifying the target genes that formed the very foundation of this project. The completion of this thesis would not have been possible without his invaluable help and guidance.

I would also like to thank Guoqing Guan, M.Sc. for providing the soil bacteria from his PhD project, which served as a vital resource for my research. My gratitude extends to Clara Priemer, M.Sc. for her expertise in operating the LC-MS system, and to Stefan Thiele, M.Sc. M.Sc. for his skillful generation of the STED images that enrich this thesis. Additionally, I would like to thank Nick Ahrends for providing the primers that were essential for the molecular work during my Master's thesis. Furthermore, I am deeply grateful to Theresa Villunger, M.Sc. for her previous analysis of the LC-MS/MS data for the knockout mutant and for being such a wonderful companion throughout the course of this work.

Abstract

Sulfonolipide, insbesondere die Klasse der Sulfobacine, sind wichtige Membranbestandteile vieler *Bacteroidota* und spielen eine wichtige Rolle bei der Gleitmotilität sowie der interzellulären Kommunikation. Trotz ihrer Bedeutung sind die subzelluläre Anordnung involvierter Enzyme und die Regulation des Biosynthesewegs bisher kaum erforscht. In dieser Masterarbeit wurden potentielle Enzyme der Sulfobacin Biosynthese in *Flavobacterium johnsoniae* mittels bioinformatischer Topologieanalysen und Fluoreszenzmikroskopie charakterisiert. Ergänzend erfolgte eine Charakterisierung der Sulfonolipid-Profile für verschiedene *Bacteroidota* Spezies.

Die bioinformatische Analyse identifizierte die Cysteat-Acyl-ACP-Transferase (SulA / Fjoh_2419) und die potentielle Sulfobacin-Synthase (Fjoh_2421) als lösliche, cytoplasmatische Proteine, während die möglichen Sulfobacin Monooxygenasen Fjoh_1748 und Fjoh_4604 als Multipass-Membranproteine vorhergesagt wurden. Zur experimentellen Validierung wurden C-terminale mScarlet-I-Fusionen mittels homologer Rekombination generiert, welche die Lokalisierung der Zielproteine mittels Fluoreszenz ermöglichte. Während die Integration von Suizidplasmiden für vier Zielgene gelang, konnte eine erfolgreiche *In-Frame*-Insertion ausschließlich für fjoh_4604 bestätigt werden. Die zusätzliche Komplementierung von *F. johnsoniae* Δ*2419* mit dem replikativen Plasmid *pCP11* ermöglichte die visuelle identifizierung des zytoplasmatischen Signals für die SulA::mScarlet-I-Fusion. Dies führte jedoch weder zur Wiederherstellung der Gleitmotilität, noch zur Sulfobacin synthese, was auf eine mögliche sterische Hinderung des aktiven Enzymzentrums durch mScarlet-I hindeutet.

Untersuchungen zur Regulation ergaben, dass die SulA-Expression durch die Wachstumsphase und die Verfügbarkeit des Präkursors Cysteat beeinflusst wird, wobei thermischer Stress (14°C und 37°C) zu einer Downregulation führte. Parallel dazu identifizierte eine Liquid chromatography-tandem mass spectrometry-basierte Analyse ein konserviertes Set an Sulfonolipiden in verschiedenen *Flavobacteriaceae* und *Weeksellaceae* Arten. Während die Supplementierung von Cysteat in *Chryseobacterium capnotolerans* zu einer erhöhten Bildung der Sulfobacin-Vorstufe Capnin sowie zur Produktion sekundärer Sulfobacine führte, verursachte sie in anderen Spezies mögliche Stressreaktionen und reduzierte die Sulfobacin-Arten.

Diese Arbeit liefert neue Einblicke in die räumliche Trennung der Sulfobacin Biosynthese und zeigt die Komplexität ihrer regulatorischen Anpassung an Umweltreize.

Abstract

Sulfobacins are important membrane sulfonolipids of select *Bacteroidota* species and play a crucial role in their gliding motility and intercellular communication. Despite their importance, the subcellular organization of the involved enzymes and the regulation of the sulfobacin biosynthesis pathway are still poorly understood. In this master's thesis, the subcellular localization of potential enzymes involved in sulfobacin biosynthesis were characterized in *Flavobacterium johnsoniae* by using bioinformatic topology analyses and fluorescence microscopy, combined with the sulfobacin profiling of selected *Bacteroidota* species.

The bioinformatic analysis identified cysteate acyl-ACP transferase (SulA / Fjoh_2419) and the potential sulfobacin synthase (Fjoh_2421) as soluble, cytoplasmic proteins, while the putative sulfobacin monooxygenases Fjoh_1748 and Fjoh_4604 were predicted to be multipass membrane proteins. For experimental validation, C-terminal mScarlet-I fusions were generated through homologous recombination, which enabled the localization of the target proteins via fluorescence. While the integration of suicide plasmids was successful for all target genes, *in-frame* insertion could only be confirmed for *fjoh_4604*. Therefore, a replicating plasmid encoding the tagged *fjoh_2419* was used to complement a *F. johnsoniae* Δ*2419* strain, which further confirmed the cytoplasmic localization of the fluorescent SulA::mScarlet-I protein. However, this did not lead to the restoration of gliding motility or sulfobacin synthesis, suggesting potential steric hindrance at the enzyme´s active site caused by the mScarlet-I tag.

Regulatory studies revealed that SulA expression is influenced by the growth phase and the availability of the precursor cysteate, with thermal stress (14°C and 37°C) leading to downregulation. In parallel, LC-MS-based analysis identified a conserved set of potential sulfobacins and derivates in various *Flavobacteriaceae* and *Weeksellaceae* species. Supplementation with cysteate showed high metabolic plasticity in *Chryseobacterium capnotolerans*, but led to possible stress responses and reduced sulfobacin production in other species.

This work provides new insights into the sulfobacin biosynthesis pathway and demonstrates the complexity of its regulatory adaptation to environmental stimuli.

List of abbreviations

Abbreviation	Definition
ACP	Acyl carrier protein
bCERs	bacterial ceramide synthase
CapA, Cys	Cysteate synthase
CapC	3-ketocapnine reductase
CerR	3-ketosphinganine reductase
CFU	Colony forming unit
CLSM	Confocal laser scanning microscopy
CoA	Coenzyme A
CYE	Casitone Yeast Extract
DAPI	4,6-Diamidino-2-phenylindole
Des2	Dehydroceramide monooxygenase
dNTP	Deoxynucleoside triphosphate
EDTA	Ethylenediaminetetraacetic acid
LB	Lysogeny broth
LPS	Lipopolysaccharide
Lpt	Lipopolysaccharide transporter
MCE	Mammalian cell entry
MD-2	Myeloid differentiation factor 2
oriT	Origin of transfer
oriV	Origin of vegetative replication
PBS	Phosphate-buffered saline
PCR	Polymerase chain reaction
PSF	Point spread function
recA	Recombinase A
RpotS	RNA-Polymerase-Omnibus-S
Spt	Serine palmitoyltransferase
STED	Stimulated emission depletion microscopy
SulA, CFAT, CapB	Cysteate acyl-ACP transferase
T_a	Annealing temperature
TAE buffer	Tris-acetate-EDTA buffer
TLR4	Toll-like receptor 4
T_m	Melting temperature
TSA	Tryptic soy agar
TSB	Tryptic soy broth
T9SS	Type IX secretion system

1 Introduction

Biological membranes are more than physical barriers, their diverse lipid composition enables bacteria to adapt to various environments (Singer and Nicolson, 1972; Sohlenkamp and Geiger, 2016). In addition to the widely known amphipathic glycerophospholipids, certain bacteria synthesize unique sulfonolipids, such as sulfobacins (Sohlenkamp and Geiger, 2016). These functional metabolites are essential for bacterial motility and act as chemical mediators in bacteria-eukaryote interactions (Abbanat et al., 1986; Older et al., 2024). However, the bacterial biosynthesis of sulfobacins remains mostly unexplored, hindering the development for targeted in vivo production strategies for future pharmacological and environmental research. The central aim of this thesis is to further elucidate the complex biosynthetic pathway of sulfobacin synthesis by investigating the subcellular localization and regulation of putative enzymes involved in this process, combined with the sulfobacin profiling of selected *Bacteroidota* species.

1.1 Bacterial sulfonolipids: structure, diversity, and biological significance

Lipids are essential components in all living cells, playing a crucial role in the development and maintenance of life (van Meer et al., 2008). In bacterial organisms, lipids function as signaling molecules and provide the structural basis for cellular membranes (Singer and Nicolson, 1972; Sohlenkamp and Geiger, 2016). Among other functions, lipid heterogeneity enables bacteria to create specialized membrane compositions that are tailored to specific ecological niches and environmental challenges (Sohlenkamp and Geiger, 2016). For example, Gram-negative bacteria are distinguished by their dual-membrane system, in which the outer membrane is characterized by the presence of lipopolysaccharides, hindering the entry of hydrophilic and large polar molecules (Raetz and Whitfield, 2002; Raetz et al., 2007). Certain Gram-negative bacteria from the phylum *Bacteroidota* (formerly *Bacteroidetes*) additionally synthesize specific sulfonolipids. These so-called sulfobacins show a structural similarity to ceramides, which form the foundation of sphingolipids (Geiger et al., 2010). Unlike sphingolipids, sulfonolipids lack the hydroxy group at C1 position, which is instead replaced by a sulfonic acid group (Sohlenkamp and Geiger, 2016) (*Figure 1*). Sulfobacins exhibit a wide structural diversity and have the amino base capnine (2-amino-3-hydroxy-15-methyl-hexadecane-1-sulfonate) as their main precursor. Diversity of these capnine derivates arise through variation in the fatty acid chain length, desaturation and or hydroxylation (Beemelmanns et al.,

(a) Sphinganine (b) Capnine

Figure 1: **Structural comparison** of the sphingoid base sphinganine and the sulfonolipid base capnine, highlighting the substitution of the primary hydroxyl group (blue) with a sulfonic acid moiety (yellow) in sulfonolipids

2014) (*Figure 2*) .

The amino base capnine ($C_{17}H_{37}O_4N_1S_1$) was identified in 1980 and serves as a fundamental precursor for sulfobacin biosynthesis. *N*-acylation of the amino group with various fatty acids yields the molecular diversity of sulfobacins (Beemelmanns et al., 2014; Godchaux and Leadbetter, 1980). These capnine derivatives are collectively referred to as capnoids (Abbanat et al., 1988; Godchaux and Leadbe1ter, 1983). Examples of well-known sulfonolipids include sulfobacin A, otherwise referred to as flavochristamide B, and sulfobacin B. Both compounds, along with flavochristamide A, have first been isolated from a *Flavobacterium sp.* in 1995 (Kamiyama et al., 1995; Kohayashi et al., 1995). While sulfobacin B consists of a C17 capnine base acylated with a non-hydroxylated *iso*-C15:0 fatty acid, sulfobacin A has a longer *iso*-C17:0 fatty acid chain with an additional hydroxy group at the β-position. In 2014, the structural diversity of sulfobacins further expanded with the identification of sulfobacin C, D, E and F. These variants are characterized by differences in the chain length, branching, and saturation of both the amino base and the N-linked fatty acid moiety (Beemelmanns et al., 2014). Named derivatives will be collectively termed "sulfobacins", in order to differentiate them from other sulfonolipids.

Furthermore, the sulfonolipids RIF-1 and RIF-2, close relatives to sulfobacins that differ by an additional hydroxy group at the capnine backbone, were first isolated in 2012 and 2016 from *Algoriphagus machipongonensis* (Alegado et al., 2012, Woznica et al., 2016).

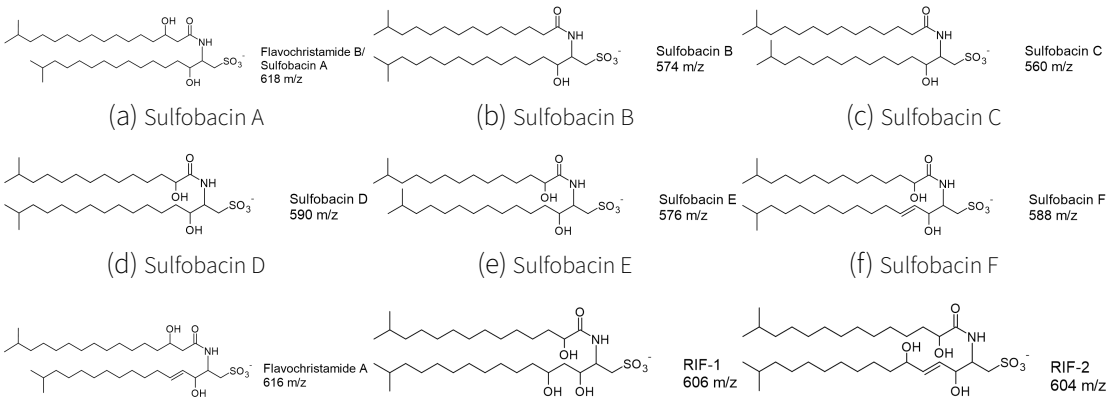

(a) Sulfobacin A (b) Sulfobacin B (c) Sulfobacin C

(d) Sulfobacin D (e) Sulfobacin E (f) Sulfobacin F

(g) Flavochristamide A (h) Rosette-inducing factor 1 (i) Rosette-inducing factor 2

Figure 2: **Chemical diversity of common sulfobacins:** Structures of various sulfonolipids, including sulfobacin A–F, flavochristamide A, and the rosette-inducing factors RIF-1 and RIF-2. This figure was made by Sebastian Tanabe.

Sulfonolipid production is a characteristic trait of several families within the phylum *Bacteroidota*, includ-

ing *Rikenellaceae*, *Marinifilaceae* and *Weeksellaceae* (Older et al., 2024). While anaerobic genera such as *Alistipes* and *Odoribacter* (Walker et al., 2017) are sulfobacin producers in the human gut, aerobic bacteria like the common soil bacterium *Flavobacterium johnsoniae* (Pitta et al., 1989) or the food associated *Chryseobacterium capnotolerans* (von Heilborn et al., 2022) also synthesize sulfobacins.
The ubiquity of constitutive sulfobacin producers across different environments suggests that these lipids provide a fundamental physiological advantage beyond simple nutrient adaptation (Abbanat et al., 1985; Sohlenkamp and Geiger, 2016). Beyond their ecological abundance, sulfobacins have also attracted attention due to their biological activities on eukaryotic organisms. Sulfobacin A and B were originally identified as von Willebrand factor receptor antagonists, demonstrating their involvement in platelet aggregation and thrombosis (Kamiyama et al., 1995). More recently, studies have indicated that both molecules exert immunomodulatory effects by blocking lipopolysaccharide (LPS) binding to the toll-like receptor 4 (TLR4) (Maeda et al., 2010; Older et al., 2024). Additionally, sulfobacin B has been reported to inhibit DNA polymerase, thereby inducing cytotoxicity in cancer cells (Maeda et al., 2010). Furthermore, the sulfonolipids RIF-1 and RIF-2 have been shown to trigger multicellular development in choanoflagellates (Alegado et al., 2012; Woznica et al., 2016).

Previous investigations into the bioactivity of sulfonolipids have relied on complex chemical synthesis, resulting in a decreased bioactivity, or on extensive purification from crude cell extracts (Beemelmanns et al., 2014). Therefore, elucidating the biosynthetic pathway of sulfobacins is crucial to facilitate further investigation into their significance as bioactive lipids (Hou et al., 2022; Y. Liu et al., 2022).
Comparison of known sulfobacins and sphingolipids revealed a high architectural similarity, suggesting an analogue biosynthetic pathway that is adapted to the structural differences (Geiger et al., 2010; Walker et al., 2017).

1.1.1 Structural similarity to sphingolipid synthesis

As with sulfonolipids, sphingolipids exhibit a high degree of structural diversity, which is mediated by acyl chain length, degree of saturation, acyl chain hydroxylation, and lipid headgroup (Brown et al., 2019; Kato et al., 1995; Stankeviciute et al., 2022). Various sphingolipids, have been observed in both eukaryotes and prokaryotes, fulfilling functions ranging from maintaining membrane integrity to signal mediation (Sohlenkamp and Geiger, 2016; Stankeviciute et al., 2019).

The bacterial sphingolipids pathway as a biosynthetic model

The *de novo* biosynthesis of ceramides, a class of sphingolipids begins with the decarboxylative, Claisen-like condensation of palmitoyl-coenzyme A (palmitoyl-CoA) and L-serine into 3-keto-sphinganine, mediated by serine palmitoyl-CoA transferase (Spt) (*Figure 3*) (Yard et al., 2007). While the Spt enzyme is

conserved across all domains, downstream enzymes in bacterial sphingolipid synthesis differ from those in eukaryotes (Stankeviciute et al., 2022). These enzymes have been identified previously and two alternative pathways have been proposed regarding the chronological order of the following N-aclytion and C3-keto reduction.

Based on the eukaryotic model, it was previously postulated that in bacteria, the reduction of the intermediate 3-keto-sphinganine occurs first via 3-keto-sphinganine reductase (CerR), followed by the N-acylation of a second acyl chain through ceramide synthase (bCerS) (Stankeviciute et al., 2022).

A newer study suggests that in many bacteria, the N-acylation occurs prior to the lipid reduction. This is supported by the spatial organization of involved enzymes, where Spt and bCerS are located in the cytoplasm, while CerR resides in the periplasm (Uchendu et al., 2024).

The resulting dihydroceramide is the starting point for various ceramide modifications. For example, the addition of a hydroxyl group by the enzyme dihydroceramide monooxygenase, which is found in fungi, plants and some animal tissues, results in the formation of phytoceramides (Kaneshiro et al., 2008; Stankeviciute et al., 2022). Due to the structural homology between sphingolipids and sulfonolipids, which primarily differ in the C1 moiety, it is postulated, that their synthesis pathway proceed in analogous manner (Geiger et al., 2010; Walker et al., 2017).

The capnoid pathway: A putative analog to sphingolipid biosynthesis

The educts for the initial sulfonolipid synthesis step are analogous to those for sphingolipid synthesis. However, instead of L-serine, the sulfur-containing amino acid cysteate is condensed with an acyl chain (acyl-ACP) (*Figure 3*). Cysteate is either synthesized by the cysteate synthase (CapA/ Cys), or scavenged from the environment. This enzyme has been identified in both *Capnocytophaga ochracea* (CapA) and *Chryseobacterium gleum* (Cys) (Hou et al., 2022; Y. Liu et al., 2022).

Previous studies have also identified the homologous enzyme cysteate acyl-ACP transferase, which catalyzes the reaction to produce 3-keto-capnine. This enzyme was identified in *F. johnsoniae* (SulA) (Vences-Guzmán et al., 2021), *Capnocytophaga ochracea* (CapB) (Hou et al., 2022), and *Chryseobacterium gleum* (CFAT) (Hou et al., 2022).

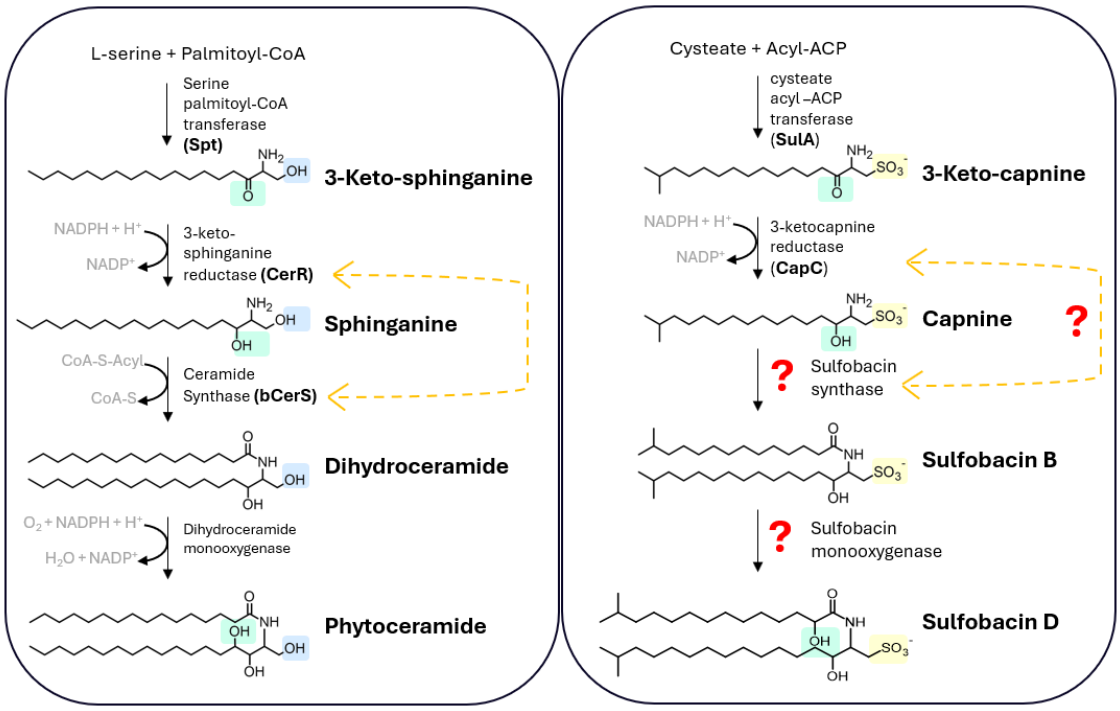

Figure 3: **Comparison of the biosynthetic pathways for sphingolipids and sulfobacins:** The left panel shows the classical eukaryotic-like sphingolipid pathway. The orange arrow hints to the recently postulated bacterial synthesis pathway, where the N-acylation (bCerS) happens prior to the reduction (CerR) (Uchendu et al., 2024). The right panel depicts the suggested sulfobacin pathway. Question marks indicate enzymes that are yet to be functionally characterized and the unknown chronological order of involved enzymes.

Although the precise chronological order of the subsequent biosynthetic steps remains to be fully elucidated, it is generally proposed that 3-keto-capnine is reduced to capnine by an NADPH-dependent 3-ketocapnine reductase (CapC), as demonstrated in *Ornithobacterium rhinotracheale* (Kongpracha et al., 2022; Y. Liu et al., 2022).

The described enzymes closely mirror those involved in sphinganine biosynthesis, suggesting that capnine is N-acylated by a ceramide-like synthase. The resulting product sulfobacin B has been previously identified in *F. johnsoniae* (Kamiyama et al., 1995). Further modifications, similar to those found in sphingolipids, could be mediated by an analogous monooxygenase, possibly resulting in the formation of sulfobacin D.

The structural similarities between sulfobacins and sphingolipids suggest that sulfonolipids likely act as replacement in bacteria that lack classical sphingolipid biosynthesis (Pitta et al., 1989; Walker et al., 2017). However, rather than imitating sphingolipids, sulfonolipids possibly fulfill different physiological roles (Older et al., 2024).

1.2 Sulfobacins in the human gut and their association with inflammatory bowel disease

While studies have shown that bacterial abundances oftentimes correlate with disease phenotypes, the mechanisms by which specific microbes potentially influence human health remain underinvestigated (Dai et al., 2023; Flint et al., 2012; Haiser and Turnbaugh, 2013). The influence of microbial metabolites on mucosal cells has been studied previously in diseases like inflammatory bowel disease, revealing complex host-microbe interactions (Chaudhari et al., 2021; Lavelle and Sokol, 2020). Driven by lifestyle changes emerging from industrialization, urbanization and westernization, this global disease affects more than 2,5 million people in Europe, resulting in a major burden on the healthcare systems (Beard and Click, 2020; Burisch et al., 2020; Kaplan and Ng, 2017; Kaplan and Windsor, 2020; Kumar et al., 2023; Omran, 2005).

These chronic inflammatory conditions, such as Crohn´s disease and ulcerative colitis affect all aspects of an individual´s life, making research into pathogenesis and treatment options so important (Burisch et al., 2013). The constant exchange between co-evolved microbes and human cells is a key driver in the pathogenesis of inflammatory bowel disease, showcasing not only beneficial synergistics like fermentation of dietary fibers or pathogen defense, but also maladaptive health responses (Buffie et al., 2014; Cummings and Macfarlane, 1997; Lavelle and Sokol, 2020).

Dysbiosis observed in inflammatory bowel disease patients is characterized by significant taxonomic shifts and altered microbial metabolites. A reduction in the abundance was observed for the genera *Alistipes* and *Odoribacter* in patients with inflammatory bowel disease (Durack and Lynch, 2019; Dziarski et al., 2016; Lima et al., 2022). Both genera are known sulfonolipid producers from the phylum *Bacteroidota* (Walker et al., 2017). Similar taxonomic shifts are observed in response to an unhealthy, westernized lifestyle. Furthermore, *Bacteroidota* and *Prevotella* abundances are associated with a lean phenotype, further underlining the importance of *Bacteroidota* for human metabolic health (Neyrinck et al., 2016).

The decreased abundances of these specific genera in the human gut, which also include common sulfonolipid producers, mirror the observed decrease in sulfobacin A and B levels in fecal samples from inflammatory bowel disease patients. This reduction indicates that the loss of immune-modulating metabolites, such as sulfobacins, may be a factor in the development or persistence of the observed chronic inflammatory state (Older et al., 2024).

The anti-inflammatory potential of these sulfobacins is credited to their ability to bind to the hydrophobic pocket within the TLR4-MD-2 complex. A pro-inflammatory signaling cascade is initiated when LPS, a key contributor to the progression of inflammatory bowel disease, binds to the myeloid differentiation factor 2 (MD-2), triggering the dimerization of the complex. This induces the release of pro-inflammatory cytokines and the polarization of M1 macrophages (X. Zhang and Mosser, 2008). Sulfobacin A and B act

as competitive antagonists by competing with the pro-inflammatory ligand LPS for this binding site. Binding of sulfobacin to the complex results in a significantly reduced immune response. Although sulfobacin A alone promotes a slight increase in cytokines in comparison to the control, the response is significantly lower than that of LPS. This suggests that sulfobacins may compete with more potent pro-inflammatory lipids to maintain intestinal immune homeostasis (Older et al., 2024). It was demonstrated, that sulfobacins generated by *Bacteroidota* can suppress ulcerative colitis in mice. Moreover, it has been observed, that these capnoids are also present in the hosts blood, suggesting a potential role in modulating immune responses beyond the intestinal tract (Older et al., 2024; Older et al., 2025; Radka et al., 2020).

Despite the promising therapeutical potential of sulfobacins, several questions, like the potential systemic effects remain unresolved (Older et al., 2024). As these bioactive sulfonolipids are not commercially available at this time, establishing a robust biotechnological production route in a genetically tractable host is of high priority for further fundamental and pharmacological research.

1.3 *Flavobacterium johnsoniae* as a genetic model for sulfobacin research

While *Alistipes sp.* and other sulfobacin producing gut commensals are relevant in the context of inflammatory bowel disease, the lack of established genetic toolkits for these organisms hinder genetic studies (Walker et al., 2017). Therefore, the Gram-negative *Flavobacterium johnsoniae* was used as a genetically tractable model to investigate the biosynthetic pathway of sulfobacins and the cellular localization of involved enzymes.

The ubiquitously distributed soil and aquatic bacterium *F. johnsoniae* is commonly used to study gliding motility. The genome is fully sequenced and is publically available, and relevant genes for gliding (Nelson et al., 2008; Shrivastava et al., 2012), type IX secretion system (Shrivastava et al., 2013) and capnine synthesis (Y. Liu et al., 2022; Vences-Guzmán et al., 2021) have already been described.

The cells are rod-shaped and are of even width (0.2 - 0.4 µm x 1.5 - 15 µm) (Stanier', 1946). Phosphatidylethanolamine has been identified as the predominant lipid of the inner membrane of *F. johnsoniae*, whereas ornithine lipids, glycine lipids, serineglycine lipids (flavolipin) and sulfonolipids (20%) have been found to be predominantly present in the outer membrane (Pitta et al., 1989; Kawazoe et al., 1991; Sohlenkamp and Geiger, 2016).

Several specialized molecular tools have already been developed, enabling fast and reproducible genetic manipulation (Agarwal et al., 1997, Mcbride and Kempf, 1996, Zhu et al., 2017).

This sulfobacin producing organism belonging to the phylum *Bacteroidota*, has been observed to glide at a rate of 2 µm/s across a variety of solid surfaces. These surfaces include Teflon, glass, and polystyrene, as well as numerous other natural surfaces (McBride and Nakane, 2015).

Genetic manipulation tools have previously enabled the deletion of the target gene *fjoh_2419* which encodes the cysteate acyl-ACP transferase (SulA) in *F. johnsoniae*. Without this enzyme, gliding was no longer possible and cells were deficient in sulfobacins (Y. Liu et al., 2022, Vences-Guzmán et al., 2021).

Gliding motility and type IX secretion system of *F. johnsoniae*

Gliding movement is triggered by lack of nutrients, leading to rapid movements of *F. johnsoniae* over solid surfaces without the help of flagella or pili (Nelson et al., 2008; Stanier', 1946; Kulkarni et al., 2017). Previous studies uncovered a connection between sulfobacin synthesis and gliding ability in *F. johnsoniae* (Abbanat et al., 1986). So far, studies have identified the cell surface adhesins SprB (Nelson et al., 2008) and RemA (Shrivastava et al., 2012), which are supported by carbohydrates, that enable efficient gliding over different surfaces (McBride et al., 2009). RemA is a galactose or rhamnose binding lectin, that moves rapidly along the cell surface. Carbohydrates likely coat the substratum, allowing gliding on otherwise poor substrates for their motility machinery (McBride et al., 2009; Shrivastava et al., 2012). SprB adhesins rapidly move on helical tracks, resulting in forward movement and rotation to the right of the cell. While SprB provides the adhesive, a rotary motor powers the motion (Shrivastava et al., 2016; Shrivastava et al., 2015). This motor, called Hub complex, is shared for both movement and secretion via the type IX secretion system (Lauber et al., 2024).

This type IX secretion pathway is needed for the secretion of numerous large proteases, polysaccharide-digesting enzymes as well as motility proteins, and bacteria possessing this system frequently exhibit gliding (Kulkarni et al., 2017; Mark and Zhu, 2013). Proteins secreted via the type IX secretion system posses N-terminal signal peptides, that are needed for the transport across the cytoplasmic membrane via the Sec system. Depending on the C-terminal domain type, proteins secreted by the type IX secretion system get released to the environment, linked to a cell surface lipopolysaccharide (type A) or get bound to carrier proteins, which link them to the cell surface after secretion (type B) (Kharade and McBride, 2015; Kulkarni et al., 2019; Kharade and McBride, 2014; Lauber et al., 2024). The architecture of this secretion system is based on the β-barrel protein SprA and an associated peptidyl-prolyl cis-trans isomerase subunit with unknown function. This complex facilitates the translocation of molecules by letting them enter the periplasmic side of the SprA pore and bind to the carrier protein PorV before they exit through a lateral opening as a substrate-carrier complex (Lauber et al., 2018, Lauber et al., 2024). This detailed investigation of system structures has been made possible through the genetic tractability of *F. johnsoniae* (Eckroat et al., 2021; Lauber et al., 2018).

1.4 Objectives of this study

To address the current knowledge gaps regarding sulfobacin biosynthesis in *Flavobacterium johnsoniae*, this master´s thesis aimed to:

(1) **Investigate the subcellular localization of candidate enzymes:** Via bioinformatic analysis and *in-frame* reporter gene fusions to selected genes, the spatial distribution of putative enzymes involved in the sulfobacin biosynthetic pathway were analyzed.

(2) **Assess protein production and gene expression:** The fluorescence reporter proteins were additionally used to monitor gene expression of the tagged proteins under defined conditions.

(3) **Characterize and compare sulfonolipid profiles across selected *Bacteroidota* species:** Using liquid chromatography-tandem mass spectrometry, molecular sulfobacin diversity was investigated to identify conserved distribution patterns and species-specific variations among selected bacteria.

Collectively, these approaches aimed to provide deeper insights into the biosynthetic pathway of sulfobacin synthesis and their spatial localization within *F. johnsoniae*. This fundamental understanding of the biosynthesis pathway should facilitate research into the bioactivity and therapeutic potential of these lipids.

2 Materials and Methods

2.1 Materials

2.1.1 Chemicals

All chemicals were sourced from Thermo Fisher Scientific (Waltham, MA, USA) and Sigma-Aldrich (St. Louis, MO, USA). Enzymes were obtained from New England Biolabs (Ipswich, MA, USA), and primers were supplied by biomers.net (Ulm, Germany). Sanger Sequencing was done by Microsynth AG (Vienna, Austria).

2.1.2 Kits

Table 1: Used Kits

Kit Name	Utilization	Producer
CytoLiner™ Fixed Cell Membrane Stain	cell staining	biotium (Fremont, CA, USA)
innuPREP PCRpure Kit	PCR purification	IST Innuscreen GmbH (Berlin, Germany)
Monarch® Spin Plasmid Miniprep Kit	Plasmid isolation	New England Biolabs (Ipswich, MA, USA)
NEBuilder® HiFi DNA Assembly	DNA assembly	New England Biolabs (Ipswich, MA, USA)
Simplex® Easy DNA Extraction Kit	DNA extraction	GEN-IAL® GmbH (Troisdorf, Germany)

2.1.3 Devices and Software

Table 2: Used devices

Device	Producer
Biological Safety Cabinet Class II	LAMSYSTEMS GmbH (Berlin, Germany)
Centrifuge 5804 R	Eppendorf (Hamburg, Germany)
Confocal Laser Scanning Microscope SP8	Leica Microsystems (Vienna, Austria)
Digital block thermostat LLG-uniBLOCKTHERM	LLG-Labware (Meckenheim, Germany)
Freeze dryer Alpha 1-4 LSCbasic	Martin Christ (Osterode, Germany)
Gel Doc XR+ Gel Documentation System	Bio-Rad (Munich, Germany)
Horizontal Gel System	Thermo Fisher Scientific (Waltham, USA)
T100™ Thermal Cycler	Bio-Rad (Munich, Germany)
MiniSpin® Mini Centrifuge	Eppendorf (Hamburg, Germany)
NanoDrop ND-100 Spectrophotometer	Thermo Fisher Scientific (Waltham, USA)
Photometer xy	Thermo Fisher Scientific (Waltham, USA)
PowerPac™ Basic Power Supply	Bio-Rad (Munich, Germany)
SONOREX ultrasonic bath	Bandelin electronic GmbH & Co. KG (Berlin, Germany)
STELLARIS 8 TAU-STED	Leica Microsystems (Vienna, Austria)
Universal Oven BE series	Memmert (Schwabach, Germany)
VWR Orbital Shaker 10000-1 ADV	VWR International GmbH (Leuven, Belgium)

Table 3: Used software

Software	Function	Source
AlphaFold2	Protein structure prediction	https://colab.research.google.com/github/sokrypton/ColabFold/blob/main/AlphaFold2.ipynb
BioRender	Scientific image and illustration software	https://www.biorender.com/
Clone Manager 9	*In silico* cloning	Scientific and educational software
Clustal Omega	Multiple sequence alignment	https://www.ebi.ac.uk/jdispatcher/msa/clustalo
daime 3.1	Image analysis and visualization software	Daims et al., 2006
DeepTMHMM	Transmembrane topology prediction and classification	https://dtu.biolib.com/DeepTMHMM
KEGG Genome	Gene sequences	https://www.genome.jp/kegg/genome/
Leica LAS X	Imaging software	https://www.leica-microsystems.com/de/produkte/mikroskop-software/p/leica-las-x-ls/
Microsoft Excel	Growth curve	Scientific and Educational Software
NEBuilder Assembly Tool	*In silico* cloning	https://nebuilder.neb.com/
NCBI GenBank database	Functional description of genes	https://www.ncbi.nlm.nih.gov/genbank/
Overleaf	Online LaTex Editor	https://www.overleaf.com
Phobius	Transmembrane helices and signal peptide prediction	https://phobius.sbc.su.se/
Reverse Complement	Sequencing analysis	https://reverse-complement.com/
SignalP-6.0	Signal peptide prediction	https://services.healthtech.dtu.dk/services/SignalP-6.0/
Skyline	LC/MS analysis	https://skyline.ms/home/project-begin.view

2.1.4 Strains, Primers and Plasmids

Table 4: Used strains

Strain	Genotype	Reference
C. capnotolerans DHB6	Wildtype	von Heilborn et al., 2022
E. coli 10 β	Δ(ara-leu) 7697 araD139 fhuA ΔlacX74 galK16 galE15 e14-ϕ80dlacδM15 recA1 relA1 endA1 nupG rpsL (StrR) rph spoT1 Δ(mrr-hsdRMS-mcrBC)	New England Biolabs (Ipswich, MA, USA)
E. coli S17-1 λ pir	(F-) RP4-2-Tc::Mu aphA::Tn7 recA λpir lysogen	Ferrières et al., 2010
F. johnsoniae UW101	Wildtype	McBride MJ et al. (2009)
Flavobacterium piscis	Wildtype	isolated by Guoqing Guan
Flavobacterium sp. LT0091	Wildtype	isolated by Guoqing Guan

Table 5: Used plasmids

Plasmid	Genotype	Reference
pCP11	*oriT, ermF, bla, oriV*	Mcbride and Kempf, 1996
prSETb mScarlet-I	*f1 ori, AmpR, oriV, mScarlet-I*	Bindels et al., 2017
pYT313	*oriT, PompA, sacB, ermF, bla, oriV*	Zhu et al., 2017

Table 6: Primers used for *in-frame* insertion

Primer	Sequence (5' → 3')	T_a (°C)	T_m (°C)	Reference
fjoh1748_up_fwd	ATTCGGGGGATCCTCTAGAGGGATCCGTTGGCTTAAC	70	74	Sebastian Tanabe
fjoh1748_up_rev	GCTTCGCCTTTAGAAACCATCGAGCCACCGCCTCCAGCAGAGCCAACTGCTAATTCAGGTTTCATTC	70	88	This thesis
fjoh1748_mSc_fwd	GAATGAAACCTGAATTAGCAGTTGGCTCTGCTGGAGGCGGTGGCTCGATGGTTTCTAAAGGCGAAGC	60	88	This thesis
fjoh1748_mSc_rev	GATTTTTTTTAGTTTTTATTACTTGTACAATTCATCCATAC	60	61	This thesis
fjoh1748_down_fwd	TGGATGAATTGTACAAGTAATAAAAACTAAAAAAAAATCTATTAATAATTAAC	55	64	This thesis
fjoh1748_down_rev	GATTACGCCAAGCTTGCATGCCCCAGGCATATTCGGC	55	79	Sebastian Tanabe
fjoh2419_up_fwd	ATTCGGGGGATCCTCTAGAGGTTACAGGCGATTTAGAGTC	55	72	Sebastian Tanabe
fjoh2419_up_rev	TCGCCTTTAGAAACCATGGAAGATCCTCCTCCTCCCGAAACGTCTACTGTTGTAC	55	81	This thesis
fjoh2419_mSc_fwd	GTACAACAGTAGACGTTTCGGGAGGAGGAGGATCTTCCATGGTTTCTAAAGGC	60	79	This thesis
fjoh2419_mSc_rev	ATTTATTTTTAAATCAATTATTACTTGTACAATTCATCCATAC	60	61	This thesis
fjoh2419_down_fwd	TGGATGAATTGTACAAGTAATAATTGATTTAAAAATAAATTCTCACATG	60	67	This thesis
fjoh2419_down_rev	GATTACGCCAAGCTTGCATGCTAGATTATGACGCCTCTGG	60	75	Sebastian Tanabe
fjoh2421_up_fwd	ATTCGGGGGATCCTCTAGAGCTTCTAACGCAACGGCAAAC	70	77	Sebastian Tanabe
fjoh2421_up_rev	TCGCCTTTAGAAACCATCGAGCCACCGCCTCCAGCAGAGCCAAGATTCTTCAAATAAGTC	70	85	This thesis
fjoh2421_mSc_fwd	ACTTATTTGAATAATCTTGGCTCTGCTGGAGGCGGTGGCTCGATGGTTTCTAAAGGCGAAGC	55	85	This thesis

Primer	Sequence (5' → 3')	T_a (°C)	T_m (°C)	Reference
fjoh2421_mSc_rev	GAACAGAAAACTTTTTTATTACTTGTACAATTCATCCATAC	55	62	This thesis
fjoh2421_down_fwd	TGGATGAATTGTACAAGTAATAAAAAAGTTTTCTGTTCAACTTACG	56	68	This thesis
fjoh2421_down_rev	GATTACGCCAAGCTTGCATGGGACAATAAGGGACCTTTAG	56	74	Sebastian Tanabe
fjoh4604_up_fwd	AAAATTCGGGGGATCCTGCGTAACACAGCCGATGTC	66	76	This thesis
fjoh4604_up_rev	GCCTTTAGAAACCATCGAGCCACCGCCTCCAGCAGAGCCAATCTCACCCGTCATTAAAATATTTTC	66	86	This thesis
fjoh4604_mSc_fwd	TTTAATGACGGGTGAGATTGGCTCTGCTGGAGGCGGTGGCTCGATGGTTTCTAAAGGCGAAGCC	66	89	This thesis
fjoh4604_mSc_rev	GTTGTGACCATGGAGGGATTCGAACCTTATTACTTGTACAATTCATCCA	66	76	This thesis
fjoh4604_down_fwd	TGGATGAATTGTACAAGTAATAAGGTTCGAATCCCTCCATGGTCACAAC	71	75	This thesis
fjoh4604_down_rev	GCTTGCATGCCTGCAGGTCGACGGTTATTATAACGATTC	71	75	This thesis

Table 7: Primers designed for positive control experiments

Primer	Sequence (5' → 3')	T_{m} (°C)	Reference
pCP11_ermFP_fwd	TCCTCTAGAGCGGCCGCCGATACCTTTGTTCCTCGGTTATATG	78	This thesis
ermFP_mSc_rev	GCTTCGCCTTTAGAAACCATTAGTAACTTCTTACAGGTGAATAC	71	This thesis
ermFP_mSc_fwd	TCACCTGTAAGAAGTTACTAATGGTTTCTAAAGGCGAAG	70	This thesis
mSc_pCP11_rev	TCTATTGCTGAATTCCCGGGTTACTTGTACAATTCATCCATAC	72	This thesis
pCP11_P+blaSigP_fwd	GGGGATCCTCTAGAGCGGCCGCCGAAGCGACTTCGCGGAGCTG	85	This thesis
P+blaSigP_mSc_rev	GCTTCGCCTTTAGAAACCATCAAACGCTTGAGTTGCGCC	77	This thesis
P+blaSigP_mSc_fwd	AGGCGCAACTCAAGCGTTTGATGGTTTCTAAAGGCGAAG	76	This thesis

Table 8: Primers used for complementation

Primer	Sequence (5' → 3')	T_{a} (°C)	T_{m} (°C)	Reference
fjoh2419_pCP11_up_fwd	GCGTCTAGAAAGCCAGAGTTAAATCTTG	53	58	Nick Ahrends
fjoh2419_pCP11_down_rev	GCGGTCGACATAAACACTTCATTTATTCTACTTTAC	53	63	Nick Ahrends

Table 9: Additional primers used for screening

Primer	Sequence (5' → 3')	T_a (°C)	T_m (°C)	Reference
sacB_fwd	CGCTTGAGGTACAGCGAAGTG	40	55	This thesis
sacB_rev	GAACATCAACGGTGTAGAG	40	42	This thesis

2.2 Molecular biological methods

2.2.1 Genomic DNA Isolation

Purification of genomic DNA from bacterial cell material was conducted in accordance with the manufacturers protocol of the Simplex® Easy DNA Extraction Kit. The extracted DNA was stored at a temperature of 4°C until further utilization.

2.2.2 Polymerase chain reaction

Copies of double stranded DNA fragments were synthesized via polymerase chain reaction (PCR) using the T100™ Thermal Cycler.

All reactions were conducted in a 25 µl reaction volume and the protocol was carried out as described by the polymerase manufacturer. Q5 high-fidelity polymerase was used to generate products for cloning (*Table 10*), whereas verification screening for correct plasmid transfer and integration was done with the taq polymerase (*Table 11*). For all experiments, reaction components were mixed on ice. After adding the polymerase, the complete mixture was transferred to a T100™ Thermal Cycler. Different annealing temperatures were tested out and elongation times were adjusted accordingly to the expected DNA fragment length as well as the used polymerase (*Table 12* & *Table 13*).

Table 10: Standard mixture for a PCR reaction using Q5 high-fidelity polymerase

Component	25 µl Reaction
5X Q5 Reaction Buffer	5 µl
10 µM Primer fwd	1.25 µl
10 µM Primer rev	1.25 µl
10 mM dNTPs	0.5 µl
Template DNA	0.5 - 1 µl
Q5 High-Fidelity DNA Polymerase	0.25 µl
Nuclease free Water	added up to 25 µl

Table 11: Standard mixture for PCR reaction using Taq polymerase

Component	25 µl Reaction
10X ThermoPol Reaction Buffer	2.5 µl
10 µM Primer fwd	0.5 µl
10 µM Primer rev	0.5 µl
10 mM dNTPs	0.5 µl
Template DNA	0.5 - 1 µl
Taq DNA Polymerase	0.125 µl
Nuclease free Water	added up to 25 µl

Table 12: PCR thermocycling conditions using Q5 high-fidelity Polymerase

Step	Temperature (°C)	Time	
Initial Denaturation	98	3 min	1x
Denaturation	98	20 sec	32x
Annealing	50-72	30 sec	32x
Elongation	72	1 - 1.5 min/kb	32x
Final Extension	72	5 min	1x
Hold	12	∞	

Table 13: PCR thermocycling conditions using Taq Polymerase

Step	Temperature (°C)	Time	
Initial Denaturation	95	3 min	1x
Denaturation	95	20 sec	30x
Annealing	45-86	30 sec	30x
Elongation	68	1 min/kb	30x
Final Extension	68	5 min	1x
Hold	12	∞	

2.2.3 Agarose gel electrophoresis

Agarose gel electrophoresis was used to separate different sized DNA fragments by applying an electric field to a polysaccharide matrix (Hjertén, 1961). The gel contains a tris-base, acetic acid and ethylenediaminetetraacetic acid (EDTA) buffer (TAE buffer) as well as different amounts of LE-Agarose, depending on the wanted separation.

A 0.5 % agarose gel was made by mixing 100 ml of TAE buffer and 0.5 g of LE-agarose before heating the mixture until the agarose dissolved. Depending on the size of the gel, different amounts of GelRed® was added to stain the DNA fragments. DNA was mixed with loading dye in a ratio of 6:1 and loaded into the desired gel pocket, which served as starting point. GeneRuler 1 kb DNA Ladder (Thermo Fisher Scientific, USA) was added in a separate pocket to identify DNA fragment size post electrophoresis. Gel electrophoresis was conducted at 100 V until adequate separation of DNA fragments was achieved. Separation is influenced by fragment size, agarose type and concentration as well as the applied current, with smaller fragments migrating faster than larger ones. The gel was examined using the Gel Doc XR+ Gel Documentation System.

2.2.4 PCR product purification

Products obtained from PCR were processed using the innuPREP PCRpure Kit according to the manufacturer's instructions. Clean PCR fragments were dissolved in 20 µl nuclease-free water and stored at -20°C until further utilization.

2.2.5 Restriction digest

Double-stranded DNA was cut at specific DNA regions using type IIP restriction enzymes (Smith and Welcox, 1970). These magnesium-dependent restriction endonucleases insert double-strand breaks at specific palindromic target sequences, leaving behind blunt- or sticky-ends (*Figure 4*).

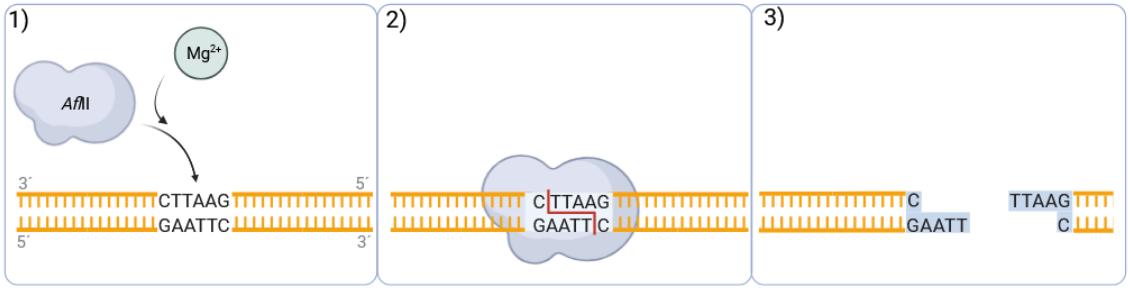

Figure 4: **Sticky-end restriction digest** using the endonuclease *Afl*II, which generates short single-stranded DNA overhangs. This figure was created with BioRender.

While blunt ended sequences do not require specific sequences to hybridize with other blunt ended sequences, sticky-ends can only hybridize with matching complementary nucleotides of another sticky ended DNA fragment. This method was implemented for linear and circular DNA fragments.
Following the manufacturers guidelines, reaction mixtures (*Table 14*) were prepared on ice and subjected to incubation at 37°C for a duration ranging from one hour to 12 hours. Mixtures intended for ligation were inactivated at 65°C for 20 minutes and stored at -20°C, whereas mixtures for control purposes were not inactivated and immediately subjected to agarose gel electrophoresis (0.5% gel (w/v), 70 minutes, 100 V).

Table 14: Standardized digest for Plasmids, linear DNA and control digests

Component	Reaction mixture (V = 20 µl)
DNA	2 µl
CutSmart® Buffer	2 µl
Restriction enzyme	1 µl
Nuclease free water	15 µl

2.2.6 Assembly of plasmids using T4 DNA ligase

To join DNA fragments, an ATP-dependent T4 DNA ligase was utilized to form a phosphodiester bond between the 5' phosphate and 3' hydroxyl ends of selected digested DNA fragments. Ligation was used to fuse a double-stranded DNA fragment, consisting of a reporter gene with flexible linker sequence and flanking up- and downstream regions of the target gene, into a digested plasmid.

The standard ligation protocol was used to insert DNA fragments into the replicating plasmids *pCP11* and *pCP23* (*Table 15*).

Plasmid and to-be inserted DNA fragment were mixed according to the manufacturers instructions in a ratio of 1:3, ideally being 0.020 pmol Plasmid to 0.060 pmol DNA fragment. The incubation period lasted 48 hours at 4°C and 2 hours at room temperature, before ligation was completed by heat inactivation at 65°C for 10 minutes. To quantify plasmid re-ligation, a control ligation reaction was performed, substituting water for the insert DNA. Subsequently, each resulting ligation reaction was used to transform competent E. coli 10β.

Table 15: Standard ligation protocol for vector and insert

Component	Reaction mixture (V = 20 µl)
T4 DNA Ligase Buffer	2 µl
T4 DNA Ligase	1 µl
Vector	variable
Insert DNA	variable
Nuclease free water	added up to 20 µl

2.2.7 Assembly of plasmids using the NEBuilder® HiFi DNA Assembly Kit

The NEBuilder® HiFi DNA Assembly Kit was used to assemble multiple linear DNA fragments, including a digested plasmid, into a complete construct. Following the Gibson Assembly approach, the supplied reaction mixture includes three distinct enzymes in a unified buffer. Exonuclease activity generates single-stranded 3´ overhangs, allowing fragments with complementary sequences to anneal. For this, an overlap of 30 to 40 base pairs between the DNA fragments should be taken into account during the primer design. Following the exonuclease, the polymerase fills in the gaps within these annealed fragments. In order to seal the nicks in the assembled DNA, a DNA ligase is also added in the buffer.

Depending on the amount of fragments used for the assembly, different ratios of plasmid and to-be inserted DNA fragments should be used. To fuse 3-5 DNA fragments into one plasmid, equimolarity should be maintained. The reaction protocol was adapted to generate successful assemblies and reactions were prepared as shown in *Table 16* and *Table 17*.

This method was utilized for the assembly of the *in-frame* insertion plasmid *pYT313* with an allelic exchange cassette, that consists of a reporter gene (*mScarlet-I*) with a flexible linker gene sequence which is flanked by approximately 3000 bp of the upstream and downstream homologous regions of the target gene. This allelic exchange cassette was assembled in a first NEB Assembly step, fusing previously produced PCR products into a single DNA fragment. Reaction mixtures were mixed on ice and incubated at 50°C for 2 hours. Correct assembly was checked with 5 µl of the reaction mixture via gel electrophoresis. The remaining reaction mixture was used to assemble the previously generated DNA fragment with the digested suicide plasmid *pYT313* by adding an equimolar amount of plasmid, 2.5 µl of NEBuilder HiFi DNA Assembly Master Mix and nuclease-free water. The assembly was completed after a 4 hour incubation at 50°C. Vector re-ligation was quantified using a control assembly reaction, where water replaced the insert DNA. Each product was subsequently introduced into E. coli 10β using the standard transformation protocol.

Table 16: Step 1: Assembly of PCR fragments into one Insert using the NEBuilder® HiFi DNA Assembly Kit

Component	Reaction mixture (V = 10 µl)
NEBuilder HiFi DNA Assembly Master Mix	5 µl
Nuclease-free water	added up to 10 µl
Upstream-Gene fragment (Fragment 1)	variable
Reporter gene with flexible linker (Fragment 2)	variable
Downstream fragment (Fragment 3)	variable

Table 17: Step 2: Assembly of Insert and Plasmid using the NEBuilder® HiFi DNA Assembly Kit

Component	Reaction mixture (V = 10 µl)	Control (V = 10 µl)
NEBuilder HiFi DNA Assembly Master Mix	2.5 µl	5 µl
Nuclease-free water	added up to 10 µl	5 µl
Digested *pYT313*	variable	
Step 1 mixture	5 µl	

2.2.8 Plasmid DNA isolation

Plasmids were isolated from liquid culture with the Monarch® Spin Plasmid Miniprep Kit following the manufacturers manual. The purified plasmids were resuspended in 50 µl nuclease-free water and stored at -20°C. To confirm successful assembly, samples of the plasmids were digested with restriction endonucleases and their digestion pattern verified using TAE agarose gel electrophoresis.

2.2.9 DNA sequencing

Samples were sent to Microsynth AG (Vienna, Austria) to perform sanger sequencing. Each sample for sequencing held 40 to 100 ng ml^{-1} plasmids or PCR-amplificates in a 15 µl volume of nuclease-free water.

2.3 Microbiological Methods

2.3.1 Bacterial cultivation

Cultivation of the bacteria strains was conducted under aerobic conditions. *Chryseobacterium capnotolerans* was cultured in liquid tryptic soy broth (TSB) or on solid tryptic soy agar (TSA) (*Table 19*) (von Heilborn et al., 2022). *C. capnotolerans* was cultured at 27°C over night in liquid medium with shaking at 180 rpm. The *Escherichia coli* strains were cultured in liquid or on solid lysogeny broth (LB) (*Table 18*) (Bertani, 1951). To prepare solid medium, 1.5 % agar-agar was added before sterilization. Following the autoclaving process, ampicillin was added to the liquid or solid medium at a ratio of 1:1000 (v/v) if needed. *E. coli* was grown on plates or in shaken liquid medium at 37°C over night. *Flavobacterium* strains were cultured in liquid or on solid Casitone-Yeast-Extract medium (CYE) and grown at 27°C over night, liquid medium being additionally shaken at 180 rpm (*Table 21*) (Mcbride and Kempf, 1996). Selected CYE media batches were supplemented with 5% (m/v) sucrose before sterilization to serve as an additional carbon source for investigation of levan production during *in-frame* insertion. Post-sterilization, some batches were further supplemented with erythromycin at a 1:1000 (v/v) ratio. Investigation of the gliding ability of *Flavobacterium johnsoniae* was performed on solid motility-medium (MM) (J. Liu et al., 2007). Erythromycin was added in a ratio of 1:1000 (v/v) after sterilization if needed (*Table 20*).

Table 18: Medium for *E.coli* cultivation

Component	LB-Medium
LB-Medium	25 gl^{-1}
Nuclease-free water	1 L
Agar-Agar	1.5 % (w/v)

Table 19: Medium for *C. capnotolerans* cultivation

Component	TS-Medium
TSB	30 gl^{-1}
Nuclease-free water	1 L
TSA	40 gl^{-1}
Nuclease-free water	1 L

Table 20: Motility Medium for *F. johnsoniae* cultivation

Component	Motility-Medium
Casitone	3.3 gl^{-1}
Yeast	1.7 gl^{-1}
Tris buffer (pH = 7.5)	.,3 mM
Nuclease-free water	1 L
Agar-Agar	1.5 % (w/v)

Table 21: Medium for *F. johnsoniae* cultivation

Component	CYE-Medium
Casitone	10 gl^{-1}
Yeast	5 gl^{-1}
Magnesium sulfate	8 mM
Tris buffer (pH = 7.5)	10 mM
Nuclease-free water	1 L
Agar-Agar	2 % (w/v)
Sucrose	5 % (w/v)

Table 22: Used antibiotics in solid and liquid medium in a ratio of 1:1000 (v/v)

Antibiotic	Concentration	Solvent	Used for
Ampicillin	100 µg ml^{-1}	Nuclease-free water	LB-Medium
Erythromycin	25 µg ml^{-1}	mol. grade ethanol	CYE-Medium

2.3.2 Production of chemical competent *E. coli* 10 β and *E. coli* S17-1 λ pir

The Calcium Chloride ($CaCl_2$) method was used, to prepare chemical competent *E. coli* 10 β and *E. coli* S17-1 λ pir cells (Dagert and Ehrlich, 1979).

For both strains, a 70 mL main culture of antibiotic-free LB medium was prepared by inoculating with a 1:100 (v/v) volume of overnight preculture. Cultures were incubated at 37°C, shaking at 180 rpm until an optical densitiy of OD_{600} = 0.6. To maintain low temperatures, all further procedures used chilled solutions and were conducted on ice. Cells were harvested via centrifugation at 4000 x g for 10 minutes and 4°C. The Pellet was transferred into a 10.5 ml solution of $CaCL_2/MgSO_4$ (70 mM $CaCl_2$, 20 mM $MgSO_4$). After

40 minutes of Incubation on ice, the cells were collected (4000 x g, 10 min, 4°C) and resuspended in a 3.5 ml $CaCl_2$/$MgSO_4$ solution. The solution was then subjected to an incubation period of 40 minutes on ice, after which 875 µl of cold, sterile glycerine was added. After mixing, the cell suspensions were aliquoted in 200 µl SafeLock Eppendorf tubes before storing them at -70°C until further usage.

2.3.3 Transformation of cells using the heat shock method

Heat shock transformation was used to introduce the assembled plasmids into competent *E. coli* 10 β or *E. coli* S17-1 λ pir cells (Hanahan, 1983).

Competent cells were slowly thawed on ice, before mixing in a small volume of Plasmid. Depending on the plasmid solution used, 1 µl of correctly assembled, free plasmid or the entire NEB Assembly/ Ligation mixture was mixed with 100 µl of thawed competent cells. Different *E. coli* strains were selected based on the purpose of transformation. *E. coli* 10 β was employed to amplify plasmids, while *E. coli* S17-1 λ pir functioned as the donor strain in conjugation experiments. The mixture was incubated on ice for 30 minutes, following a heatshock at 42°C for 90 seconds. Subsequently the cells were incubated on ice for 2 minutes before adding 800 µl of LB Medium. After 1 hour of Incubation at 37°C, cells were pelleted at 2000 rpm for 4 minutes at room temperature and resuspended in the residual liquid. A volume of 100 µl of the cell suspension was plated on a LB plate substituted with ampicillin and incubated at 37°C overnight. Plates were then stored at 4°C for up to three weeks.

2.3.4 Conjugation of plasmids into cells

This method utilizes the ability of horizontal gene-transfer to get Plasmid-DNA from a donor cell into an acceptor cell via cell-cell contact (Lederberg and Tatum, 1946). Employing this method, the assembled vector is transferred from *E.coli* S 17-1 λ pir to the *F. johnsoniae* Mcbride and Kempf, 1996.

Transformed *E. coli* S 17-1 λ pir were cultured overnight in liquid LB-medium, supplemented with Ampicillin (1000:1, v/v), at 37°C while shaking at 180 rpm. Separately, *F. johnsoniae* was cultured overnight in CYE-medium at 27°C, also shaking at 180 rpm. 1 ml of both cultures were centrifuged at 5000 rpm for 1 minute and the *F. johnsoniae* pellet was resuspended in 50 µl of CYE-medium. The *E.coli* pellet was resuspended in 1000 µl CYE-medium and centrifuged again to remove excess ampicillin. Subsequently the pellet was resuspended in 50 µl CYE-medium followed by mixing 25 µl of *E. coli* and 25 µl of *F. johnsoniae* in a new tube. The mixed 50 µl were then spotted on a CYE plate, previously coated with 100 µl of sterile 1 M $CaCl_2$ and incubated at 27°C over night. As control, 25 µl of the *F. johnsoniae* suspension was spotted and incubated on a $CaCl_2$ covered CYE plate. After overnight incubation, *F. johnsoniae* cells were scraped from the plates and serially diluted from 10^{-1} to 10^{-5}. 100 µl of each dilution was then plated onto seperate CYE plates supplemented with 25 µg/ml erythromycin. Plates were incubated at 27°C for 2-3 days to select for successful conjugative transfer.

2.3.5 *In-frame* insertion

In-frame insertion was used to investigate the activity and localization of a protein without disrupting its natural gene locus. This method utilizes a suicide plasmid carrying a previously inserted allelic exchange cassette, two positive selection markers and a counter-selection marker. The allelic exchange cassette consists of the reporter gene fragment to be inserted, flanked by upstream and downstream homologs that define the target insertion site. The positive selection markers, usually antibiotic resistance genes, are used to select for cells that have successfully taken up the plasmid. A counter-selection marker is a gene whose expression is lethal when the cells are grown under specific conditions.

In-frame insertion is achieved following two successive crossover events. Through a first crossover event, the suicide plasmid is integrated either via upstream or downstream homologous region, mediating the integration of the entire plasmid into the genome. A positive selection marker enables screening at this stage, as only colony forming units (CFU) that have successfully integrated the plasmid can grow on the selective medium. The presence of the reporter gene, and therefore the presence of the entire plasmid, is validated by performing a PCR as an additional confirmatory step. Confirmed clones with the integrated plasmid are then grown without selection pressure, initiating the second crossover event and the loss of the plasmid. The outcome of the event is determined by the alignment of the integrated plasmid segment relative to the homologous wildtype region, resulting in either the restoration of the original sequence or the stable *in-frame* insertion. Confirmation of the insertion of the reporter gene fragment is done via PCR.

In-frame insertion was performed using the suicide plasmid *pYT313* as a vector to insert the fluorescent reporter gene onto a targeted gene of *F. johnsoniae*. This *in-frame* approach ensures that both genes are situated within a single continuous open reading frame, resulting in a protein where the fluorescent marker is covalently linked to the target protein. This strategy allows for the visualization of the fusion protein while preserving its physiological wildtype function (Smeyne et al., 1992).

The assembled vector has two antibiotic resistance genes. The *bla* gene confers resistance to ampicillin, enabling transformed *E. coli* cells to grow on ampicillin-supplemented LB medium, while the *ermF* gene, encoding for erythromycin resistance, is the positive selection marker during markerless in-frame insertion. A counter selection marker called *sacB* was used after the first crossover event, to visually differentiate between spontaneous mutants to erythromycin compared to cells, that integrated the plasmid into the nucleoid. The allelic exchange cassette consists of the to-be inserted reporter gene *mScarlet-I* with a flexible G-S-A-G-G-G-G-S-Linker, flanked by roughly 3000 bp of upstream and downstream homologous region of the targeted *F. johnsoniae* gene. These fragments were generated via PCR and fused into one fragment with the NEBuilder HiFi DNA Assembly Kit. The empty suicide plasmid was digested by type IIP restriction endonucleases and the plasmid was fused to the allelic exchange cassette through a second NEBuilder HiFi DNA Assembly.

The assembled suicide plasmid was introduced into *F.johnsoniae* via conjugative transfer. Selected CFU were streaked onto two different selective plates: erythromycin enriched CYE plates and CYE plates supplemented with 5 % sucrose. Colonies that were erythromycin resistant and had sucrose activity indicated the presence of an integrated plasmid, which was additionally confirmed via PCR for *sacB* or *mScarlet-I*. Colonies with confirmed integration were grown in liquid CYE-medium for 1-2 days at 27°C and shaking at 180 rpm, triggering the second crossing over event. Thereafter, serial dilution was conducted by mixing 180 µl of CYE and 20 µl of preculture. Diluted cultures ranging from 10^{-5} to 10^{-10} were plated on CYE + 5% Saccharose plates and grown for 2 to 3 days at 27°C. Obtained clones were transferred to a fresh CYE plate and genomic DNA isolates were tested for *sacB* absence and *mScarlet-I* presence via PCR.

2.3.6 Preparation of cryo-cultivates

Used bacteria and genetically modified clones were stored at -75°C using cryo-cultivates. Therefore, 1000 µl of an overnight liquid culture of the wanted bacteria was mixed with 250 µl of a sterile 75% glycerol solution. Subsequently, 250 µl of this mixture was transferred into 0.5 µl Safelock tubes. After a five minute incubation on ice, the cryo-cultures were placed in a -75°C freezer for long time storage.

2.3.7 Processing cells for imaging and growth experiment

Confocal microscopy was used to examine the activity and subcellular localization of translated, modified proteins in *F. johnsoniae*. For sample processing, cells were grown in liquid medium, fixed with a 2% Formaldehyde solution, washed, dried and stained with 4‘,6 Diamidino-2-phenylindole (DAPI), before mounting the spotted cells in CitiFluor™.

Liquid precultures of *Flavobacterium* strains were grown overnight at 27°C at 180 rpm in CYE-medium, enriched with erythromycin if needed (1:1000 v/v). Subsequently, 500 µl of the overnight preculture was inoculated into 50 ml of CYE medium, which had been supplemented with 1 mg/ml cysteate and or 25 µg/ml erythromycin as required. Cultures were incubated at 27°C while shaking at 180 rpm for 49 hours. For certain cultures, OD_{600} measurements were obtained every two hours to identify different growth stages over a period of 49 hours. In accordance with the early (2h) and late stages (6h) of the exponential phase, as well as the stationary phase (10h, some at 25h mark), 500 µl of culture was sampled and processed for imaging. Identical experimental procedures were carried out for *E. coli* S 17-1 λ pir and *C. capnotolerans*. *E. coli* was grown in LB medium at 37°C, whereas *C. capnotolerans* was incubated in TSB medium at a lower temperature of 27°C. The shaking speed for both organisms was maintained at 180 rpm. Certain *F. johnsoniae* cultures were grown for 4 hours at 27°C while shaking at 180 rpm, before 500 µl were sampled and processed.

Cells of isolated samples were centrifuged at 2000 rpm for 4 minutes. The pellet was resuspended in 200 µl of a 2% Formaldehyde solution and incubated in the dark at room temperature for 30 minutes.

Cells were subjected to three washing cycles, using 300 µl of 1x phosphate-buffered saline (1x PBS, pH = 7.4) and centrifugation (2000 rpm for 4 minutes) for each step. Resulting fixed cell pellets were mixed with 50 µl of 70% ethanol and archived at -20°C until the imaging day. As needed, 10 µl of the fixed cell suspension was spotted on a microscope slide and dried for 15 to 25 minutes at 46°C. General staining was performed using DAPI (1 µg/µL) by applying 10 µL to the dried specimen, followed by incubation in the dark for 10 min at room temperature. Microscopy slides were washed with nuclease-free water and 96% Ethanol. CitiFluor™ was used as mounting medium after the slides were dry and specimen were imaged immediately after. Certain specimen were additionally stained using the CytoLiner™ Fixed Cell membrane stain. Fixed cells were stained following the manufacturers instructions. The cell pellet was diluted in 50 µl of 1x PBS. 10 µl of the suspension was spotted onto a microscope slide followed by 30 minutes drying at 46°C. Dried spots were mounted in 1x PBS and immediately imaged.

2.3.8 Imaging of cells using CLSM

Cell imaging was aquired using Leica Confocal Laser Scanning Microscope SP8 (CLSM) or Leica STELLARIS 8 TAU-STED. For the CLSM SP8, optical magnification was provided by a x100 glycerine-immersion objective (1.30 NA) and images were aquired using the corresponding Leica camera. Data acquired via STELLARIS 8 TAU-STED was done with a HC PL APO CS 100x oil-immersion objective (1.40 NA) and images were obtained with the corresponding Leica camera. Fluorescence images were collected at laser power of 4-8% for DAPI, 20-30% for *mScarlet-I* and 10% for CytoLiner™ . Cells expressing *mScarlet-I* and stained with DAPI and CytoLiner™ were imaged using the fluorescence parameters listed in *Table 23*. Images were captured at a spatial resolution of 1024 x 1024 pixels using a scan speed of 200Hz and a line average of 2. Raw data was analyzed using the Leica LAS X software and 3D cell imaging was done using the z-stack function.

Table 23: Photophysical protperties of the utilized fluorescent markers

	mScarlet-I	DAPI	CytoLiner™
Max. excitation	569 nm	354 nm	492 nm
Max. emission	594 nm	456 nm	510 nm

2.4 Biochemical Methods

2.4.1 Lipid extraction

Lipids of *Flavobacterium* strains and *C. capnotolerans* were extracted using the method as described previously (BLIGH and DYER, 1959). Overnight precultures were used to inoculate 5 ml of medium (1:100, v/v). The cultures were prepared in duplicate, with only one culture additionally supplemented with 1 mg/ml of cysteate. Following 6 hours of incubation at 27°C while shaking at 180 rpm, cells were harvested (10000

rpm, 2 min) and subjected to overnight freeze-drying. The resulting dry pellet was resuspended using 1 ml of molecular grade methanol. For cell lysis, samples were incubated in a cooled sonication bath for 1 hour, followed by a 2 hour incubation at room temperature. To separate cell debris, the samples were centrifuged at maximum relative centrifugal force for 15 minutes. Thereafter, 800 µl of the supernatant was transferred to an HPLC glass vial and evaporated overnight using a nitrogen evaporator. Subsequently, solutions with a lipid concentration of 1-2 mg/ml were prepared using the evaporated supernatant and molecular grade methanol. Thereafter, a diluted solution with a concentration of 50 µg/ml was prepared. To remove insoluble impurities, the diluted solution was centrifuged at 14000xg for 20 minutes before 100 µl of the supernatant was transferred into a new HPLC glass vile. The lipid extraction was performed on the day of the LC-MS/MS analysis and stored at 14°C.

2.4.2 Liquid chromatography-tandem mass spectrometry

Liquid chromatography-tandem mass spectrometry (LC-MS/MS) was employed to identify sulfobacins and biosynthetic intermediates produced by *F. johnsoniae* wildtype and mutant strains, as well as *C. capnotolerans*. Furthermore, two additional *Flavobacterium species* provided by Guoqing Guan were screened as potential candidates for sulfobacin production. The LC-MS/MS analysis followed a protocol adapted from Pekkle Lam et al., 2023. Lipid extracts were analyzed using a UHPLC system equipped with a reversed-phase C8 column, which enabled the efficient separation of lipid species based on their hydrophobicity. Following chromatographic separation, analytes were ionized and detected using an Orbitrap mass spectrometer operated in tandem MS (MS/MS) mode. Structural characterization of sulfobacins and related intermediates was achieved through accurate mass measurements and the evaluation of characteristic fragmentation patterns. Raw data processing and analysis were performed using Skyline software

2.5 Analysis methods

2.5.1 *In silico* protein topology prediction using Phobius and DeepTMHMM

Transmembrane topology and signal peptide prediction were assessed using Phobius and DeepTMHMM. Based on Hidden-Marcov models, Phobius estimates posterior probabilities for each amino acid position to belong to distinct topological states. This includes transmembrane helices, cytoplasmic regions, non-cytoplasmic regions and signal peptides. Resulting probabilities were visualized along the protein sequence. DeepTMHMM uses convolutional neural networks (deep learning) to recognize which parts of an amino acid sequence passes through a biological membrane via transmembrane helices and which parts are located in the cytoplasm or periplasm. Resulting probabilities were visualized along the protein sequence (Hallgren et al., 2022).

Encoded protein sequences of the target genes *fjoh_1748* (possible sulfobacin monooxygenase), *fjoh_2419* (cysteate-acyl-ACP transferase), *fjoh_2421* (possible sulfobacin synthase) and *fjoh_4604* (possible sulfobacin monooxygenase) were each entered into both models.

2.5.2 *In silico* protein structure prediction using AlphaFold2

Protein structure predictions were perfomed using AlphaFold2 (Jumper et al., 2021).

Protein structure predictions for Fjoh_2419 (cysteate-acyl-ACP transferase) and Fjoh_4604 (possible sulfobacin monooxygenase) and the corresponding fusion proteins were each entered into AlphaFold2.

2.5.3 Analysis of fluorescence intensity and spatial overlap using *daime* 3.1

Quantitative evaluation of the fluorescence intensities of the tagged target enzymes was done using *daime* 3.1 software (Daims et al., 2006).

Cell recognition was based on two-dimensional segmentation using a local thresholding method (Sauvola). Additionally, objects with a size of $\leq$ 20 pixels were excluded, reducing image noise. Cells from five independent images per condition were pooled for quantitative analysis by combining them into one object layer. Quantitative intensity parameters were extracted for each object using the *Measure Object Features* function. The median object intensity was used as a measure of fluorescence intensity. Resulting object intensities were statistically compared between the four experimental categories using the Kruskal-Wallis test.

Subcellular topology comparison between mScarlet-I fluorescence and CytoLiner™ signals was performed using daime 3.1 (Daims et al., 2006). Automated cell recognition was achieved through two dimensional segmentation using the Sauvola algorithm, followed by appropriate image noise reduction. Quantitative morphological parameters were extracted for each object using the *Measure Object Features* function. One representative image per fluorescence channel was analyzed, and the median object size was utilized for statistical comparison (Kruskal-Wallis test) between the two experimental categories.

3 Results

In this study, the previously described SulA encoding gene *fjoh_2419*, as well as previously unidentified genes possibly encoding the sulfobacin synthase (*fjoh_2421*), and the sulfobacin monooxygenase (*fjoh_1748*, *fjoh_4604*) were targeted. These genes were identified through a sequence-based homology search using BLAST against the *F. johnsoniae* genome, using analogue genes involved in the sphingolipid biosynthesis.

3.1 *In silico* topology prediction and structural modeling of putative sulfobacin biosynthetic enzymes

Transmembrane topology and signal peptide prediction were assessed using Phobius and DeeptMHMM (Hallgren et al., 2022). Phobius predicts a non-cytoplasmic orientation for the cysteate acyl-ACP transferase (Fjoh_2419) with an 80% probability across the majority of the sequence, despite the absence of a predicted signal peptide. However, additional validation using deepTMHMM yielded no probability of a transmembrane sequence, instead predicting a cytoplasmic, globular protein (Figure 5c; *Figure 5d*). Phobius and deepTMHMM did not predict transmembrane sequences or signal peptides for the protein Fjoh_2421, indicating that the putative sulfobacin synthase is a soluble and cytoplasm-associated enzyme (*Figure 5e; Figure 5f*). Both putative sulfobacin monooxygenases Fjoh_1748 and Fjoh_4604 show no N-terminal signal peptides. Predictive analysis suggests four transmembrane helices located approximately between the amino acid position 50-100 and 200-250 for Fjoh_1748 (*Figure 5a; Figure 5b*), whereas the output for the Fjoh_4604 indicates four transmembrane helices at the positions 50-100 and 230-280 (*Figure 5g; Figure 5h*). To evaluate the structural architecture of the fusion proteins, 3D models were generated using AlphaFold2 (Jumper et al., 2021). Both native enzymes, representing a putative cytoplasmic (Fjoh_2419) and an integral membrane (Fjoh_4604) protein, exhibited a high confidence fold (pLDDT > 90, dark blue) within their potential catalytic domains (Figure 6a & Figure 6c). The structure prediction for the cysteate acyl-ACP transferase (Fjoh_2419) revealed a c-shaped architecture, whereas Fjoh_4604 (putative sulfobacin monooxygenase) was predicted to adopt a diamond-shaped conformation. In both fusion protein models, the barrel shaped mScarlet-I fluorophore (highlighted in pink) demonstrated high confidence scores. In contrast, the putative linker sequence exhibited a very low confidence score (pLDDT < 50, highlighted in orange), highlighting the flexibility of the used linker (Figure 6b & Figure 6d).

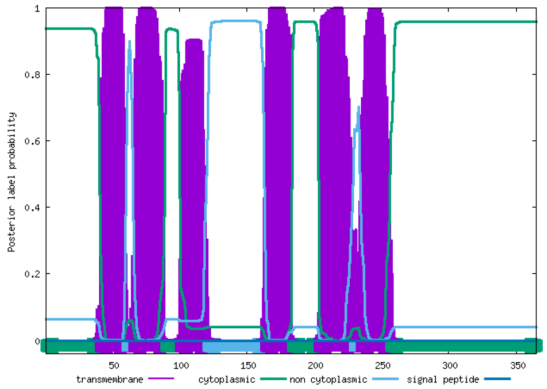

(a) Phobius: *fjoh_1748*

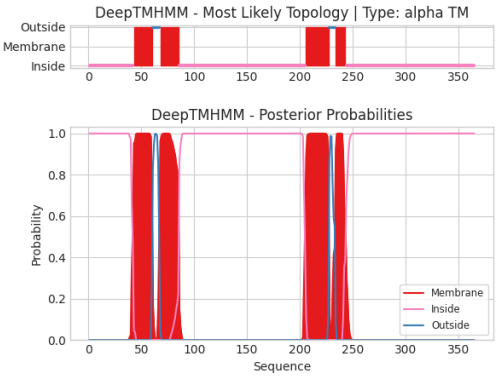

(b) DeepTMHMM: *fjoh_1748*

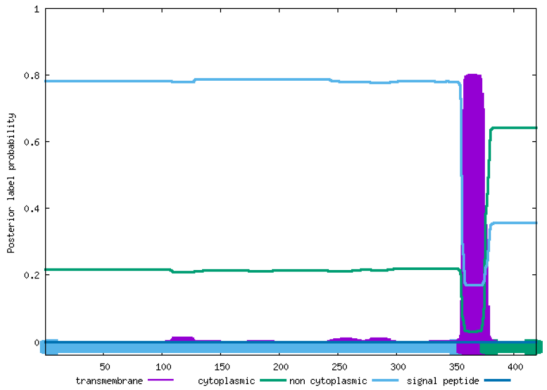

(c) Phobius: *fjoh_2419*

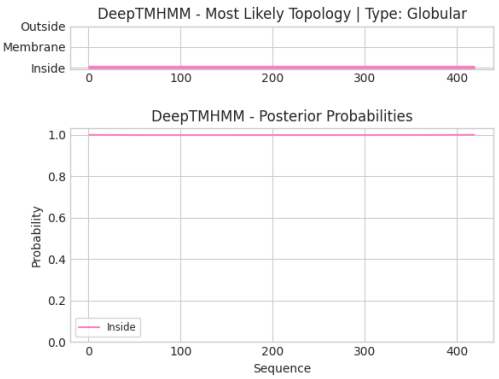

(d) DeepTMHMM: *fjoh_2419*

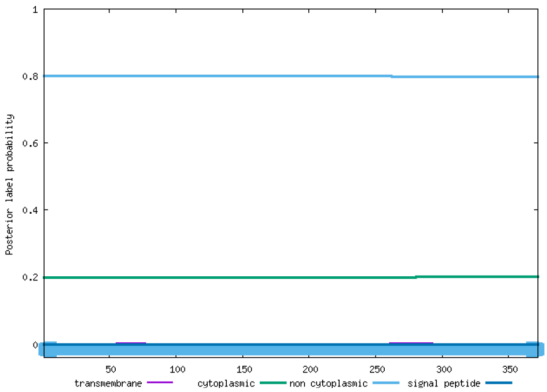

(e) Phobius: *fjoh_2421*

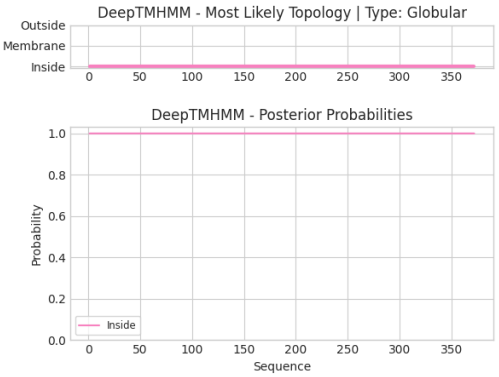

(f) DeepTMHMM: *fjoh_2421*

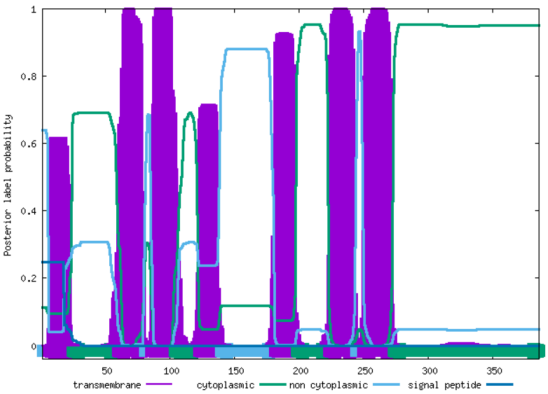

(g) Phobius: *fjoh_4604*

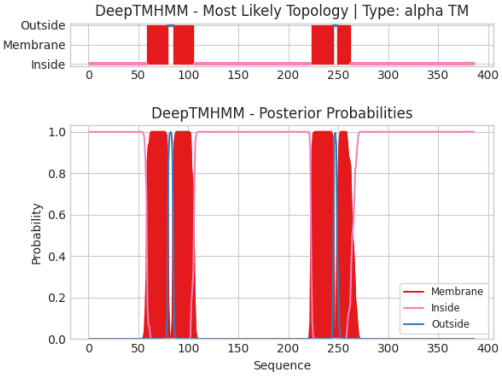

(h) DeepTMHMM: *fjoh_4604*

Figure 5: **Position-wise probabilities for topological states predicted by Phobius and DeepTMHMM** indicating the likelihood of each amino acid belonging to a given topological class for selected *F. johnsoniae* proteins.

(a) Predicted 3D structure of the cysteate acyl-ACP transferase (SulA)

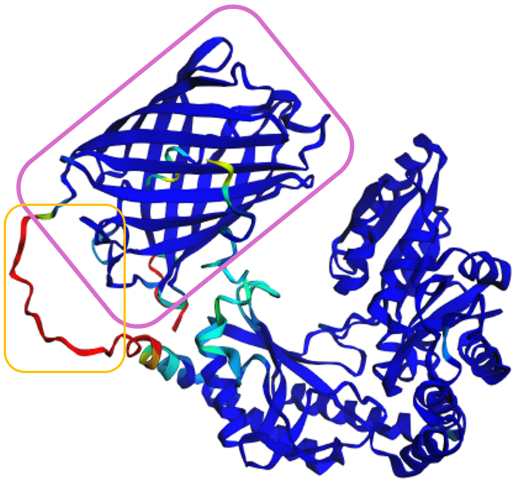

(b) Predicted 3D structure of the mScarlet-I tagged cysteate acyl-ACP transferase

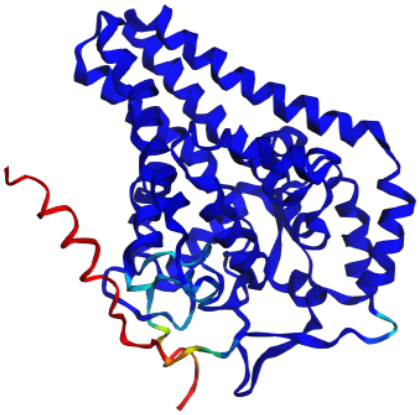

(c) Predicted 3D structure of the putative sulfobacin monooxygenase (Fjoh_4604)

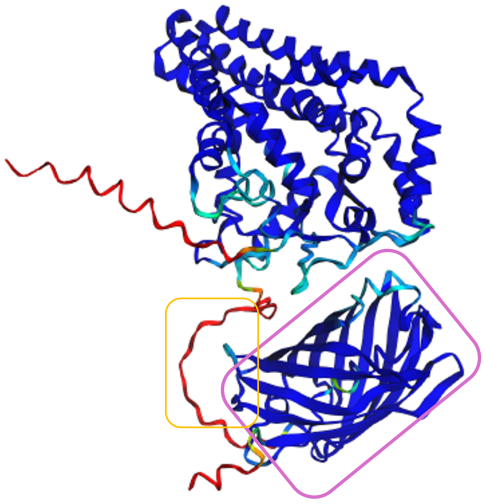

(d) Predicted 3D structure of the putative tagged sulfobacin monooxygenase (Fjoh_4604)

Figure 6: **AlphaFold2-predicted structural models of representative enzymes in the sulfobacin pathway:** The models illustrate two architectural classes: (a & b) Fjoh_2419, representing a putative soluble cytoplasmic protein and (c & d) Fjoh_4604, representing a putative integral membrane protein. The mScarlet-I tagged proteins feature the fluorophore highlighted by a pink box, while the connecting flexible linker is indicated by an orange box.

3.2 Design and construction of plasmids for *in-frame* gene insertion and complementation

Previous studies introduced a cloning strategy for genes of *F. johnsoniae* and a deletion system has been successfully applied previously (Vences-Guzmán et al., 2021; Mcbride and Kempf, 1996). Primer and Plasmid design, as well as *in silico* cloning was conducted with Clone Manager 9. The cloning strategy was based on established vector backbones for *F. johnsoniae*. Based on these, the non-replicative plasmid *pYT313* for genomic integration and the autonomously replicating plasmid *pCP11* for complementation was modified. (Mcbride and Kempf, 1996; Zhu et al., 2017).

The chromosomal integration-based plasmid *pYT313* carries resistance genes for ampicillin and erythromycin, which are used as positive selection markers at different cloning stages, as well as the levansucrase gene (*sacB*) as a counter-selection marker. This plasmid can replicate in the employed *E. coli* 10 β and *E. coli* S 17-1 λ pir, but not in *F. johnsoniae*, as the origin of replication (*oriV*) only gets recognized by *E. coli* strains.

The empty *pYT313* plasmid and the allelic exchange cassette fragment used for *in-frame* insertion were assembled using the NEBuilder® HiFi DNA Assembly Kit. To generate the allelic exchange cassette, three distinct fragments were used. The heterologous reporter gene *mScarlet-I* was inserted between the fragment containing the upstream region and the target gene, and the fragment containing the downstream region. These flanking regions define the precise insertion site within the *F. johnsoniae* genome. In a first assembly step, the three amplified fragments were fused together using their complementary terminal sequences, which featured overlaps of about 40 base pairs. Amplification of the upstream fragment did not include the stop codon of the respective *F. johnsoniae* target gene. Via NEBuilder HiFi DNA Assembly, the 5´end of the upstream fragment was fused to the 3´end of the reporter gene fragment via overlapping homologous sequences. The *mScarlet-I* reporter gene fragment was amplified using the *prSETb mScarlet-I* Plasmid as DNA template during PCR. The used forward primer was designed to contain a homologous region corresponding to the 5' end of the upstream fragment and the initial nucleotides of the reporter gene, combined by a flexible linker encoding the amino acid sequence glycine–serine–alanine–glycine–glycine–glycine–glycine–serine (G–S–A–G–G–G–G–S). This linker sequence, adjacent to the start codon of *mScarlet-I* does not disrupt the open reading frame of the target gene and is therefore translated with the target gene sequence into one modified protein. Two stop codons, derived from the original *mScarlet-I* gene and the *F. johnsoniae* wildtype target gene, were integrated into the reverse primer. The amplified downstream fragment corresponded to the respective wildtype genomic region and was fused via NEBuilder HiFi DNA Assembly to the 5' end of the reporter gene *mScarlet-I* with the help of overlapping homologous sequences. The assembled allelic exchange cassette fragment, consisting of the upstream region with the target gene, reporter gene with link to the

target gene, and homologous downstream region of the target gene, was then fused into the digested *pYT313* in a second assembly.

In addition to the *in-frame* insertion plasmid, a complementation plasmid for the target gene *fjoh_2419* was made using the *pCP11* plasmid as vector backbone. Same as for *pYT313*, the replicating vector *pCP11* encodes an ampicillin and erythromycin resistance, which are used as positive selection markers. This vector gets replicated both in the utilized *E. coli* strains and *F.johnsoniae* due to the recognition of the origin of replication (*oriV*). The inserted fragment was amplified using the previously assembled *pYT313* suicide plasmid for *fjoh_2419* as template DNA, making the structure equivalent as described above. Digested plasmid and PCR fragment was then fused using T4 ligase.

Positive controls for *mScarlet-I* fluorescence signals were also constructed using the *pCP11* replicating plasmid. Depending on the subcellular destination of the translated reporter gene, two different vectors were constructed. Both control constructs, one designed to produce a cytoplasmic signal and the other a transmembrane signal, were exclusively assembled *in silico* (*Figure 17*; Figure 19). For each vector, a localization-determining sequence and the heterologous reporter gene *mScarlet-I* fragment were amplified and fused together. The plasmid constructed for cytoplasmic reporter protein localisation, consisted of the *pCP11* plasmid backbone as well as the *ermF* promoter region fused to the reporter gene *mScarlet-I*. The *pCP11* plasmid constructed for transmembrane localisation comprised the plasmid backbone, the *bla* promoter region, a signal peptide encoding sequence, and the reporter gene *mScarlet-I*. Using *in-silico* overlap extension PCR, the 3' end of the localization-determining sequence was fused to the 5' end of the reporter gene. The resulting fragment was then ligated *in-silico* into the digested plasmid backbone.

3.2.1 Suicide plasmid strategy for *in-frame* tagging of the putative sulfobacin monooxygenase Fjoh_4604

The NCBI GenBank database provides a functional annotation for the 1098 nucleotide long *fjoh_1748* as putative linoleoyl-CoA desaturase. However, prior comparative genomic analyses have revealed sequence similarities between the dihydroceramide monooxygenase gene involved in sphingolipid biosynthesis and the *fjoh_1748* gene. This suggests that *fjoh_1748* might represent an ortholog encoding the sulfonolipid-specific analog sulfobacin monooxygenase. The open reading frame upstream of the target gene *fjoh_1748* is encoding the 16S rRNA methyltransferase GidB, while the downstream gene encodes putative aspartate aminotranserase. The gene encoding the aspartate aminotransferase and *fjoh_1748* are oriented in the same transcriptional direction, suggesting a co-transcription of the aminotransferase as part of a single operon.

The plasmid *pYT313* encoded levansucrase *sacB* and conferred resistance to erythromycin and ampicillin. *Sal*I and *Sph*I were used to digest the suicide plasmid. The fragment used for the homologous recombination event was inserted using the NEBuilder® HiFi DNA Assembly Kit (*Figure 8*) This fragment contained approximately 2.400 bp of upstream and downstream regions of *fjoh_1748*. Within this sequence, the target gene *fjoh_1748* was fused to the reporter gene *mScarlet-I* via a G–S–A–G–G–G–G–S linker sequence and positioned between the flanking regions (*Figure 7*).

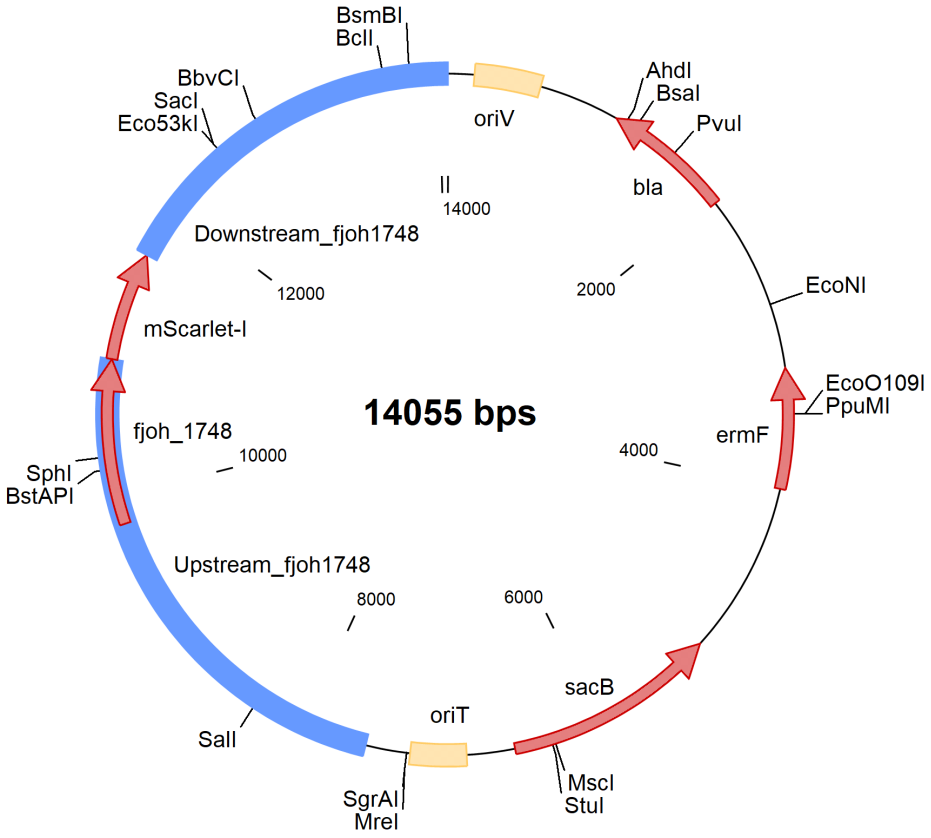

Figure 7: **Plasmid map of *pYT313_1748_mScarlet-I*** The 14.055 bp suicide vector was designed for the C-terminal mScarlet-I tagging of the target gene fjoh_1748 via homologous recombination. The plasmid contains upstream and downstream flanking regions (blue) of fjoh_1748. Selection markers include an erythromycin resistance gene (*ermF*) for selection in *F. johnsoniae* and a beta-lactamase gene (*bla*) for ampicillin selection in *E. coli*. The *sacB* gene is incorporated as a counter selection marker for sucrose sensitivity. The plasmid additionally features an oriV and oriT. This figure was created with Clone Manager 9.

Figure 8: **Primer binding sites of the allelic exchange cassette for the target gene *fjoh_1748:*** *In-frame* fusion between the C-terminus of the target gene *fjoh_1748* and the N-terminus of the *mScarlet-I* reporter. Specific attention was paid to the removal of the original stop codon of *fjoh_1748* and the insertion of a flexible linker to prevent steric hindrance and ensure independent folding of both the target protein and the fluorophore. The yellow highlights the binding positions of the primers. The consistent open reading frame across the junctions was verified *in silico* to ensure functional translation of the fusion protein. This figure was created with Clone Manager 9.

3.2.2 Suicide plasmid strategy for *in-frame* tagging of the cysteate acyl-ACP transferase

A study by Vences-Guzmán et al., 2021 revealed that *fjoh_2419* encodes a cysteate acyl-ACP transferase. The NCBI GenBank database provides a functional annotation for *fjoh_2419* as 8-amino-7-oxononanoate synthase.

The 1.260 bp long gene *fjoh_2419* is flanked by an upstream gene encoding a nitrite reductase and a downstream gene encoding a hypothetical lipoprotein. Notably, *fjoh_2419* and the downstream lipoprotein gene are oriented in the same transcriptional direction and may constitute to a single operon.

The plasmid *pYT313* encoded levansucrase *sacB* and the antibiotic resistance genes for erythromycin and ampicillin. *Sal*I and *Sph*I were used to digest the suicide plasmid. The fragment used for the homologous recombination event was inserted using the NEBuilder® HiFi DNA Assembly Kit (*Figure 10*).

This allelic exchange cassette fragment contained approximately 2.300 bp of upstream and downstream regions of *fjoh_2419*. The target gene *fjoh_2419* was fused to the reporter gene *mScarlet-I* via a G–S–A–G–G–G–G–S linker sequence and positioned between the flanking regions (*Figure 9*).

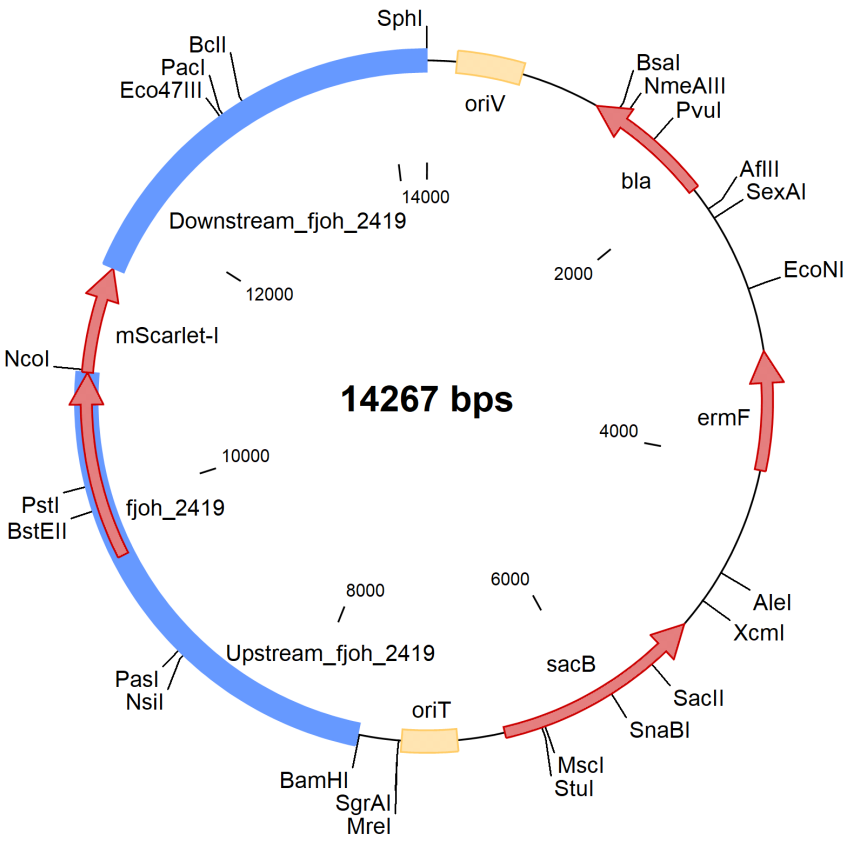

Figure 9: **Plasmid map of *pYT313_fjoh_2419::mScarlet-I*** The 14.267 bp suicide vector was designed for the C-terminal mScarlet-I tagging of the target gene fjoh_2419 via homologous recombination. The plasmid contains upstream and downstream flanking regions (blue) of fjoh_2419. Selection markers include an erythromycin resistance gene (*ermF*) for selection in *F. johnsoniae* and a beta-lactamase gene (*bla*) for ampicillin selection in *E. coli*. The *sacB* gene is incorporated as a counter selection marker for sucrose sensitivity. The plasmid additionally features an oriV and oriT. This figure was created with Clone Manager 9.

Figure 10: **Primer binding sites of the allelic exchange cassette for the target gene *fjoh_2419*:** *In-frame* fusion between the C-terminus of the target gene *fjoh_2419* and the N-terminus of the *mScarlet-I* reporter. Specific attention was paid to the removal of the original stop codon of *fjoh_2419* and the insertion of a flexible linker to prevent steric hindrance and ensure independent folding of both the target protein and the fluorophore. The yellow highlights the binding positions of the primers. The consistent open reading frame across all junctions was verified *in silico* to ensure functional translation of the fusion protein. This figure was created with Clone Manager 9.

3.2.3 Suicide plasmid strategy for *in-frame* tagging of the putative sulfobacin synthase

The NCBI GenBank database provides a functional annotation for the 1119 basepair long *fjoh_2421* as a hypothetical protein. Comparative genomic analyses revealed sequence similarities between the ceramide synthase involved in sphingolipid biosynthesis and the *fjoh_2421* gene, possibly being an ortholog encoding the sulfonolipid-specific analog sulfobacin synthase. The open reading frame upstream of the target gene is encoding a hypothetical lipoprotein, while the downstream gene encodes an additional hypothetical protein. The downstream gene is oriented in the same transcriptional direction, suggesting both genes being part of a single operon.

The plasmid *pYT313* encoded levansucrase *sacB* and conferred resistance to erythromycin and ampicillin. *Sal*I and *Sph*I were used to digest the suicide plasmid. The fragment used for the homologous recombination event was inserted using the NEBuilder® HiFi DNA Assembly Kit (*Figure 12*) This fragment contained approximately 2.000 bp of upstream and downstream regions of *fjoh_2421*. Within this sequence, the target gene was fused to the reporter gene *mScarlet-I* via a G–S–A–G–G–G–G–S linker sequence and positioned between both flanking regions (*Figure 11*).

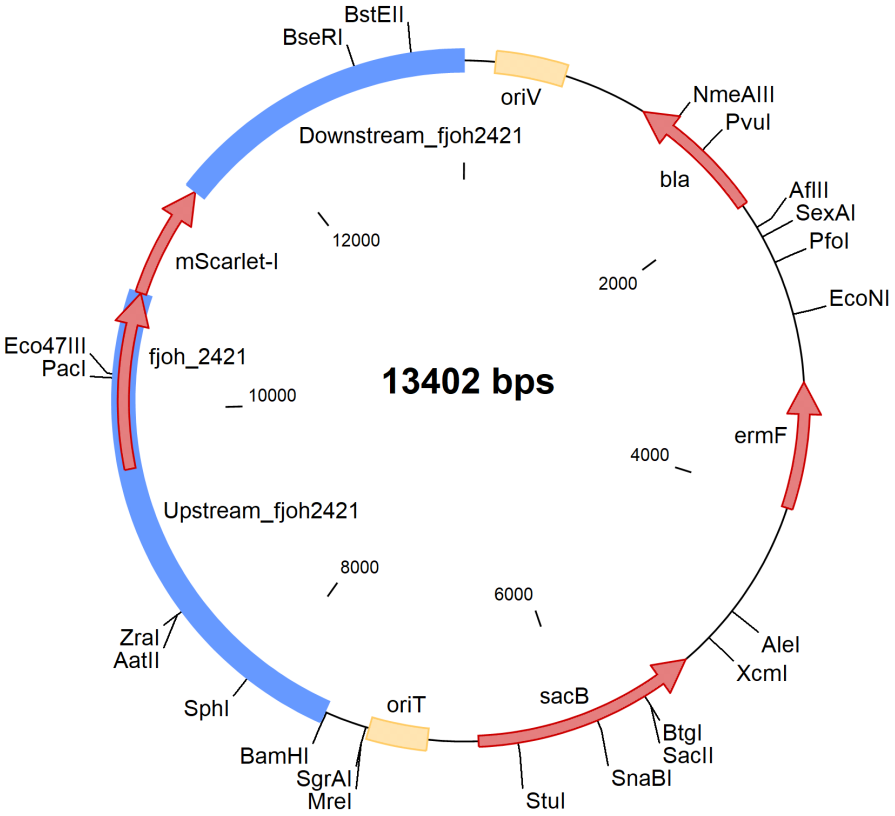

Figure 11: **Plasmide map of *pYT313_fjoh_2421::mScarlet-I*** The 13.402 bp suicide vector was designed for the C-terminal mScarlet-I tagging of the target gene fjoh_2421 via homologous recombination. The plasmid contains upstream and downstream flanking regions (blue) of fjoh_2421. Selection markers include an erythromycin resistance gene (*ermF*) for selection in *F. johnsoniae* and a beta-lactamase gene (*bla*) for ampicillin selection in *E. coli*. The *sacB* gene is incorporated as a counter selection marker for sucrose sensitivity. The plasmid additionally features an oriV and oriT. This figure was created with Clone Manager 9.

Figure 12: **Primer binding sites of the allelic exchange cassette for the target gene *fjoh_2421*:** *In-frame* fusion between the C-terminus of the target gene *fjoh_2421* and the N-terminus of the *mScarlet-I* reporter. Specific attention was paid to the removal of the original stop codon of *fjoh_2421* and the insertion of a flexible linker to prevent steric hindrance and ensure independent folding of both the target protein and the fluorophore. The yellow highlights the binding positions of the primers. The consistent open reading frame across all junctions was verified *in silico* to ensure functional translation of the fusion protein. This figure was created with Clone Manager 9.

3.2.4 Suicide plasmid strategy for *in-frame* tagging of the putative sulfobacin monooxygenase Fjoh_4604

The NCBI GenBank database provides a functional annotation for the 1161 nucleotide long *fjoh_4604* as fatty acid desaturase. Yet, prior comparative genomic analyses have revealed sequence similarities between the dihydroceramide monooxygenase gene involved in sphingolipid biosynthesis and the *fjoh_4604* gene. This suggests that *fjoh_4604* might represent an ortholog encoding the sulfonolipid-specific analog sulfobacin monooxygenase. The open reading frame upstream of the target gene is encoding hypothetical proteins of unknown function, while the downstream region encodes putative proteins involved in protein degradation.

The plasmid *pYT313* encoded levansucrase *sacB* and conferred resistance to erythromycin and ampicillin. *Sal*I and *Xba*I were utilized to digest the suicide plasmid, as the restriction site for *Sph*I was present in the to be inserted upstream fragment. The fragment used for homologous recombination event was inserted using the NEBuilder® HiFi DNA Assembly Kit (*Figure 14*) This fragment contained approximately 2,500 bp of upstream and downstream regions of *fjoh_4604*, flanking the target gene *fjoh_4604* that was linked to

the reporter gene *mScarlet-I* via a G–S–A–G–G–G–G–S linker sequence (*Figure 13*).

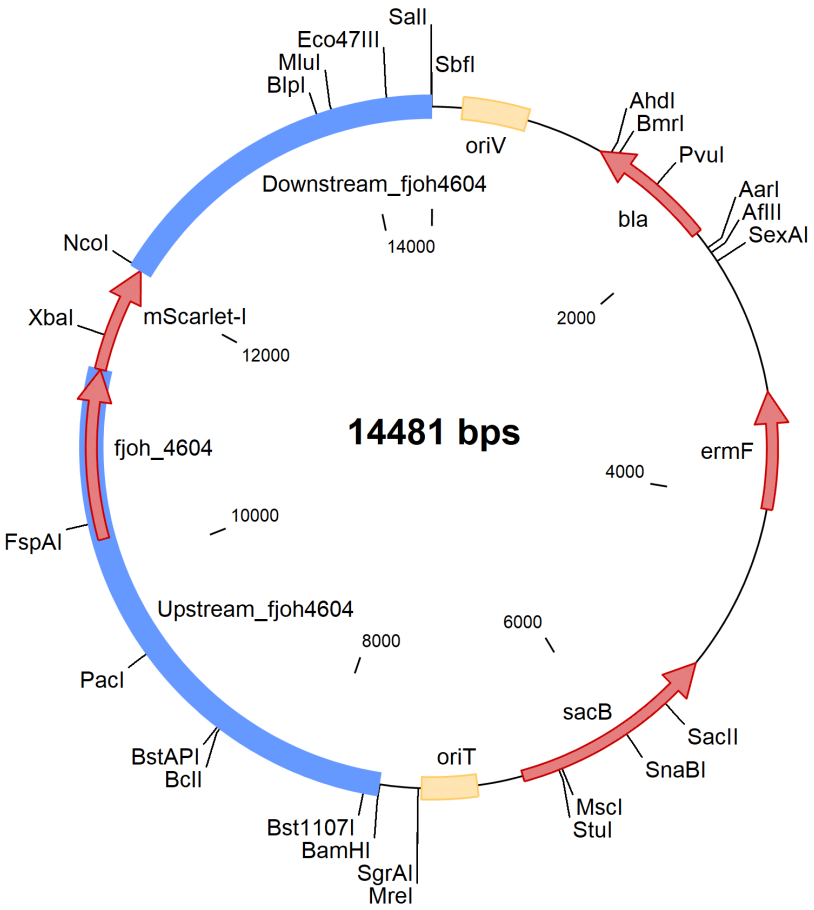

Figure 13: **Plasmid map of *pYT313_fjoh_4604::mScarlet-I*** The 14.481 bp suicide vector was designed for the C-terminal mScarlet-I tagging of the target gene fjoh_4604 via homologous recombination. The plasmid contains upstream and downstream flanking regions (blue) of fjoh_4604. Selection markers include an erythromycin resistance gene (*ermF*) for selection in *F. johnsoniae* and a beta-lactamase gene (*bla*) for ampicillin selection in *E. coli*. The *sacB* gene is incorporated as a counter selection marker for sucrose sensitivity. The plasmid additionally features an oriV and oriT. This figure was created with Clone Manager 9.

Figure 14: **Primer binding sites of the allelic exchange cassette for the target gene *fjoh_4604*:** *In-frame* fusion between the C-terminus of the target gene *fjoh_4604* and the N-terminus of the *mScarlet-I* reporter. Specific attention was paid to the removal of the original stop codon of fjoh_4604 and the insertion of a flexible linker to prevent steric hindrance and ensure independent folding of both the target protein and the fluorophore. The yellow highlights the binding positions of the primers. The consistent open reading frame across all junctions was verified *in silico* to ensure functional translation of the fusion protein. This figure was created with Clone Manager 9.

3.2.5 Design of the autonomously replicating plasmid for SulA::mScarlet-I expression

The plasmid *pCP11*, used for the introduction of the modified *fjoh_2419* gene into the knockout *F. johnsoniae* Δ *2419*, was digested using the restriction endonucleases *Sma*I and *Sal*I. Subsequently, the plasmid was left behind with a blunt end at the 3´ terminus and a sticky end at the 5´terminus. The inserted fragment was amplified using the assembled *pYT313* suicide plasmid for *fjoh_2419* as template DNA, making the structure equivalent as described above. The upstream fragment contained 142 bp and terminated one base before the start codon of *fjoh_2419*, whereas the downstream fragment encompassed 614 bp that initiated one base after the two encoded stop codons (**Figure 15**). The amplified fragment was then subjected to digestion with *Sal*I, a process that resulted in the formation of a blunt end at the 3´end and a sticky end at the 5´end. The digested fragment was then fused to the digested *pCP11* using the compatible sticky and blunt ends via T4 ligase (**Figure 16**).

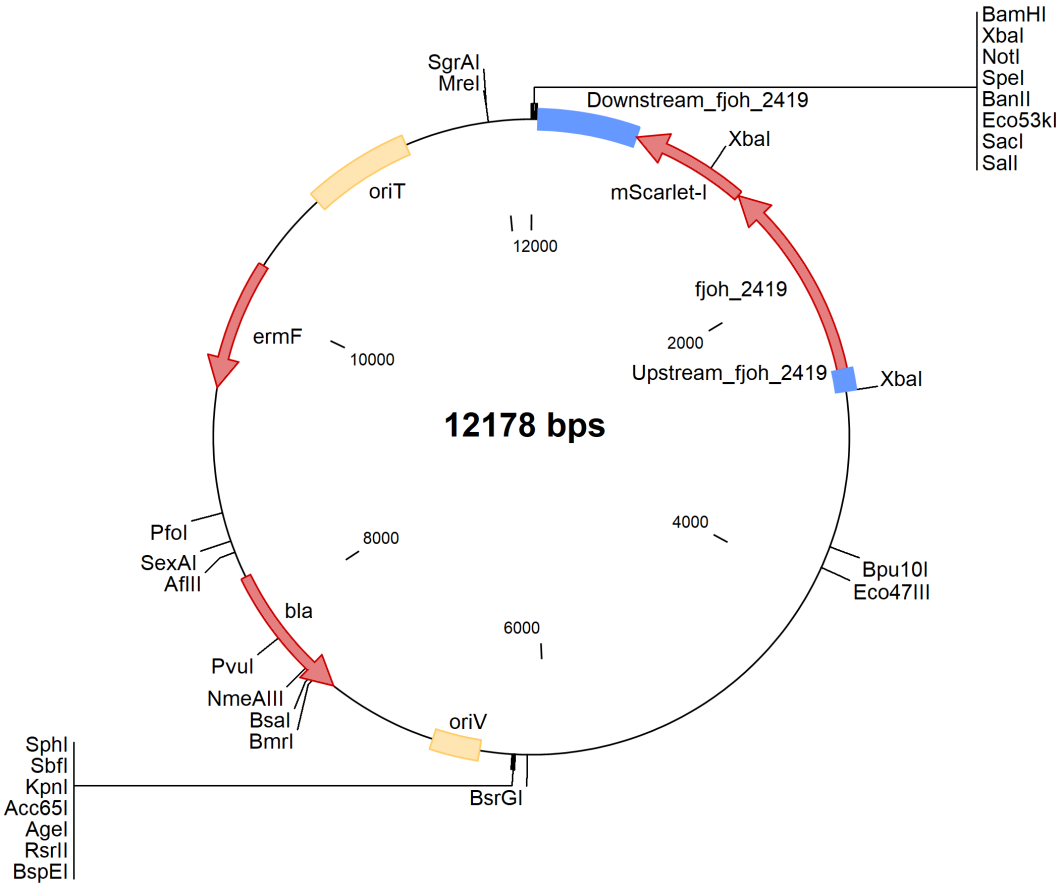

Figure 15: **Plasmid map of *pCP11_fjoh_2419::mScarlet-I*** This 12.178 bp replicating vector was constructed for the genetic complementation of the knockout strain *F. johnsoniae* Δ *2419*. The plasmid carries the target gene *fjoh_2419* and a C-terminal fusion with *mScarlet-I* to restore sulfonolipid biosynthesis and fluorescence-based localization. It contains an erythromycin resistance gene (*ermF*) for selection in *F. johnsoniae* and a beta-lactamase gene (*bla*) for ampicillin resistance in *E. coli*, as well as an OriV and OriT. Genetic engineering and visualization were performed using Clone Manager 9.

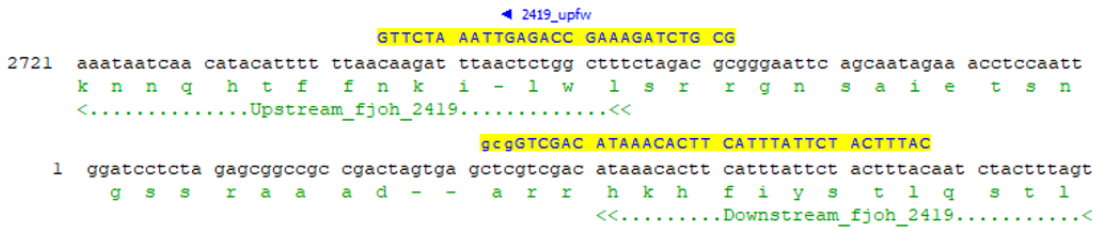

Figure 16: **Primer binding sites of the *pCP11_fjoh_2419::mScarlet-I* shuttle plasmid:** The alignment confirms the seamless transition between the upstream region of *fjoh_2419::mScarlet-I* and the downstream components within the vector. The highlighted yellow regions represent the binding sites for the used primers.

3.2.6 *In silico* design of a replicating *pCP11* vector for fluorescent signal protein expression

The replicating plasmid *pCP11* was used to poduce a fluorescent transmembrane reporter signal in *F. johnsoniae*. The plasmid encoded for erythromycin and beta lactamase resistance and contained the localization-determining sequence and the reporter gene *mScarlet-I* (*Figure 17*). *pCP11* was digested using the restriction endonucleases *Sal*I and *Spe*I. The localization-determining sequence region of the inserted fragment contained the promoter region and the corresponding signal peptide. This fragment was amplified *in-silico*, using the on *pCP11* already encoded *bla* gene as template DNA. The 5´end of the upstream fragment was fused to the 3´end of the reporter gene *mScarlet-I* through *in-silico* overlap extension PCR. The resulting DNA fragment was digested *in-silico* with *Sal*I and *Spe*I and ligated into the cut *pCP11* plasmid via the compatible ends (*Figure 18*).

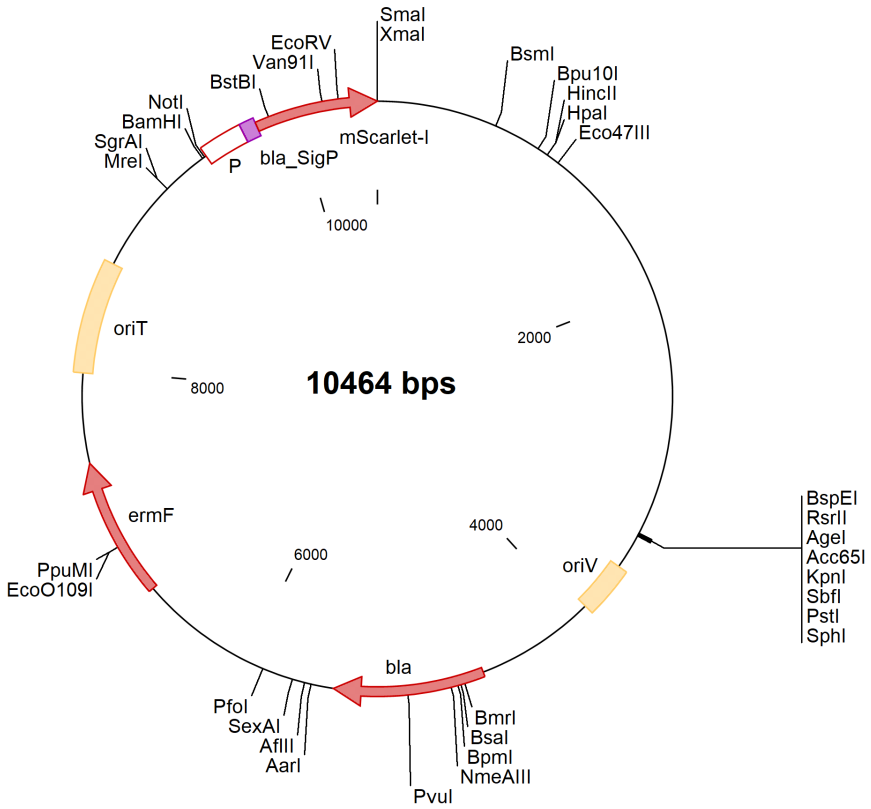

Figure 17: **Plasmid map of *pCP11_blaSigP-P_mScarlet-I*** This 10.464 bp replicating plasmid was designed as a localization control. It features the *bla* signal peptide (blaSigP) fused to mScarlet-I to direct the fluorescent protein to the periplasmic space or the outer membrane of the target organism. The plasmid includes an erythromycin resistance gene (*ermF*) for selection in *F. johnsoniae* and a second beta-lactamase gene (*bla*) for ampicillin resistance during cloning in *E. coli*, as well as on oriV and oriT. Genetic visualization was performed using Clone Manager 9

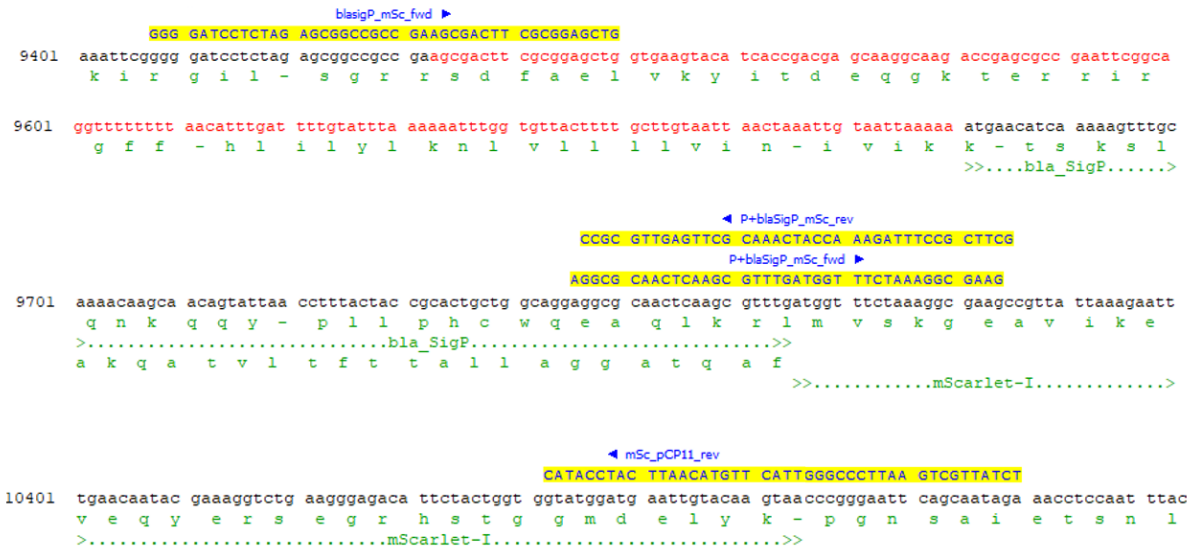

Figure 18: **Primer binding sites for the *pCP11_blaSigP-P_mScarlet-I* shuttle plasmid:** The sequence shows the fusion of the bla promoter and its corresponding N-terminal signal peptide (*blaSigP*) to the *mScarlet-I* gene. The signal sequence is highlighted in red and yellow highlights show the primer binding sites This figure was created with Clone Manager 9.

3.2.7 *In silico* design of a *pCP11*-based positive control for cytoplasmic *mScarlet-I* expression

The replicating plasmid *pCP11* was used to produce a fluorescent cytoplasmatic reporter signal in *F. johnsoniae in-silico*. The plasmid encoded for erythromycin and beta lactamase resistance and contained the localization-determining sequence and the reporter gene *mScarlet-I* (*Figure 19*).

pCP11 was digested using the restriction endonucleases *Sal*I and *Spe*I. The localization-determining sequence region of the inserted fragment contained the *ermF* promoter region. This fragment was amplified *in-silico*, using the on *pCP11* already encoded *ermF* gene as template DNA.

The 5´end of the upstream fragment was fused to the 3´end of the reporter gene *mScarlet-I* through *in-silico* overlap extension PCR. The resulting DNA fragment was digested *in-silico* with *Sal*I and *Spe*I and ligated into the cut *pCP11* plasmid via the compatible ends (*Figure 20*).

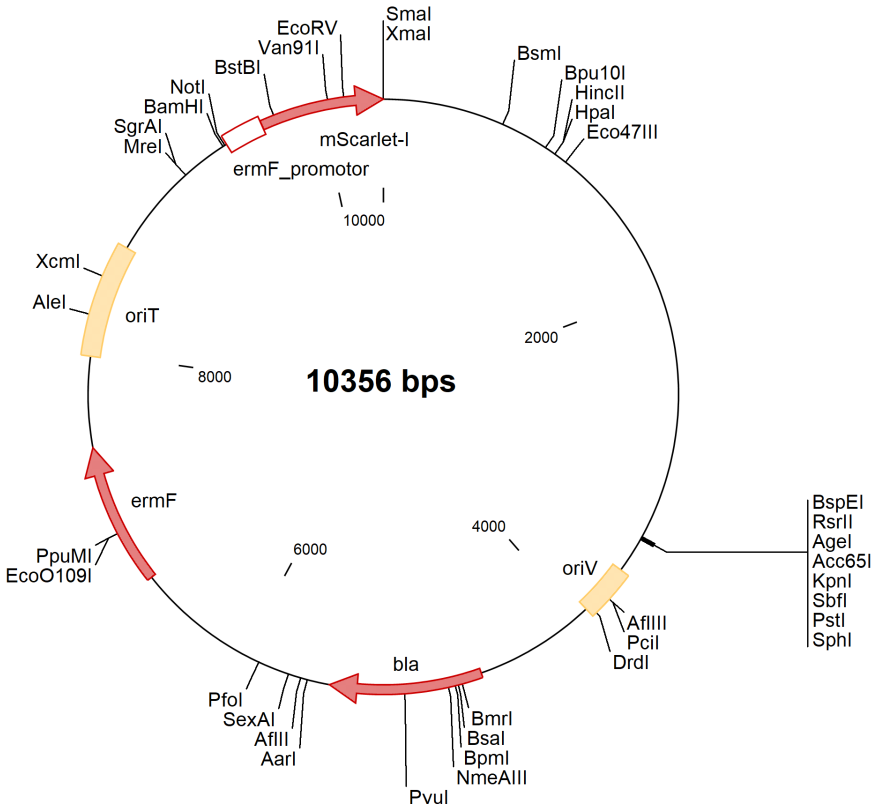

Figure 19: **Plasmid map of *pCP11_ermF-P_mScarlet-I*** This 10.356 bp replicating vector serves as a cytoplasmic localization control. In this construct, *mScarlet-I* is expressed under the control of the *ermF* promoter. The vector contains an erythromycin resistance gene (*ermF*) for selection in *F. johnsoniae* and a beta-lactamase gene (*bla*) for ampicillin resistance in *E. coli*, as well as an oriV and an oriT. Visualization was performed using Clone Manager 9

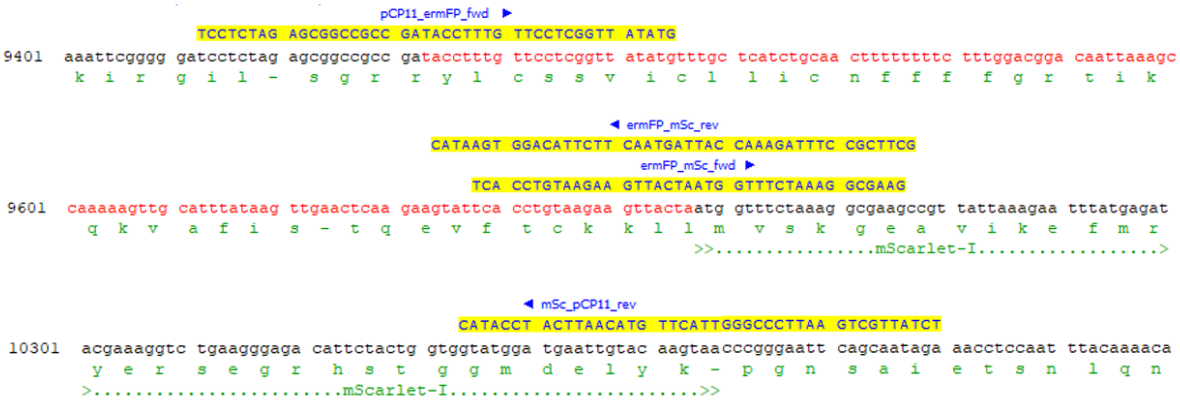

Figure 20: **Primer binding sites for the *pCP11_ermF-P_mScarlet-I shuttle plasmid:*** The sequence shows the fusion of the *ermF* promoter region to the *mScarlet-I* gene. The promoter region is coloured in red and yellow highlights show the primer binding sites. This figure was created with Clone Manager 9.

3.3 *In-frame* insertion of *mScarlet-I*

3.3.1 Generation and molecular cloning of *mScarlet-I* fusion constructs

PCR amplification of DNA fragments used for *in-frame* insertion

For the *in-frame* insertion of *mScarlet-I* onto the target genes *fjoh_1748, fjoh_2419, fjoh_2421* and *fjoh_4604*, suicide plasmids with the *pYT313* backbone were constructed.

The upstream, reporter gene and downstream fragments for each target gene were amplified, in accordance with the *in-silico* cloning strategy (*section 3.2*). Genomic DNA of *F. johnsoniae* and plasmid DNA of prSETb *mScarlet-I*, utilized as DNA template during PCR, were isolated. Estimated primer annealing temperatures were tested out alongside two additional ones to cover broader temperature range using 25 µl PCR reaction volumes. The primers for the construction of the allelic exchange cassettes are named according to their respective gene and fragment orientation (*Table 6*). Upstream fragments were amplified using specific primer pairs labeled with the respective gene name followed by _up_fwd and _up_rev, and the genomic DNA of the wildtype *F. johnsoniae*. Amplification of the reporter gene fragments (*mScarlet-I*) was achieved through the utilisation of the primer pairs labeled with the respective gene name followed by _mSc_fwd and _mSc_rev, and the plasmid DNA of prSETb *mScarlet-I* as DNA template. The downstream fragments were amplified using the specific primer pairs labeled with the gene name followed by _down_fwd and _down_rev, and the genomic wildtype DNA of *F. johnsoniae*. Examination of amplified fragments was done through TAE agarose gel electrophoresis using 1% LE-agarose. Each amplified upstream fragment had a size of about 3000 bp. This corresponded to the expected sizes of 3333 bp for the *fjoh_1748* upstream fragment, 3291 bp for the *fjoh_2419* upstream fragment, 3139 bp for the *fjoh_2421* upstream fragment and 3791 bp for the *fjoh_4604* upstream fragment. The amplified reporter gene fragments were 725 bp long. Due to a shift on the gel mediated by GelRed®, the amplified *mScarlet-I* fragment for *fjoh_4604* appears smaller. Amplified downstream fragments ranged between 2000 to 2500 basepairs in size, which corresponded to the predicted sizes of 2425 bp for the *fjoh_1748* downstream fragment, 2655 bp for the *fjoh_2419* downstream fragment, 1937 bp for the *fjoh_2421* downstream fragment and 2359 bp for the *fjoh_4604* downstream fragment (*Figure 21*). PCR reactions with the correct amplified fragments were purified using the innuPREP PCRpure Kit and concentrations were measured using NanoDrop.

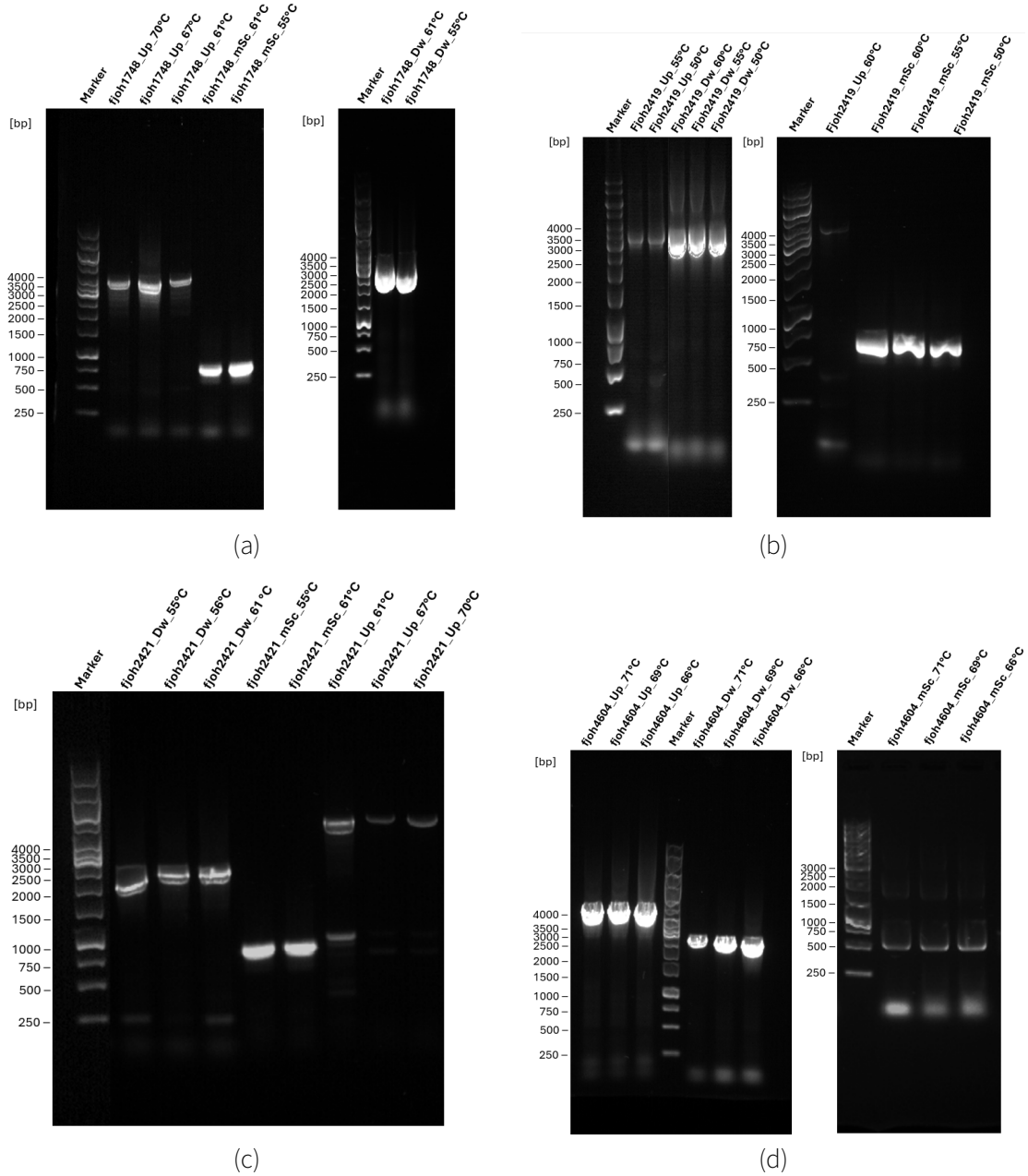

Figure 21: **Allelic exchange cassette fragments after gel electrophoresis:** Upstream, downstream and reporter gene fragments for the target genes **(a)** *fjoh_1748*, **(b)** *fjoh_2419*, **(c)** *fjoh_2421*, **(d)** *fjoh_4604* obtained via PCR.

HiFi DNA Assembly and restriction analysis of suicide plasmid constructs

For insertion of the allelic exchange cassette into the suicide plasmid *pYT313*, the empty plasmid was first isolated from *E.coli* using the Monarch® Spin Plasmid Miniprep Kit. The resulting plasmid was digested in a 20 µl reaction volume using assembly-specific restriction endonucleases. For the target genes *fjoh_1748, fjoh_2419* and *fjoh_2421*, 0,5 µl of both *Sal*I and *Sph*I were used. For the target gene *fjoh_4604*, the restriction enzymes *Sal*I and *Xba*I were used. Both reaction mixtures were incubated for one hour at 37°C and inactivated at 65°C for 20 minutes.

Depending on the concentration of clean amplified PCR fragments, different volumes were added to the NEBuilder® HiFi DNA Assembly reaction mixture while still maintaining equimolarity. The digested plasmid and fragments were assembled in a 2:1 molar ratio using the NEBuilder® HiFi DNA Assembly Kit. Each allelic exchange cassette for the *pYT313_fjoh_1748::mScarlet-I*, *pYT313_fjoh_2419::mScarlet-I*, *pYT313_fjoh_2421::mScarlet-I* and *fjoh_4604* plasmid was assembled individually by mixing 0,01 pmol of the corresponding upstream, *mScarlet-I*, and downstream fragment in a total reaction volume of 10 µl. After a 2 hour incubation at 50°C, a 5 µl aliquot of each reaction mixture was removed and analyzed using gel electrophoresis, verifying successful fusion of the three mixed fragments. The remaining mixture was substituted with 0,02 pmol of the corresponding digested plasmid *pYT313*. The reaction mixtures were additionally substituted with NEBuilder HiFi DNA Assembly Master Mix and nuclease-free water up to the previous volume of 10 µl and incubated at 50°C for four hours.

For each reaction mixture, vector re-ligation was quantified using a control assembly reaction, where water replaced the insert DNA.

Each of the NEBuilder® HiFi DNA Assembly reaction mixtures was introduced into competent *E.coli* 10*β* and plated onto ampicillin enriched LB plates. The plates were incubated overnight at 37 °C, after which selected CFUs were inoculated into ampicillin supplemented LB broth. After another overnight incubation at 37°C while shaking at 180 rpm, the plasmid DNA was isolated following the Monarch® Spin Plasmid Miniprep Kit´s instructions. Plasmids were resuspended in 50 µl of nuclease-free water and prior to storage at -20 °C, a 2 µl aliquot was removed. Correct assembly of the plasmid was verified via restriction digestion with *EcoR*V and *EcoR*I, which yielded distinct banding patterns upon gel electrophoresis. The digestion reaction mixtures, containing the 2 µl plasmid aliquots, were subjected to incubation at 37°C for a duration of one hour.

Examination of amplified fragments was done via agarose gel electrophoresis using 0,5% LE-agarose. While the *pYT313* suicide plasmids designed for the target gene *fjoh_1748, fjoh_2419* and *fjoh_2421* were digested with *EcoR*V, the plasmid for *fjoh_4604* was additionally digested with *EcoR*I (*Table 24*).

The fused *pYT313_fjoh_1748::mScarlet-I* contains three *EcoR*V restriction sites at positions 11506 bp, 12009 bp and 12010 bp. Digestion of the plasmid resulted in two fragments measuring about 500 and 13,000 bp. This corresponded with the expected fragment sizes of 503 and 13645 bp.

The fused *pYT313_fjoh_2419::mScarlet-I* contains four *EcoR*V restriction sites at positions 9265 bp, 10027 bp, 10794 bp and 11392 bp. Digestion resulted in the anticipated fragment sizes of 597 bp, 761 bp, 768 bp and 12141 bp. As two fragments were of a similar size, only three bands at 600 bp, 750 bp, and 12,000 bp were visible on the gel.

The *pYT313_fjoh_2421::mScarlet-I* contains three *EcoR*V restriction sites at positions 11245 bp, 12270 bp, and 13038 bp. Digestion yielded the expected fragments in the sizes 768 bp, 1025 bp and 11609 bp (*Figure 22*).

Digestion of *pYT313_fjoh_4604::mScarlet-I* with *EcoR*I and *EcoR*V resulted in eight different fragments. Fragment sizes were 224 bp, 404 bp, 796 bp, 217 bp, 1612 bp, 2179 bp, 2680 bp and 5369 bp and showed up on the gel correspondingly. Due to reduced electrophoretic mobility caused by the use of GelRed®, larger DNA fragments migrated more slowly and therefore deviated from the correct sizes (*Figure 23*).
Plasmids displaying the correct fragment pattern were further verified via Sanger sequencing using the *M13r* primer, which covers part of the plasmid and the downstream fragment.

Table 24: Fragment sizes after restriction digest

Plasmid	Restriction enzyme	Fragment sizes (bp)							
pYT313_fjoh_1748::mScarlet-I	*EcoR*V	503	13645						
pYT313_fjoh_2419::mScarlet-I	*EcoR*V	597	761	768	12141				
pYT313_fjoh_2421::mScarlet-I	*EcoR*V	768	1025	11609					
pYT313_fjoh_4604::mScarlet-I	*EcoR*I & *EcoR*V	224	404	796	1217	1612	2179	2680	5369

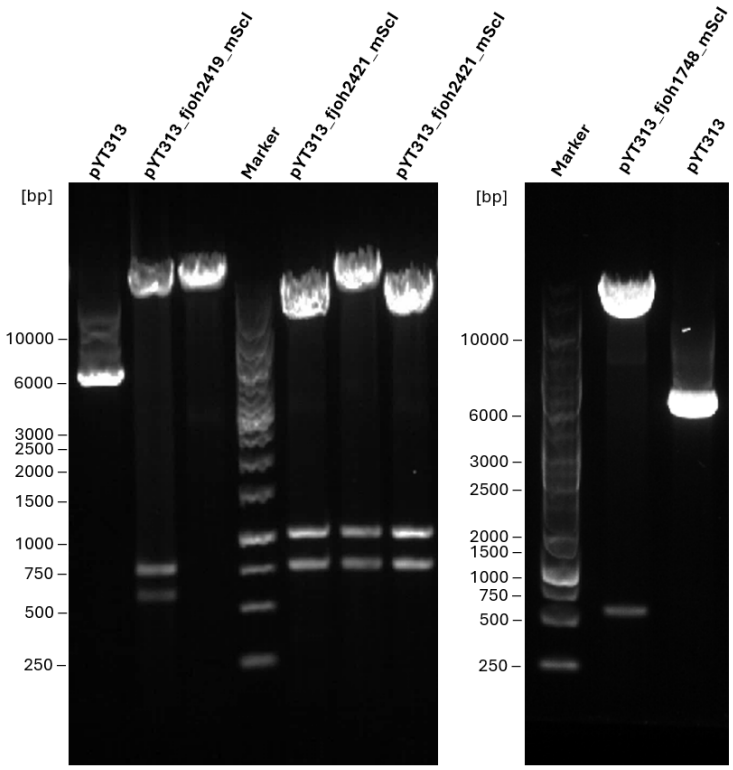

Figure 22: **Gel electrophoresis of the assembled suicide plasmids** for the target genes *fjoh_1748, fjoh_2419* and *fjoh_2421* after digestion with *EcoR*V

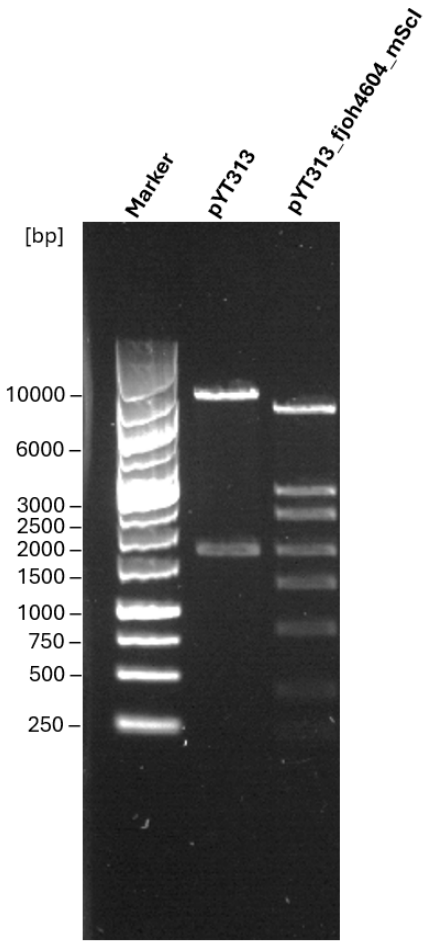

Figure 23: **Gel electrophoresis of the assembled suicide plasmid** for the target gene *fjoh_4604* after digestion with *EcoR*I and *EcoR*V

3.3.2 Generation of the replicating *pCP11* plasmid for *fjoh_2419::mScarlet-I* complementation

PCR amplification of the DNA fragment

For the complementation of the *F. johnsoniae* Δ*2419* strain with SulA::mScarlet fusion protein, a fragment containing the genetic fusion of *fjoh_2419::mScarlet-I* was amplified using *pYT313_fjoh_2419::mScarlet-I* as template. Experimental validation was performed in 25 µl PCR reaction volumes using the primer pair fjoh2419_pCP11_up_fwd and fjoh2419_pCP11_down_rev.

Estimated primer annealing temperature was tested alongside two additional ones to cover broader temperature range (*Figure 24*). Examination of amplified fragments was performed via agarose gel electrophoresis using 0,5% LE-agarose. All tested annealing temperatures led to an amplification of a 3000 bp fragment, which corresponded to the expected size of 2741 bp of the *fjoh_2419::mScarlet-I* fragment.

The fragment generated by PCR (T_a = 55°C) was purified using the innuPREP PCRpure Kit and the concentration was measured using NanoDrop.

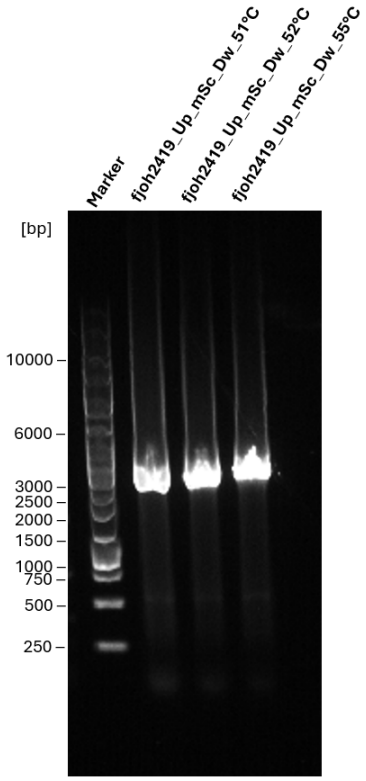

Figure 24: **PCR amplification** of the *fjoh_2419_Up::mScarlet-I_Down* fragment for insertion into *pCP11* using different annealing temperatures (51°C, 52°C and 55°C)

Ligation assembly and molecular validation of the expression vector

For insertion of the expression cassette into *pCP11*, the empty shuttle plasmid was first isolated using the Monarch® Spin Plasmid Miniprep Kit. The isolate was digested with *Sma*I in a 20 µl digestion reaction volume (*subsection 2.2.5*). Following an initial incubation period of one hour at 37°C, 1 µl of *Sal*I was added, as *in-silico* cloning revealed restriction enzyme site interference, hindering digestion with both enzymes in one reaction process. After an additional incubation period of one hour, the reaction was inactivated at 65°C for 20 minutes.

The digested *pCP11* backbone and *fjoh_2419_Up::mScarlet-I_Down* fragment were fused into the functional shuttle vector using T4 ligase. For this purpose, the digested plasmid and DNA fragment were mixed at a 1:3 molar ratio as suggested by the ligase manufacturer. A total of 4 µl (0,06 pmol) of the digested PCR fragment and 0,34 µl (0,02 pmol) of the digested *pCP11* were combined in a 20 µl ligation reaction (*subsection 2.2.6*). The mixture was incubated for 48 h at 4°C, followed by a 2 h incubation at room temperature. Subsequently, the ligation mixture was introduced into competent *E.coli* 10β cells via transformation. Plated cells were incubated overnight on ampicillin enriched LB plates at 37°C before selected CFUs were inoculated into ampicillin supplemented LB broth. Cultures were grown overnight at 37°C while shaking at 180 rpm, before isolating the plasmid-DNA using the Monarch® Spin Plasmid Miniprep Kit.

The plasmids were resuspended in 50 µl of nuclease-free water. Prior to storage at -20°C, a 2 µl sample was removed for control purposes.

The correct assembly of the plasmid was verified via restriction digestion with *EcoR*I, which produced distinct banding patterns in a gel electrophoresis analysis (**??**). Digestion of the *pCP11_fjoh_2419::mScarlet-I* shuttle vector resulted in five fragments lying at 250 bp, 1000 bp, 1700 bp, 3000 bp and 6000 bp. This corresponded with the expected sizes of 172, 1331, 2063, 3407 and 5205 bp. Plasmids with correct fragment pattern were further verified via Sanger sequencing using the fjoh2419_pCP11_down_rev primer.

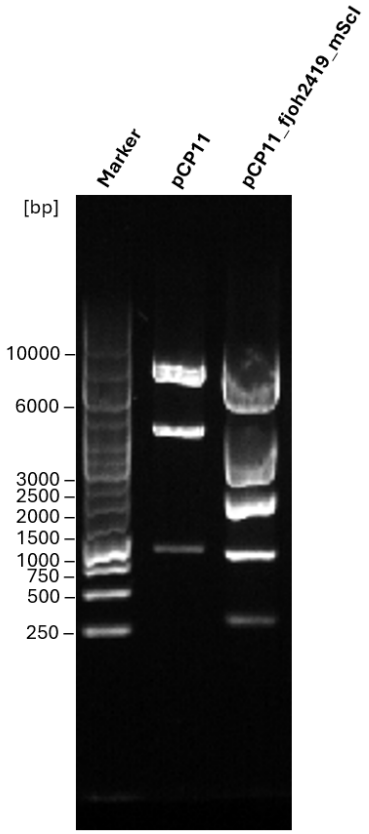

Figure 25: **Gel electrophoresis** of the assembled shuttle vector *pCP11_fjoh_2419::mScarlet-I* after digestion with *EcoR*I

3.3.3 Generation of *mScarlet-I* fusion mutants via allelic exchange

In-frame insertion requires two homologous recombination events. In the first crossover event, the suicide plasmid is integrated via the upstream or downstream homologous region of the targeted wildtype gene, thereby mediating the integration of the entire plasmid into the genome. The outcome of the second recombination event is determined by the alignment of the integrated plasmid segment relative to the homologous wildtype region, resulting in either the restoration of the original sequence or the stable *in-frame* insertion. Positive and counter selection markers are used during these two events to obtain successive recombinants (*subsection 2.3.5*).

The assembled plasmids *pYT313_fjoh_1748::mScarlet-I*, *pYT313_fjoh_2419::mScarlet-I*, *pYT313_fjoh_2421::mScarlet-I* and *pYT313_fjoh_4604::mScarlet-I* were introduced into competent *E.coli* S17-1 λ pir cells via transformation as described in *subsection 2.3.3*.

Conjugation between *E. coli* S17-1 λ pir and *F. johnsoniae* was performed, followed by selective recovery of *F. johnsoniae* transconjugants (*subsection 2.3.4*). Colonies that were resistant to erythromycin were obtained and subsequently screened using PCR, confirming the presence of the *sacB* gene. Additional visual confirmation of the *sacB* activity of colonies growing on saccharose-enriched CYE plates was not observed. For each transconjugant, the *sacB* gene fragment was amplified using the primer pair sacB_fwd and sacB_rev (T_a = 40°C) and their isolated genomic DNA. For the *sacB* positive control, plasmid *pYT313* was used as the DNA template.

PCR products were visualized using 1% LE-agarose gel electrophoresis (*Figure 26*). The *sacB* presence was confirmed for all four colonies. All amplified fragments migrated between 500 and 750 bp, which matched the expected fragment size of 640 bp. This PCR analysis confirmed the first homologous recombination event, corresponding to the integration of the plasmid into the genome.

The positive transconjugant CFUs were streaked onto erythromycin enriched CYE plates (1:1000, v/v) and stored at 4°C for up to three weeks. Additionally, cryo-cultures were prepared and stored at -75°C.

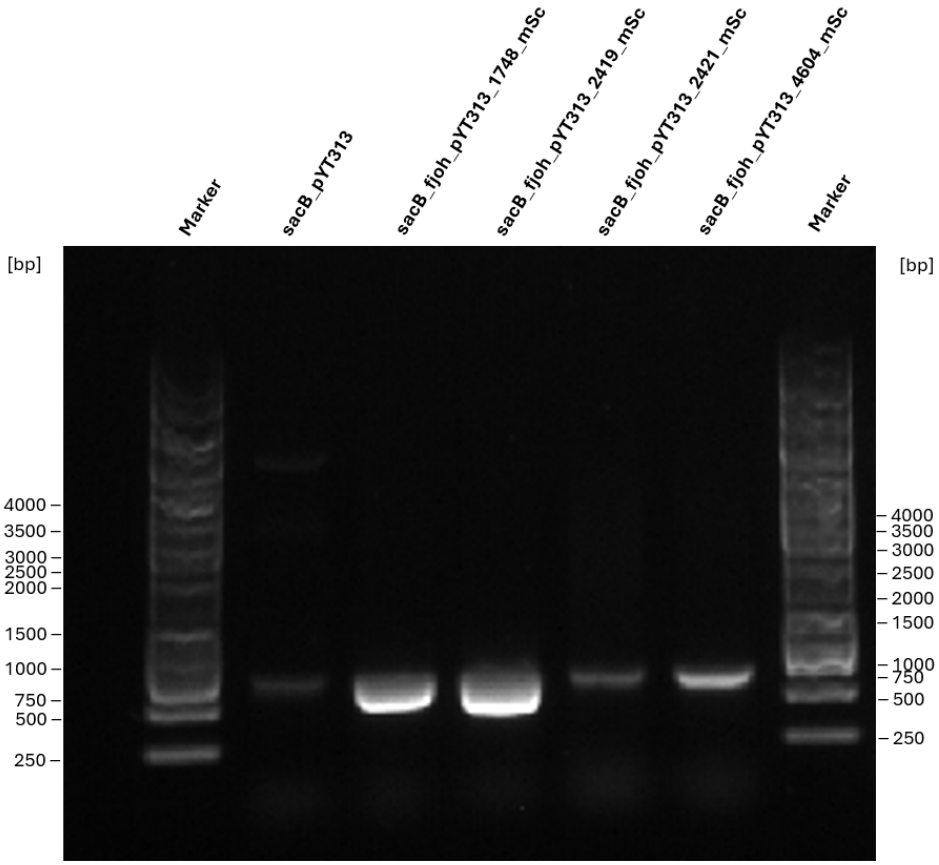

Figure 26: **Amplified *sacB* gene fragments** from isolated *F. johnsoniae* transconjugants for all four targeted genes (*fjoh_1748, fjoh_2419, fjoh_2421, fjoh_4604*) after the first homologous recombination event.

The second recombination event was induced by removing selection pressure, as described in *subsection 2.3.5*. Certain CFU were obtained and subsequently screened via PCR, confirming the *sacB* gene absence but presence of the *mScarlet-I* gene. The *sacB* gene fragment was amplified using the primer pair sacB_fwd and sacB_rev (T_a = 40°C) and isolated genomic DNA The *mScarlet-I* fragment was obtained using the primer pair fjoh2421_mSc_fwd and fjoh2421_mSc_rev (T_a = 55°C). As *mScarlet-I* positive control, the plasmid *prSETb mScarlet-I* was used as the DNA template.

PCR products from *F. johnsoniae* isolates after the second homologous recombination event were visualized using gel electrophoresis with 1% LE-agarose.

PCR amplification showed *sacB* gene absence and *mScarlet-I* presence for the target gene *fjoh_4604*, possibly encoding the enzyme sulfobacin monooxygenase (*Figure 27*). The amplified *mScarlet-I* fragment migrated between 750 and 1000 bp, which corresponded to the expected size of 725 bp. The positive in-frame insertion CFU was streaked onto a CYE plate and stored at 4°C for up to three weeks. Additionally, a cryo-culture was made and stored at -75°C. *F. johnsoniae fjoh_4604::mScarlet-I* was then examined using CLSM.

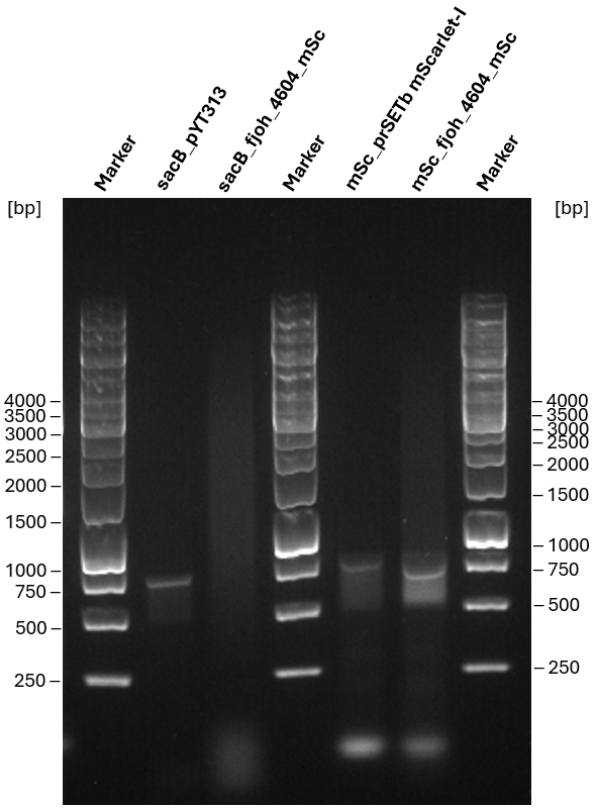

Figure 27: **Amplified *sacB* and *mScarlet-I* gene fragments** from isolated *F. johnsoniae fjoh_4604::mScarlet* CFU after the second homologous recombination event. *SacB* absence and *mScarlet-I* presence confirmed *in-frame* insertion of *mScarlet-I* to the *fjoh_4604*.

PCR analysis of the screening products for the intended *in-frame* insertions of *fjoh_1748, fjoh_2419* and *fjoh_2421* showed no positive reporter gene insertions, showing a reversion to the wildtype genotype. As

shown in Figure 28, amplification of the *mScarlet-I* reporter gene yielded no detectable product, whereas the positive control showed the expected amplification of 725 bp. Induction of the second homologous recombination event was repeated several times before *in-frame* insertions for the target genes *fjoh_1748, fjoh_2419* and *fjoh_2421* was abandoned.

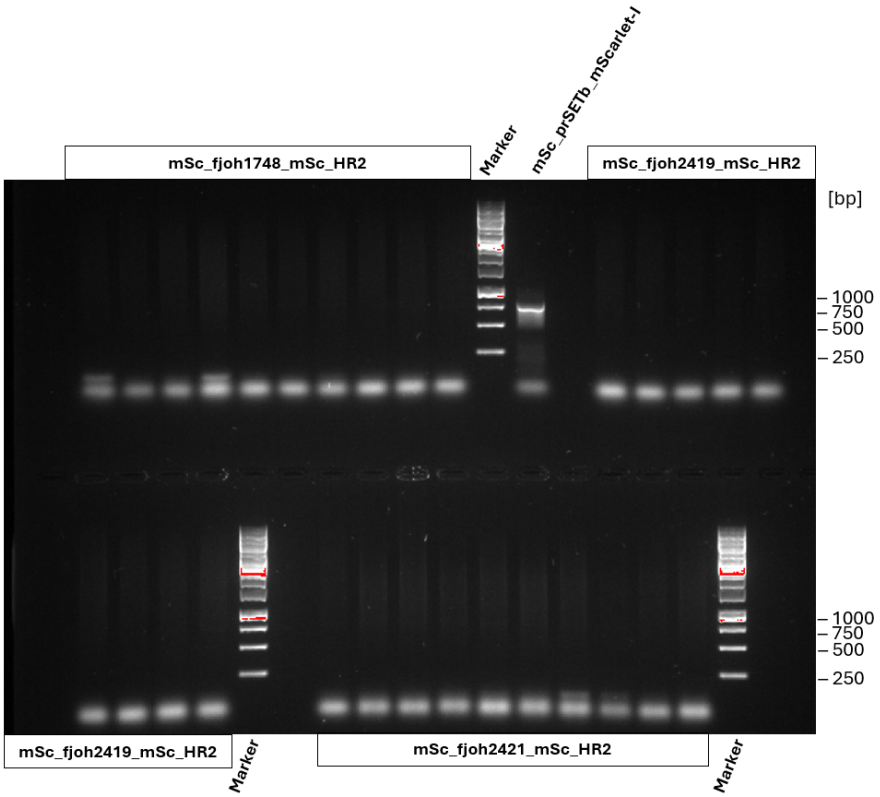

Figure 28: **Amplified *mScarlet-I* gene fragments** from isolated *F. johnsoniae* after the second homologous recombination event for the *in-frame* insertions of *mScarlet-I* onto the target genes *fjoh_1748, fjoh_2419* and *fjoh_2421*.

3.3.4 Conjugal transfer of the shuttle vector into *F. johnsoniae* Δ*2419*

The *pCP11_fjoh_2419::mScarlet-I* vector is introduced into *F. johnsoniae* Δ*2419* using conjugation. Due to the properties of the assembled shuttle vector, the transconjugant retains the plasmid as an independent element in the cell, rather than integrating it into the genomic DNA. The *F. johnsoniae* Δ*2419* mutant strain lacks the gene *fjoh_2419*, which provides the possibility for *in trans* complementation of the *fjoh_2419::mScarlet-I* protein. This should enable the production of the fusion protein at physiologically relevant levels of expression. Positive selection markers are used during the conjugation process to obtain positive transconjugants (*subsection 2.3.4*).

The assembled plasmid *pCP11_fjoh_2419::mScarlet-I* was introduced into competent *E.coli* S17-1 λ pir cells via transformation, as described in *subsection 2.3.3*.

Subsequently, conjugation between the donor *E. coli* S17-1 λ pir and recipient *F. johnsoniae* Δ*2419* was performed as described in *subsection 2.3.4*. Following selective recovery, erythromycin resistant transcon-

jugants were screened via PCR, confirming the presence of the *mScarlet-I* gene using the primer pair fjoh2421_mSc_fwd and fjoh2421_mSc_rev (T_a = 55°C)(*subsection 2.3.4*). Possible transconjugants were grown overnight in erythromycin enriched CYE broth (1:1000, v/v) before isolating the plasmids with the Monarch® Spin Plasmid Miniprep Kit. Subsequently, 5 ml of each isolated plasmid was digested using the restriction enzyme *EcoR*I. Additionally, the empty plasmid *pCP11* was digested as negative control.
Digested products were visualized using 1% LE-agarose gel electrophoresis *Figure 29*. This resulted in four fragments lying at 2500 bp, 4000 bp, 6000 bp and 9000 bp, which did not correspond with the expected sizes of 172, 1331, 2063, 3407 and 5205 bp. However, since it differs greatly from the digested empty *pCP11* plasmid, it was assumed that the isolated *pCP11_fjoh_2419::mScarlet-I* plasmid had migrated differently due to the GelRed® used during gel electrophoresis. Additional confirmation was done via CLSM microscopy. The transconjugant strain *F. johnsoniae* Δ*2419, pCP11_fjoh_2419::mScarlet-I* was streaked onto an erythromycin enriched CYE plate (1:1000, v/v) and stored at 4°C for up to three weeks. Additionally, a cryo-culture was made and stored at -75°C. Additionally, lipid profiles were investigated using LC-MS/MS (*subsection 3.5.1*).

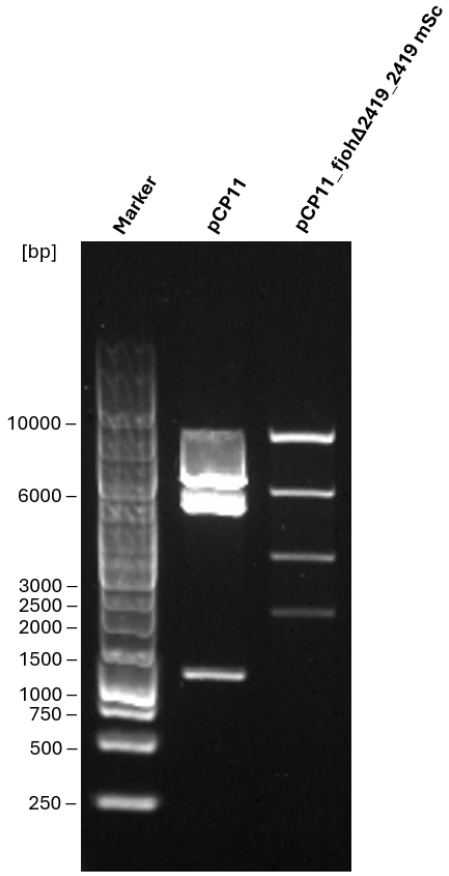

Figure 29: **Digested *pCP11_fjoh_2419::mScarlet-I* DNA**, isolated from transconjugant *F. johnsoniae* Δ*2419, pCP11_fjoh_2419::mScarlet-I*. The empty *pCP11* was digested with *EcoR*I as negative control.

3.4 Microscopic analysis

3.4.1 Localisation of the tagged cysteate acyl-ACP transferase in *F. johnsoniae* Δ*2419, pCP11_fjoh_2419::mScarlet-I*

To ensure precise sampling for microscopy imaging, a preliminary growth experiment was conducted with *F. johnsoniae* Δ*2419, pCP11_fjoh_2419::mScarlet-I*. This allowed for the determination of different growth phases, enabling the harvest of cells accordingly. Following harvest, cells were processed for microscopy as described in *subsection 2.3.7*.

The growth experiment was conducted over a 49 hour period. *F. johnsoniae* Δ*2419, pCP11_fjoh_2419::mScarlet-I* showed a lag phase of 2 hours, followed by exponential growth between 2 and 10 hours. After 10 hours, the culture transitioned into the stationary phase. The culture exhibited a doubling time of 1.86 hours and the specific growth rate μ was determined to be 0.37 h^{-1} (*Figure 30*).

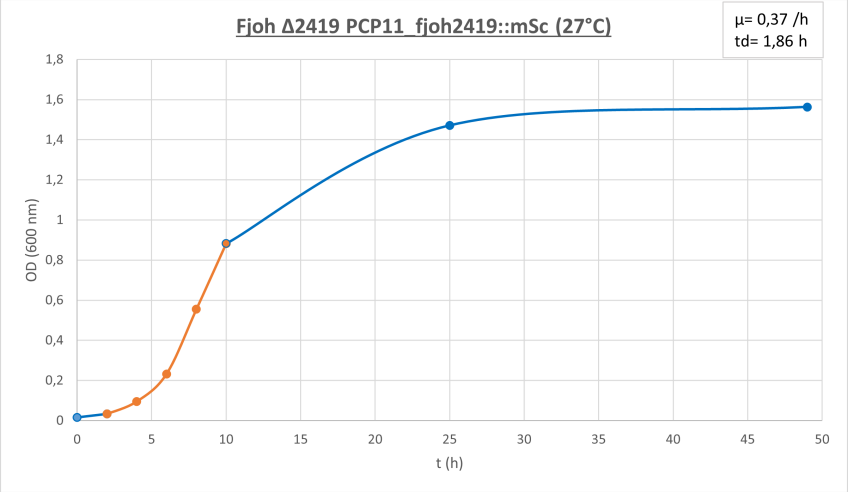

Figure 30: **Growth curve of *F. johnsoniae* Δ*2419, pCP11_fjoh_2419::mScarlet-I*** over a 49 hour period. The culture exhibits a short lag phase until t = 2h, followed by an exponential growth phase between t = 2h and t = 10h (orange). Data points represent measurements from a single experimental run.

First images were acquired using the Confocal Laser Scanning Microscope SP8. As described in *subsection 2.3.7*, the culture was grown for a period of 49 hours in CYE medium supplemented with erythromycin (1:1000, v/v) at a temperature of 27°C whilst shaking at 180 rpm. Cells were harvested and processed for imaging via CLSM, which included DAPI staining (1 mg/ml). As shown in Figure 31, the rod shaped cells stained with DAPI exhibited not only a DAPI signal but also a signal corresponding to *mScarlet-I*, indicating that the protein production of the cysteate acyl-ACP transferase::mScarlet-I fusion protein was restored.

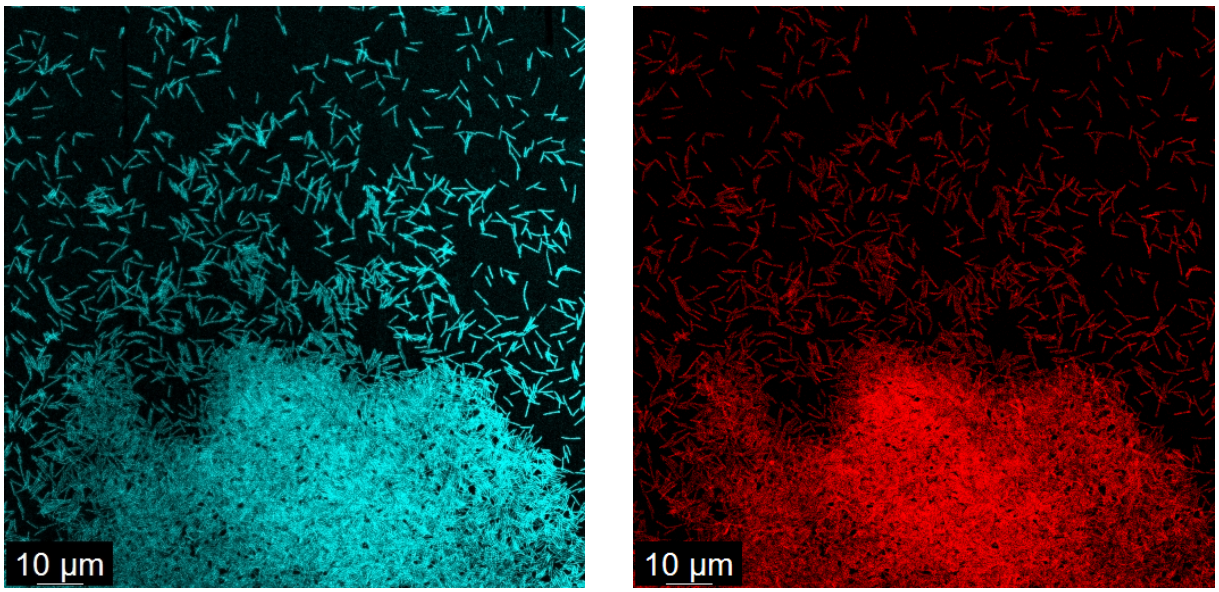

(a) DAPI staining (λ_{ex} = 354 nm, λ_{em} = 456 nm) (b) *mScarlet-I* fluorescence (λ_{ex} = 569 nm, λ_{em} = 594 nm)

Figure 31: **CLSM SP8-imaging of *F. johnsoniae* Δ*2419, pCP11_fjoh_2419::mScarlet-I*** grown for 10 hours at 27°C, shown in two separate channels (a) and (b).

Additionally, certain *F. johnsoniae* Δ*2419, pCP11_fjoh_2419::mScarlet-I* cells were stained with the CytoLiner™ fixed cell membrane stain and imaged by Stefan Thiele using the STELLARIS 8 TAU-STED microscope. Visual inspection suggests a slightly narrower distribution of the red *mScarlet-I* signal compared to the broader green CytoLiner™ signal within the cells (*Figure 32*). However, quantitative image analysis using *daime* 3.1 did not reveal statistically significant differences in the cell widths or localization pattern (Daims et al., 2006).

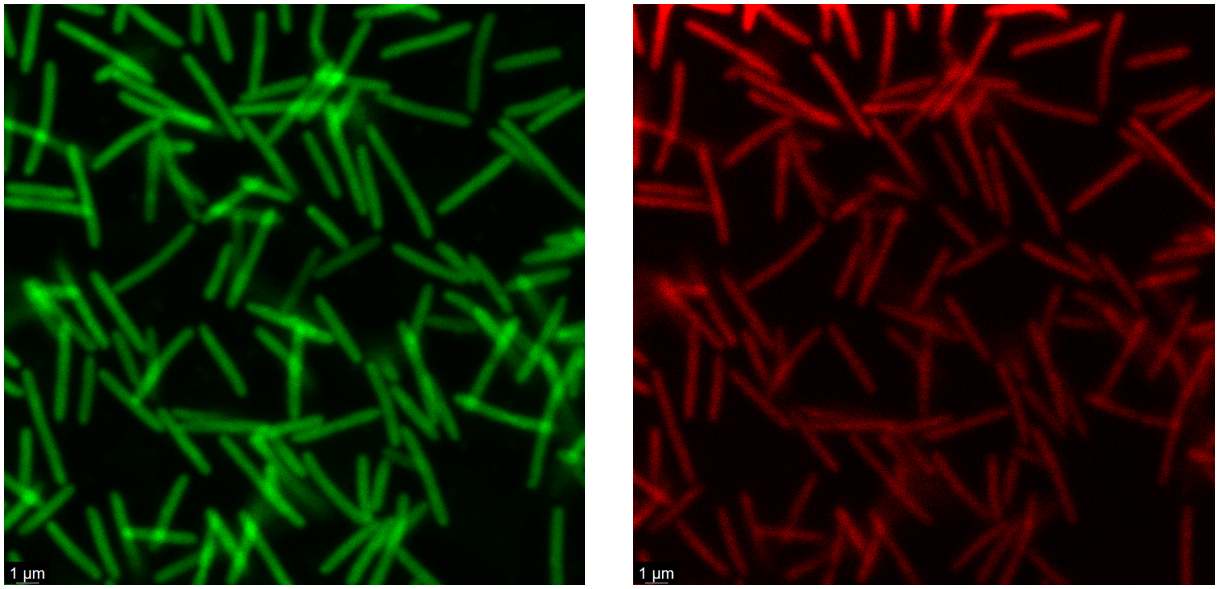

(a) CytoLiner™ staining (λ_{ex} = 492 nm, λ_{em} = 510 nm) (b) *mScarlet-I* fluorescence (λ_{ex} = 569 nm, λ_{em} = 594 nm)

Figure 32: **Stellaris 8 TAU-STED imaging of *F. johnsoniae* Δ*2419, pCP11_fjoh_2419::mScarlet-I*** grown for 10 hours at 27°C, shown in two separate channels (a) and (b).

Effect of external stimuli on cysteate acyl-ACP transferase expression

Successful production of the mScarlet-I fusion protein was confirmed by the detection of red fluorescence emission. To evaluate the impact of external stimuli on the cysteate acyl-ACP transferase (SulA) production, various growth conditions were tested. For this, images generated via Confocal Laser Scanning Microscope SP8 were analysed using *daime* 3.1 (Daims et al., 2006).

Liquid precultures of *F. johnsoniae* Δ*2419, pCP11_fjoh_2419::mScarlet-I* were used to inoculate 5 ml of CYE medium supplemented with erythromycin (1:1000, v/v). The cultures were grown under four conditions: at 27°C (control), at 27°C supplemented with 1 mg/ml cysteate (precursor addition), at 14°C, and at 37°C. To identify potential time dependent variations in the fusion protein production, samples were harvested for analysis after 6 and 10 hours of incubation (*Figure 33, Figure 34*). Images were analyzed as described in *subsection 2.5.3*. Median fluorescence intensities were determined and compared between the four experimental categories using the Kruskal-Wallis test.

Median fluorescence intensities after 6 hours of growth indicated that the null hypothesis of equal distribution could be rejected, showing a statistically significant difference between at least two of the experimental groups (p = 0,0085). Cells grown under normal conditions (2419_6h; OD_{600}= 0.233) showed a median fluorescence intensity of 110. Cells supplemented with cysteate (2419_cyst_6h; OD_{600}= 0.073) exhibited a higher median of 130 and showed the greatest spread in data across all groups. In contrast, cells grown at 14°C (2419_14C_6h; OD_{600}= 0.051) showed a suppressed intensity (median = 40). Cells grown at 37°C (2419_37C_6h; OD_{600}= 0.081) exhibited a median similar to the cysteate group (*Figure 33*).

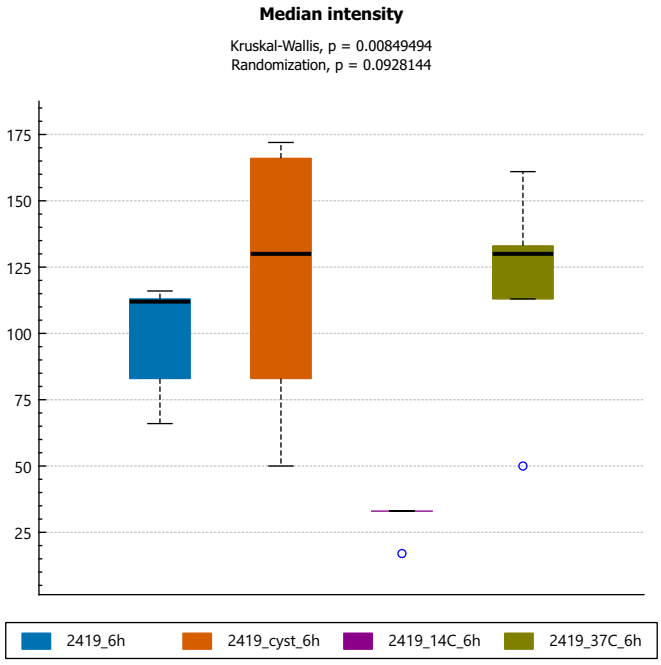

Figure 33: **Median fluorescence intensities of the transconjugant grown for 6h** at 180 rpm in liquid CYE medium at 27°C (blue), at 27°C substituted with 1 mg/ml cysteate (orange), at 14°C (purple) and at 37°C (green). Fluorescence was quantified in arbitrary units (A.U.) representing the median intensity per cell. Statistical significance was assessed using a Kruskal-Wallis test.

After a growth period of 10 hours, shifts in intensity profiles were observed. Cells grown under normal conditions (2419_10h; OD_{600}= 0.883) had an increase in fluorescent signal strength (median = 150). While cells supplemented with cysteate (2419_cyst_10h; OD_{600}= 0.216) maintained a similar median of 145, the distribution was more skewed toward lower values. Cells grown at 14°C (2419_14C_10h; OD_{600}= 0.162) had the lowest intensity (median = 25) and cells grown at 37°C (2419_37C_10h; OD_{600}= 0.024) exhibited a decrease in intensity compared to the cells harvested after 6 hours (median = 65). The Kruskal-Wallis test showed a significant difference between at least two experimental groups (p-value = 0.0030) and a significant randomization test (p-value = 0.0020) (*Figure 34*).

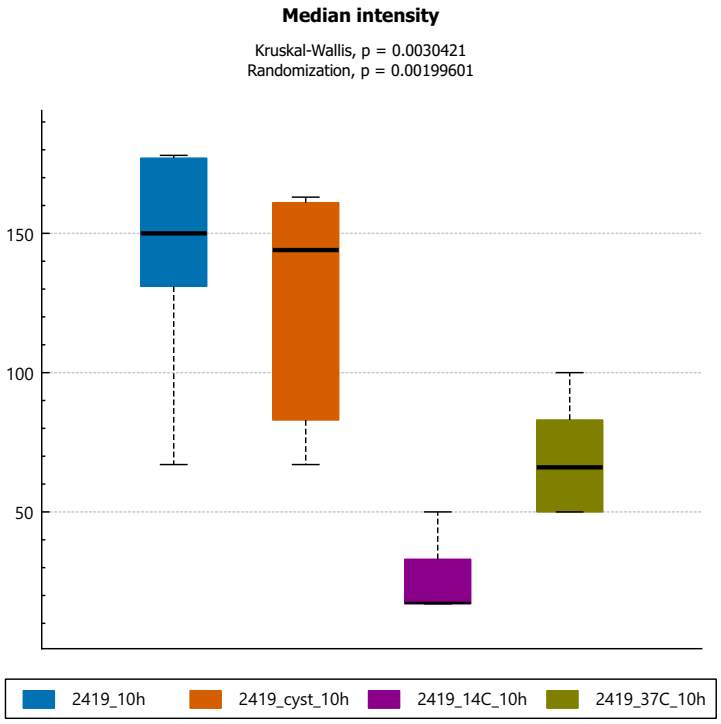

Figure 34: **Median intensities of the transconjugant grown for 10 h** at 180 rpm in liquid CYE medium at 27°C (blue), at 27°C substituted with 1 mg/ml Cysteate (orange), at 14°C (purple) and at 37°C (green). Fluorescence was quantified in arbitrary units (A.U.) representing the median intensity per cell. Statistical significance was assessed using a Kruskal-Wallis test

Promotor recognition of *fjoh_2419::mScarlet-I* by *E.coli* S17-1 λ pir

The *E.coli S17-1 λ pir, pCP11_fjoh_2419::mScarlet-I* exhibited a light pink pellet during conjugation, indicating fusion protein expression. Therefore, the strain was cultivated in liquid ampicillin enriched LB medium (1:1000, v/v) and grown overnight for 15 hours at 37 °C with shaking at 180 rpm. In parallel, a growth experiment was conducted to characterize the growth states of *E.coli S17-1 λ pir, pCP11_fjoh_2419::mScarlet-I*. After 15 hours of incubation, cells were harvested and processed for imaging as described in *subsection 2.3.7*.

The growth experiment was conducted over a 49 hour period. *E.coli S17-1 λ pir, pCP11_fjoh_2419::mScarlet-I* showed a lag phase of 4 hours, followed by rapid exponential growth

between 4h and 10 h. After 10 hours, the culture grew slower, transitioning into the stationary phase. The culture had a doubling time of 1.30 hours and the specific growth rate μ was determined to be 0.53 h^{-1} (*Figure 35b*).

The culture reached the early stationary phase prior to being harvested and imaged via CLSM SP8. Cells exhibited a distinct *mScarlet-I* fluorescence, showing that the cysteate acyl-ACP transferase::mScarlet protein production also occurs in *E.coli S17-1 λ pir*, driven by the native *F. johnsoniae* promotor present on the *pCP11* construct (*Figure 35a*).

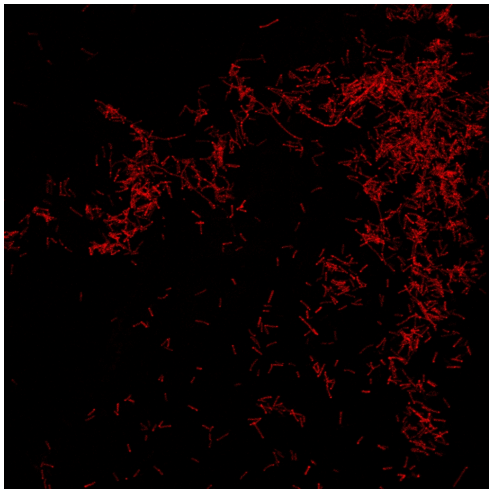

(a) *mScarlet-I* fluorescence (λ_{ex} = 569 nm, λ_{em} = 594 nm)

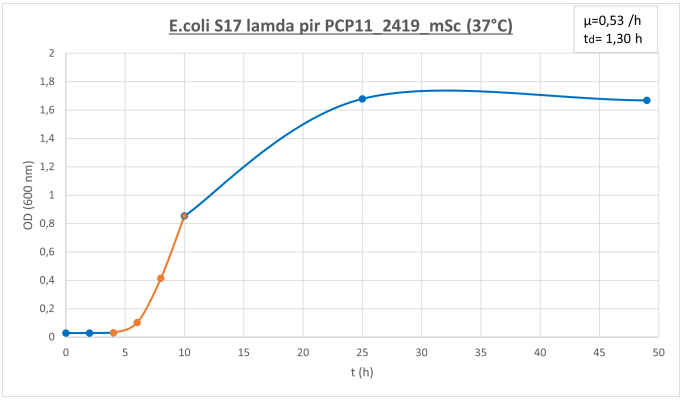

(b) Growth curve over a 49 hour period. The culture exhibits a lag phase until t = 4h, followed by an exponential growth phase between t = 4h and t = 10h (orange). Data points represent measurements from a single experimental run.

Figure 35: ***E.coli S17-1 λ pir, pCP11_fjoh_2419::mScarlet-I*** imaged by CLSM after an overnight cultivation (15 hours) at 37°C (a) and growth curve over a 49 hour period (b).

3.4.2 Investigation of the subcellular localisation of Fjoh_4604::mScarlet-I

To ensure correct sampling times for microscopy imaging, a preliminary growth experiment was conducted with *F. johnsoniae fjoh_4604::mScarlet*. This showed the different growth phases, enabling the harvest of cells accordingly. Following harvest, cells were processed for microscopy as described in *subsection 2.3.7*.

The growth experiment was conducted over a period of 49 hours. *F. johnsoniae fjoh_4604::mScarlet* showed a short lag phase of 2 hours, followed by exponential growth between 2 and 10 hours. After 10 hours, the culture transitioned into the stationary phase. The culture exhibited a doubling time of 1.22 hours and the specific growth rate μ was determined to be 0.57 h^{-1} (*Figure 36*).

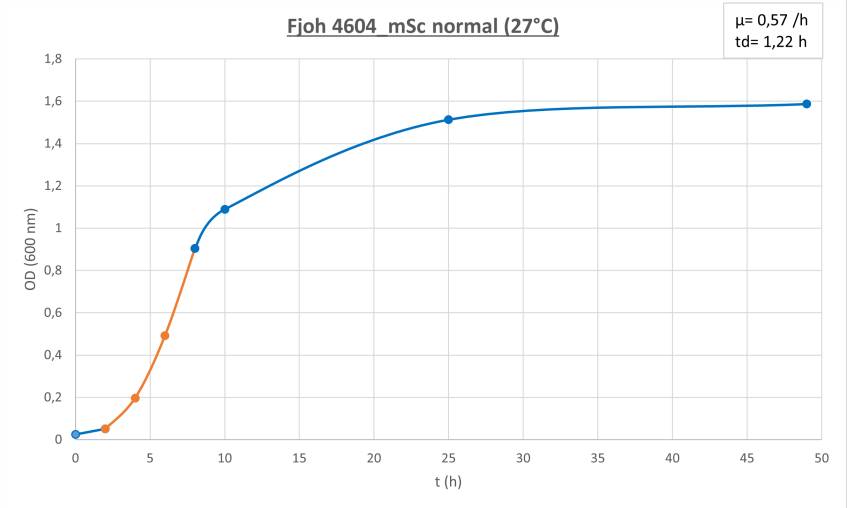

Figure 36: **Growth curve of *F. johnsoniae fjoh_4604::mScarlet-I* over a 49 hour period.** The culture exhibits a short lag phase until t = 2h, followed by an exponential growth phase between t = 2h and t = 8h (orange). Data points represent measurements from a single experimental run.

Cells were imaged using the confocal laser scanning microscope SP8. The culture was incubated for six hours in liquid CYE medium at 27°C with shaking at 180 rpm, which corresponded to the exponential growth phase. Subsequently, the cells were harvested and processed for imaging, which included DAPI staining (1 mg/ml) for general bacterial localization. Imaging revealed rod shaped cells but no red fluorescence upon excitation at 569 nm Figure 37.

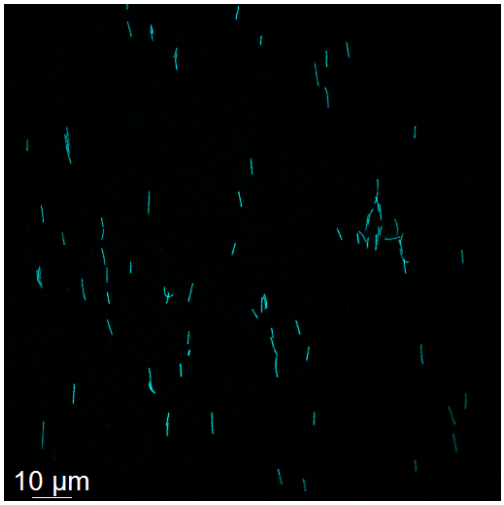

(a) DAPI staining (λ_{ex} = 354 nm, λ_{em} = 456 nm)

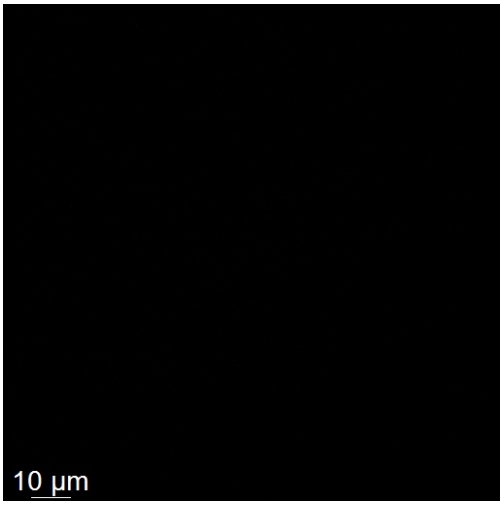

(b) *mScarlet-I* fluorescence (λ_{ex} = 569 nm, λ_{em} = 594 nm)

Figure 37: ***F. johnsoniae fjoh_4604::mScarlet-I* grown for 6h**, imaged by CLSM SP8, shown in two separate channels (a) and (b).

Time-dependent protein expression was assessed by performing additional imaging after 10 and 25 hours of growth. However, imaging yielded no red fluorescence upon excitation at 569 nm Figure 38. Additionally, a range of external stimuli were tested, including the supplementation of the sulfonolipid precursor cysteate (1 mg/ml) and different growth temperatures. However, these stimuli did not elicit a fluorescent

mScarlet-I response from *F. johnsoniae fjoh_4604::mScarlet-I*.

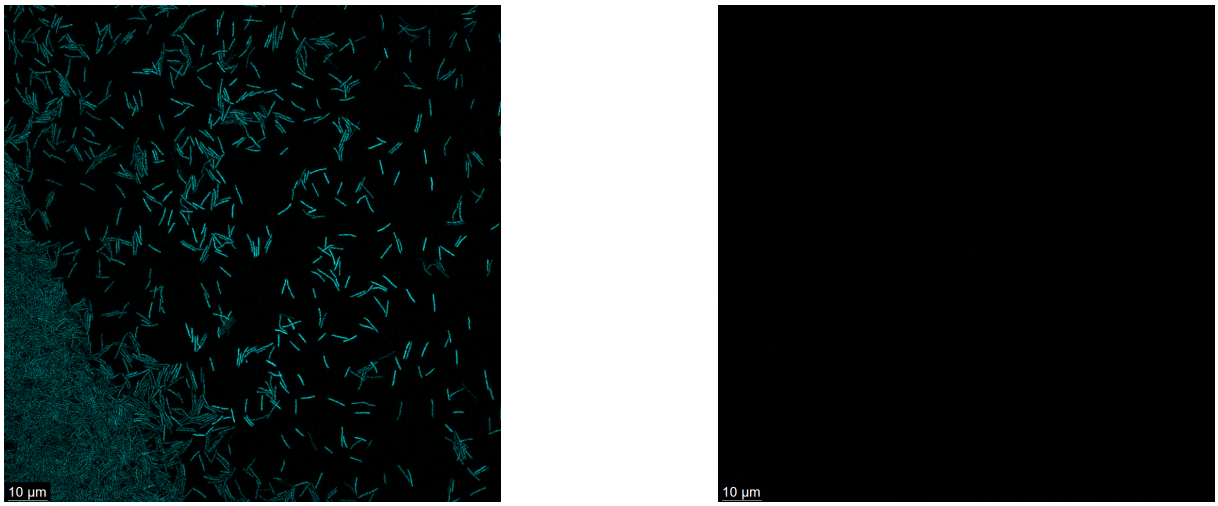

(a) DAPI staining (λ_{ex} = 354 nm, λ_{em} = 456 nm)

(b) *mScarlet-I* fluorescence (λ_{ex} = 569 nm, λ_{em} = 594 nm)

Figure 38: ***F. johnsoniae fjoh_4604::mScarlet-I* grown for 10h**, imaged via CLSM SP8, shown in two separate channels (a) and (b).

3.4.3 Imaging of *Chryseobacterium capnotolerans DHB6*

Morphological characterization of *C. capnotolerans* was done via confocal laser scanning microscope SP8. Cells were harvested and processed for imaging as described in *subsection 2.3.7*. Additionally, a growth experiment was conducted to determine the specific growth rate and doubling time.

Precultures demonstrated rapid growth. Consequently, the culture was subjected to an incubation period of two hours in liquid TSB at a temperature of 27°C, with shaking at 180 rpm. Subsequently, cells were harvested and processed for imaging. General bacterial localisation was done using DAPI staining (1 mg/ml). Imaging revealed short rod-shaped bacteria (1-2 µm) with a uniform morphology Figure 39a.

The growth experiment was carried out over a period of 49 hours. *C. capnotolerans* showed a short lag phase of 2 hours, followed by rapid exponential growth between 2 and 8 hours. During this experiment, the culture exhibited a doubling time of 3.94 hours and the specific growth rate was µ = 0.18 h^{-1} (*Figure 39b*).

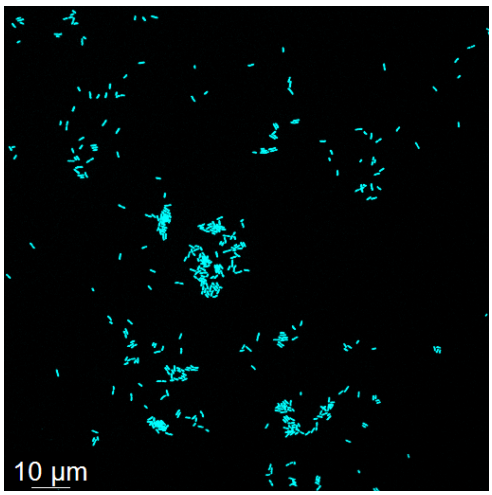

(a) *C. capnotolerans* grown for 2h, imaged by fluorescence microscopy,DAPI stained (λ_{ex} = 354 nm, λ_{em} = 456 nm).

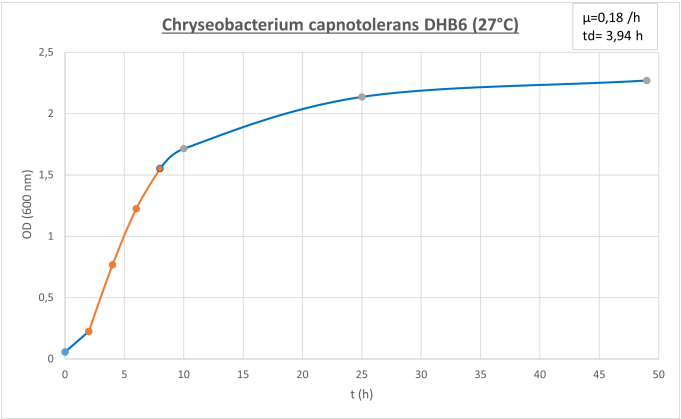

(b) Growth curve of *C.capnotolerans* over a 49 hour period. The culture exhibits a distinct lag phase until t = 2h, followed by an exponential growth phase between t = 4h and t = 8h (orange). The transition to the stationary phase is observed starting at t = 10h. Data points represent measurements from a single experimental run.

Figure 39: ***Chryseobacterium capnotolerans DHB6***

3.4.4 Imaging of *Flavobacterium piscis*

Visual assessment of *F. piscis*, which was previously isolated from soil by Guoqing Guan, was done using the CLSM SP8. Cells were harvested and processed for imaging as described in *subsection 2.3.7*. A growth experiment was additionally conducted to determine the specific growth rate and doubling time.

The culture was subjected to an incubation period of 25 hours in liquid CYE medium at a temperature of 27°C with shaking at 180 rpm. Cells were harvested and processed for imaging after six and 25 hours of growth. General bacterial localization under the microscope was done via DAPI staining (1 mg/ml). Imaging after 6 hours of growth showed elongated Rods with variable length. Additionally, filamentation is visible, which can be seen more clearly after 25 hours of growth (*Figure 40*).

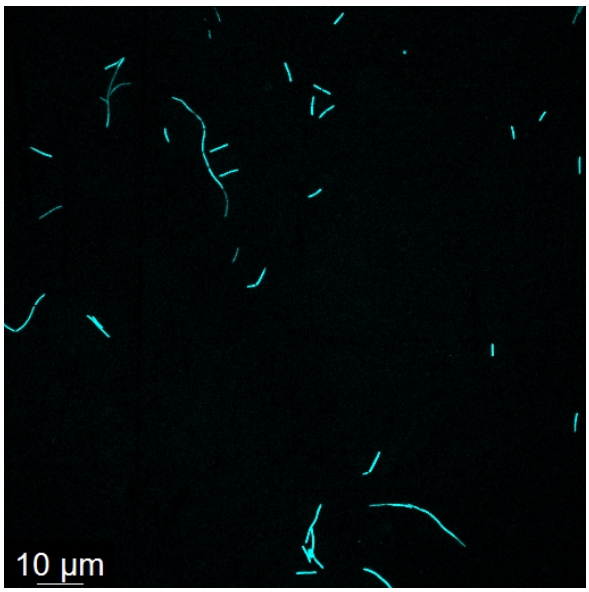

(a) DAPI stained *F. piscis* during exponential growth phase (6h).

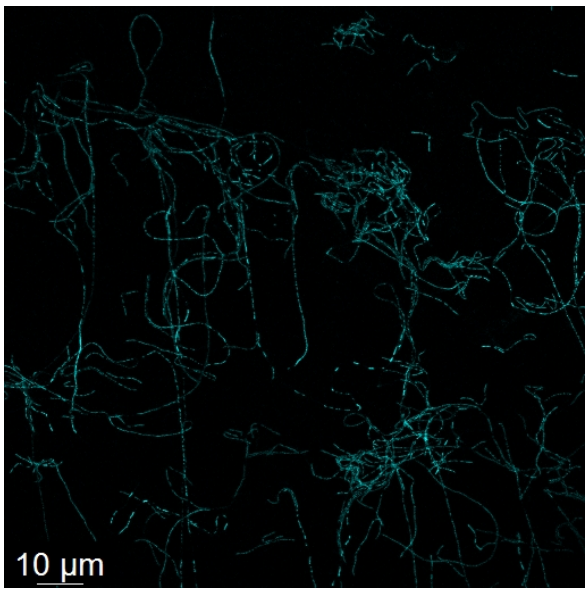

(b) DAPI stained *F. piscis* during stationary phase (25 h).

Figure 40: ***F. psicis* imaged by CLSM SP8** after 6 (a) and 25 hours (b) growth in liquid CYE medium. Stained with 1 µg/µL DAPI (λ_{ex} = 354 nm, λ_{em} = 456 nm).

The growth experiment was carried out over 49 hours. *F. piscis* showed a lag phase of 2 hours, followed by an exponential growth phase between 2 and 10 hours. During this experiment, the culture exhibited a doubling time of 2.34 hours and the specific growth rate was µ = 0.29 h^{-1} (*Figure 41*).

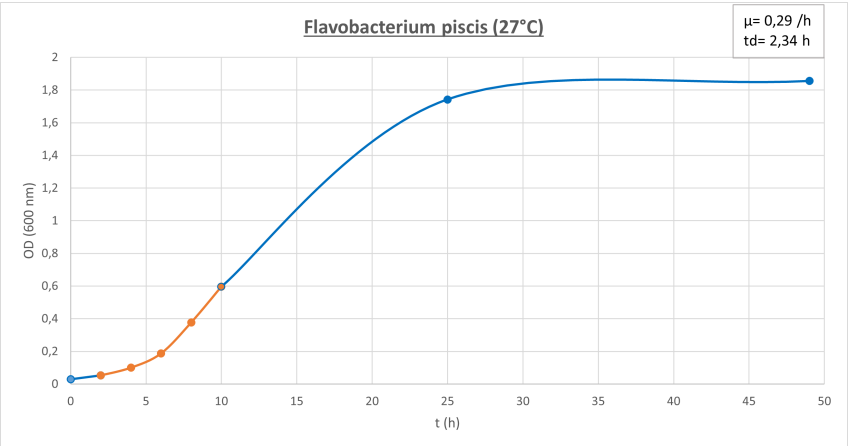

Figure 41: **Growth curve of *F. piscis*** over a 49 hour period. The culture exhibits a short lag phase until t = 2h, followed by an exponential growth phase between t = 2h and t = 10h (orange). Data points represent measurements from a single experimental run.

3.4.5 Imaging of *Flavobacterium LT0091*

The CLSM SP8 was used to visually assess *F. LT0091*, which was isolated from soil by Guoqing Guan. Cells were harvested and processed for imaging as described previously and a growth experiment was conducted additionally to determine the specific growth rate and doubling time.

The culture was incubated for 25 hours in liquid CYE medium at a temperature of 27°C, while shaking at 180 rpm. Part of the cells was harvested and processed for imaging after 6 and 25 hours of growth.

Localization and visual assessment of bacteria was facilitated by DAPI staining (1 mg/ml). After 6 h of growth, imaging revealed short rods forming small clusters (*Figure 42a*). After 25 hours of growth, this progressed into a biofilm structure, where rod-shaped cells were organized into large, interconnected cellular sheets (*Figure 42b*).

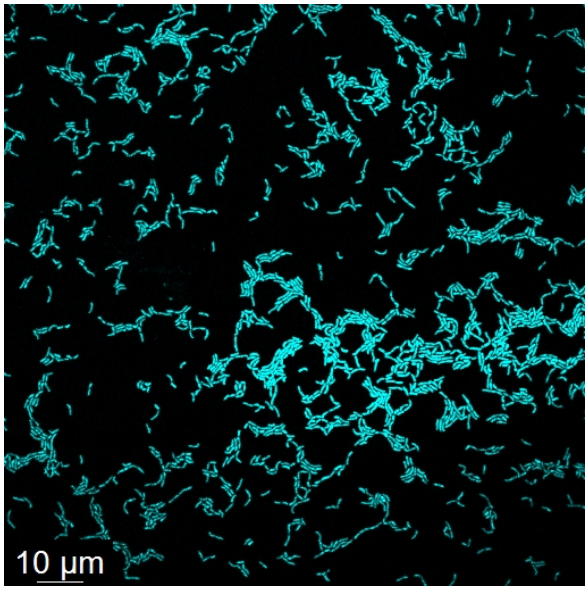

(a) DAPI stained *F. LT0091* during exponential growth phase (6h).

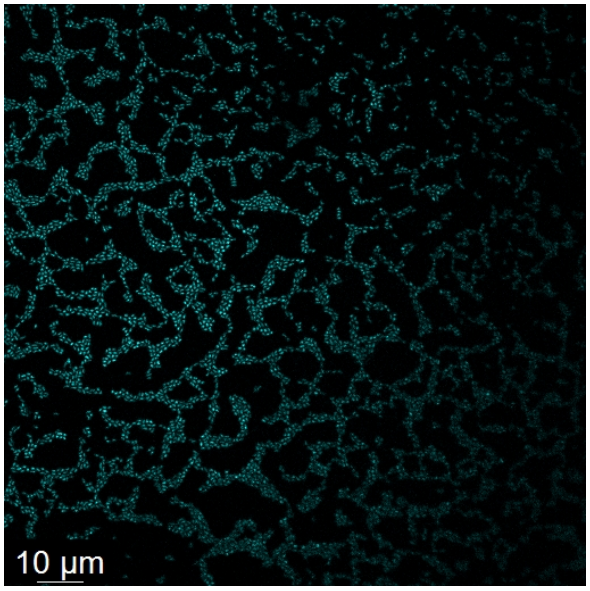

(b) DAPI stained *F. LT0091* during stationary phase (25h).

Figure 42: ***F. LT0091* imaged via CLSM SP8** after 6 (a) and 25 hours (b) growth in liquid CYE medium. Stained with 1 µg/µL DAPI (λ_{ex} = 354 nm, λ_{em} = 456 nm).

The growth experiment was carried out over a period of 49 hours. *F. LT0091* showed a lag phase of 4 hours, followed by an exponential growth phase between 6 and 10 hours. During this experiment, the culture exhibited a doubling time of 1.30 hours and the specific growth rate was µ = 0.53 h^{-1} (*Figure 43*).

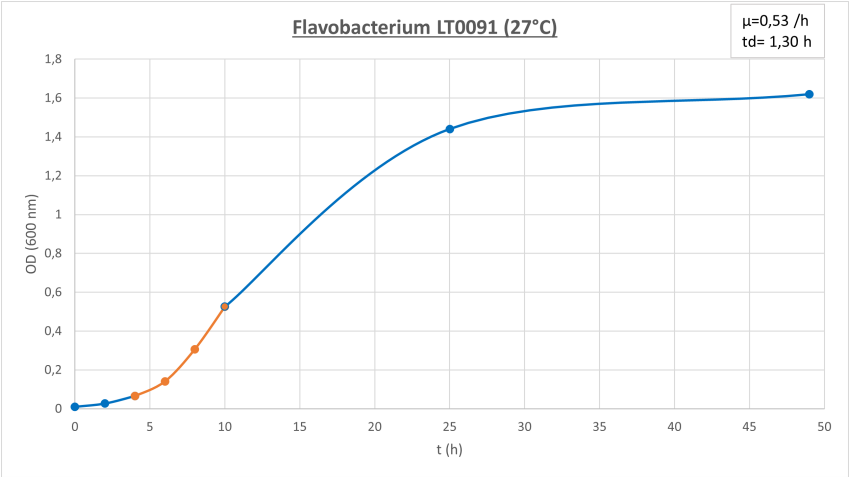

Figure 43: **Growth curve of *F. LT0091*** over a 49 hour period. The culture exhibits a distinct lag phase until t = 4h, followed by an exponential growth phase between t = 6h and t = 10h (orange). Data points represent measurements from a single experimental run.

3.5 Lipid profile analysis

Identification of sulfobacins and their intermediates in *F. johnsoniae, F.piscis, F. sp. LT0091* and *C. capnotolerans* was carried out using liquid chromatography-tandem mass spectrometry (LC-MS/MS). Targeted data processing was conducted via Skyline. Putative and established sulfobacins were identified based on a comprehensive transition list, which integrated previously identified sulfobacin structures by Beemelmanns et al., 2014 and Hou et al., 2022. In order to ensure data integrity, it was necessary to consider signals as detected only if their intensity exceeded a threshold of twice the signal intensity observed in the blank. Consequently, only mass traces surpassing this detection limit are displayed in the corresponding chromatograms.

3.5.1 Sulfonolipid profile of *F. johnsoniae* $\triangle$*2419, pCP11_fjoh_2419::mScarlet-I*

Baseline lipidomic profiles for *F. johnsoniae* wildtype and *F. johnsoniae* Δ*2419* were assessed to identify changes after the introduction of the complementing plasmid *pCP11_2419::mScarlet-I* into the knockout strain *F. johnsoniae* Δ*2419*.

LC-MS analysis of the *F. johnsoniae* wildtype exhibited nine peaks of established sulfobacins, as well as 14 unidentified putative sulfobacin (-derivate) species (*Figure 44*).

Signals corresponding to sulfobacin D (*m/z* = 590.4451) and an uncharacterized sulfobacin (*m/z* = 604.4608) were detected at retention times of 14.6 and 14.9 minutes. Both lipids exhibited a characteristic MS/MS fragmentation pattern of a sulfate fragment (*m/z* = 80.96) and capnine product ions (*m/z* = 333.2102 and 350.2357). Potential sulfobacin A and sulfobacin B signals were both identified using the expected *mass-to-charge* ratios of 618.4768 (SulA) and 574.4501 (SulB) at a retention time of 15.3 minutes. A signal for an unknown sulfobacin (*m/z* = 588.4662) was detected at a retention time of 15.7 minutes. MS/MS analysis revealed the presence of the expected fragments with a *mass-to-charge* ratio of 80.9652 (sulfonate) as well as 333.2100 and 350.2344 (capnine product ions). A potential signal for sulfobacin F was identified using the specific *mass-to-charge* ratio of 588.4589 and the retention time at 15.7 minutes. Furthermore, a putative sulfobacin (*m/z* = 686.4645) was identified at a retention time of 16.7 minutes.

Due to their low relative intensities, the following signals are less prominent in the visual representation of the chromatograms, although they exceeded the detection threshold. These signals, which lacked a detailed MS/MS analysis were ketocapnine (*m/z* = 349.2253), sulfobacin E (*m/z* = 574.9927), capnine (*m/z* = 350.2372), sulfobacin C (*m/z* = 558.9927) and RIF2 (*m/z* = 603.4539). Similarly, several signals for putative sulfobacins were detected with *mass-to-charge* ratios of 588.4298, 634.4670, 602.4455, 658.4325, 572.4349, 630.4761, 644.4877, 686.4645 and 598.4505.

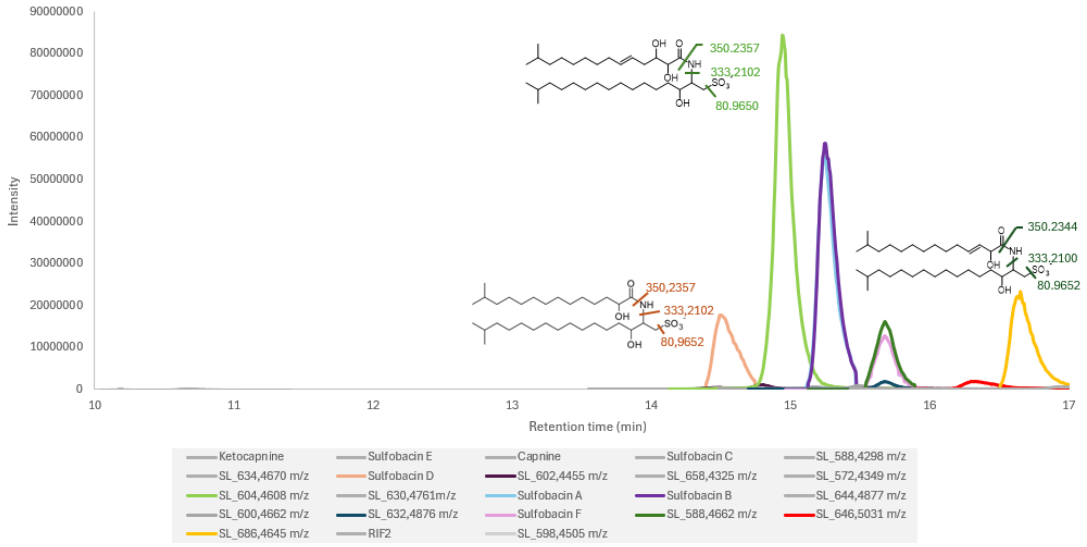

Figure 44: **Lipid analysis of the *F. johnsoniae* wildtype strain** revealed 23 peaks for possible sulfobacins, comprising of 9 previously described, as well as 14 unknown putative sulfobacins. MS/MS data was available for sulfobacin D (*m/z* = 590.4451), and two unknown sulfobacins with *mass-to-charge* ratios of 504.4608 and 588.4662. Peak intensities were plotted in arbitrary units.

Lipid analysis of *F. johnsoniae* Δ*2419* was conducted by Theresa Villunger. As shown in *Figure 45*, an accumulation of the sulfobacin precursor capnine (*m/z* = 350.2372) at a retention time of 10.7 minutes was observed for *F. johnsoniae* Δ*2419* . A possible signal for ketocapnine was additionally detected with a *mass-to-charge* ratio of 349.2253 at a retention time of 10.9 minutes. Sulfobacins derived from the capnine backbone were absent as no other significant peak was detected.

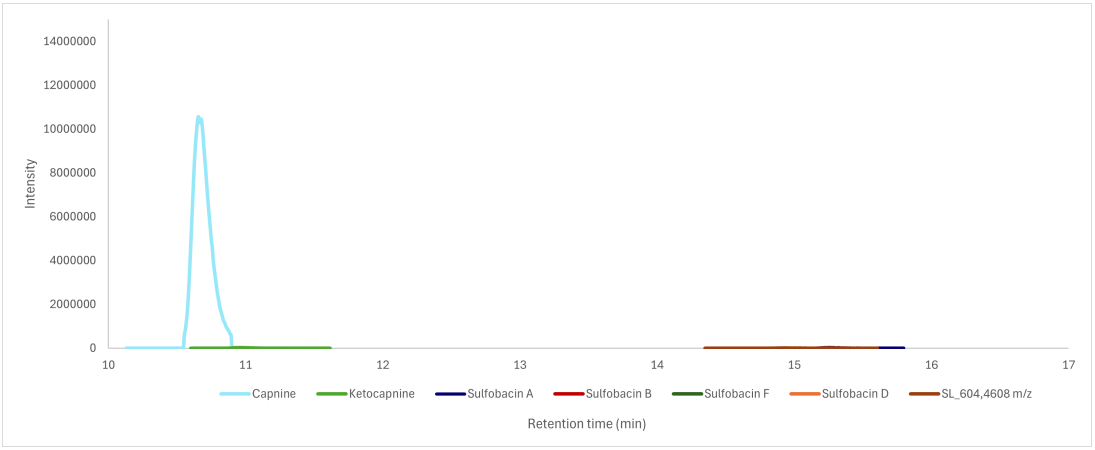

Figure 45: **Lipidomic analysis of *F. johnsoniae* Δ*2419*** revealed the absence of capnine derived sulfobacins. Peak intensities were plotted in arbitrary units.

Complementation with the *pCP_fjoh_2419::mScarlet-I* plasmid did not restore the *F. johnsoniae* wild-type sulfobacin production

LC-MS analysis of lipid extracts from *F.johnsoniae* Δ*2419, pCP11_fjoh_2419::mScarlet-I* demonstrated that the expression of the SulA::mScarlet-I fusion protein failed to restore the wildtype sulfobacin phenotype. Complementation with the plasmid resulted in the detection of a possible signal for capnine (*m/z* =

350.2372) at a retention time of 10.7 minutes. Additionally, possible signals for sulfobacin E (*m/z* = 574.9927), ketocapnine (*m/z* = 349.2253) and several unknown sulfobacins (*m/z* = 658.4325, 646.5032, 616.4611 and 576.4307) exceeded the baseline threshold. No other significant peaks for possible capnoids were observed (*Figure 46*).

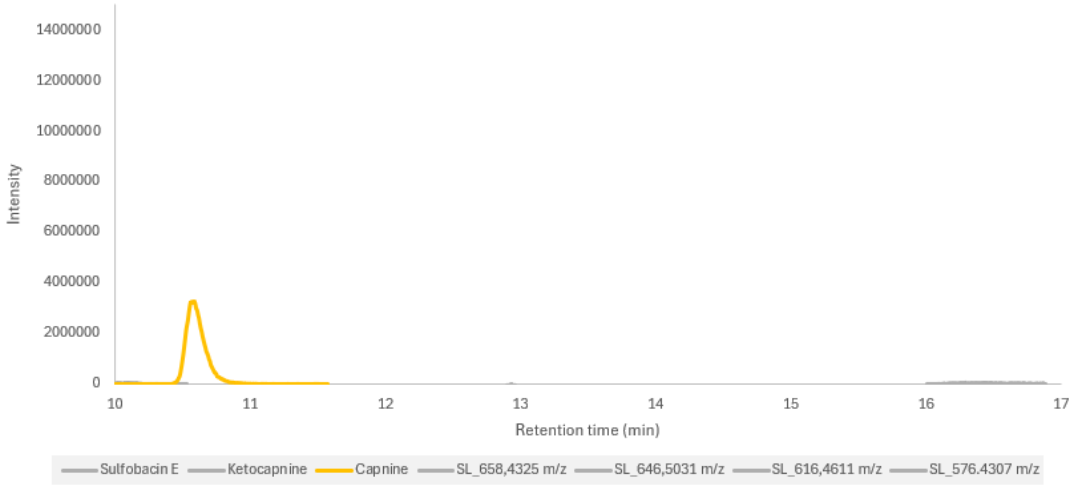

Figure 46: **Lipidomic analysis of *F. johnsoniae* Δ*2419, pCP11_fjoh_2419::mScarlet-I*** showed, that the complementation of the knockout with the SulA::mScarlet-I did not restore the sulfobacin production. Peak intensities were plotted in arbitrary units.

Addition of the precursor cysteate altered the lipid profile of the tranconjugant *F. johnsoniae* Δ*2419, pCP11_fjoh_2419::mScarlet-I*

Cysteate supplementation (1 mg/ml) of the liquid CYE-erythromycin medium altered the sulfonolipid production, as possible signals for sulfobacin C (*m/z* = 558.9927; RT = 3.6 min) and sulfobacin F (*m/z* = 588.4589; RT = 17.7), as well as an unknown sulfobacin (*m/z* = 644.4877; RT = 17.4) were significantly above the background level of the blank sample (*Figure 47*).

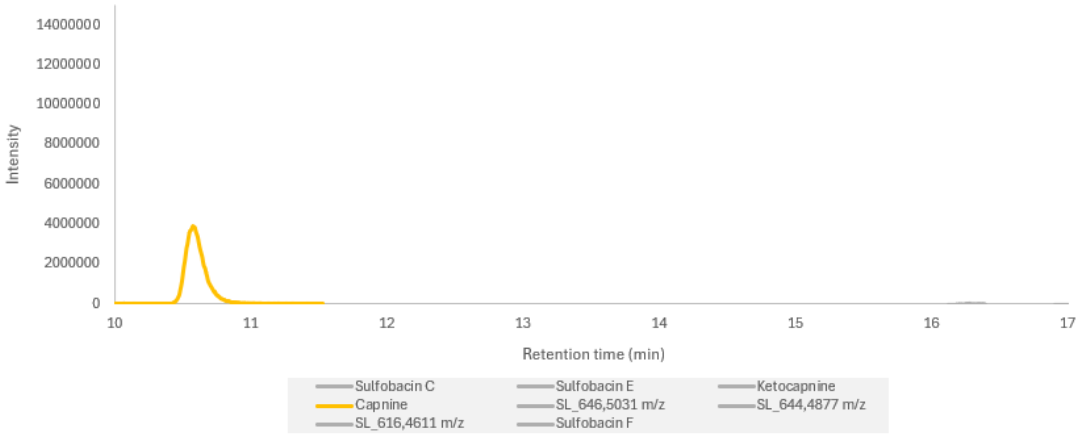

Figure 47: **Lipidomic analysis of *F. johnsoniae* Δ*2419, pCP11_fjoh_2419::mScarlet-I*, substituted with 1 mg/ml cysteate** altered the sulfobacin targeted lipid profile, as possible signals for sulfobacin C (*m/z* = 558.9927), sulfobacin F (*m/z* = 588.4589) and and unknown sulfonolipid (*m/z* = 644.4877) were additionally detected. Peak intensities were plotted in arbitrary units.

3.5.2 Sulfonolipid profile of *Chryseobacterium capnotolerans*

LC-MS analysis revealed 23 signals for possible sulfobacins. The lipid profile for *C. capnotolerans* comprised seven significant peaks for known sulfobacins (*Figure 48*). A signal for sulfobacin A (m/z = 618.4768) was detected at a retention time of 15.2 minutes. Additionally, possible signals for sulfobacin E (m/z = 574.9927; RT = 10.0 min), capnine (m/z =350.2372; RT = 10.6 min), ketocapnine (m/z = 349.2253; RT = 10.9 min), sulfobacin F (m/z = 588.4589; RT = 15.5 min) and RIF 2 (m/z = 603.4539; RT = 16.9 min) were detected. Furthermore, several unknown sulfobacins or potential derivates were identified, as shown in *Figure 48*.

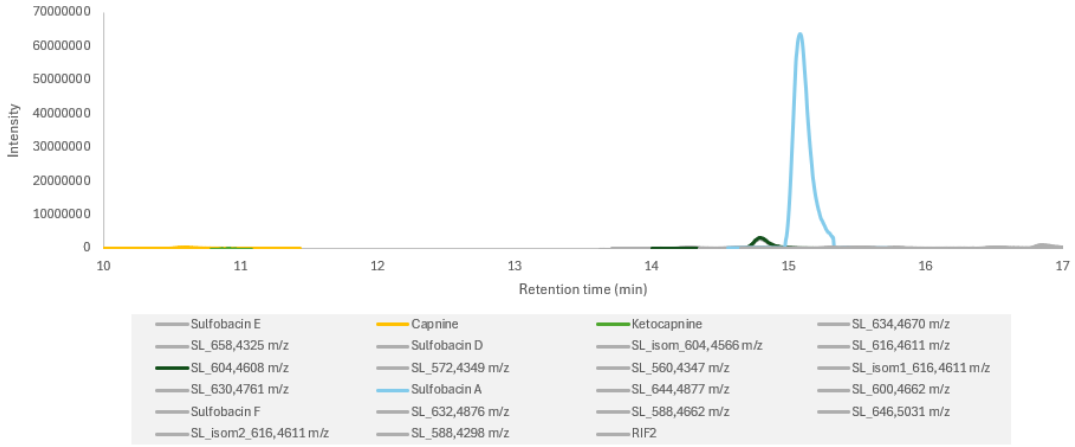

Figure 48: **Lipidomic analysis of *C. capnotolerans*** revealed 23 possible sulfobacins, comprising of 7 known capnoids and 16 unknown sulfobacin species. Peak intensities were plotted in arbitrary units.

Cysteate induced shift in sulfobacin composition of *C. capnotolerans*

The addition of 1 mg/ml cysteate to the *C. capnotolerans* strain medium resulted in a significant shift of the lipid composition. In addition to a signal for sulfobacin A (*m/z* = 618.4768), sulfobacin B (*m/z* = 574.4501) was detected at the same retention time of 15.1 minutes. Sulfobacin A was additionally identified through the specific MS/MS pattern, revealing the diganostic ion capnine (*m/z* = 350.23369). The supplementation of cysteate resulted in a high signal intensity for the sulfobacin precursor capnine (*m/z* = 350.2372; RT = 10.6 min) compared to the standard medium. MS/MS analysis revealed ion fragments with a mass to charge ratio of 80.9535 (sulfonate) and 174.9551. Other significant signals for sulfobacin C (*m/z* = 558.9927; RT = 3.6 min) , ketocapnine (*m/z* = 349.2253; RT = 10.9 min), sulfobacin D (*m/z* = 590.4451; RT = 14.4 min), sulfobacin F (*m/z* = 588.4589; RT = 15.5 min) and RIF 2 (*m/z*= 603.4539; RT = 16.9 min) were detected, though lacking MS/MS data for further confirmation. Additionally, various unknown sulfobacin signals were detected and can be seen in *Figure 49*.

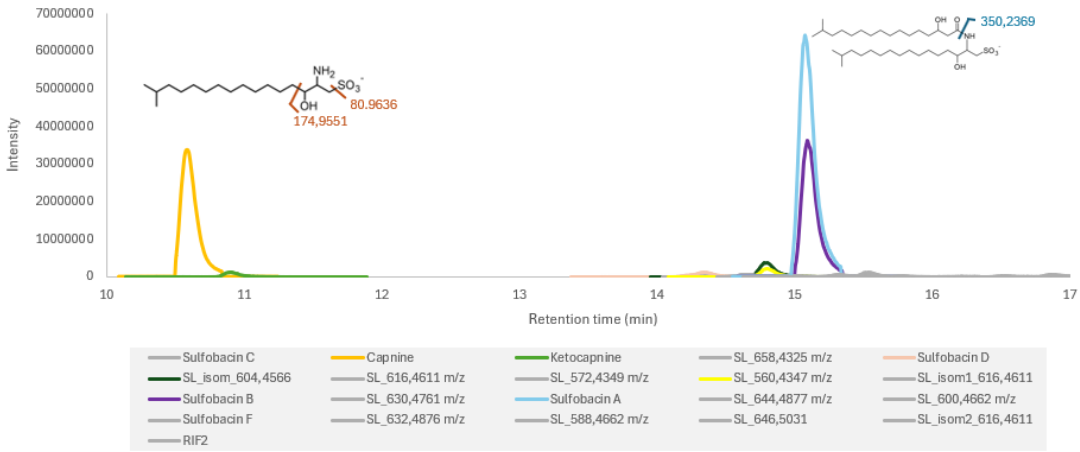

Figure 49: **Lipidomic analysis of *C. capnotolerans*, substituted with 1 mg/ml cysteate** increased the capnine (*m/z* = 350.2369) signal. MS/MS data was available for capnine and sulfobacin A (*m/z* = 618.4768). Peak intensities were plotted in arbitrary units.

3.5.3 Sulfonolipid profile of *Flavobacterium piscis*

Analysis of the *F. piscis* lipid profile revealed 25 signals for possible sulfonolipids (*Figure 50*).

A potential signal for sulfobacin D was detected at a *mass-to-charge* ratio of 590.4451 and a retention time of 14.4 min. An unknown sulfobacin, as well as their isomer (*m/z* = 604.4566) were detected at 14.7 minutes. Signals for sulfobacin A (*m/z* = 618.4768) and sulfobacin B (*m/z* = 574.4501) were detected at a retention time of 15.1 minutes. Sulfobacin A was additionally fragmented. The MS/MS output revealed the diagnostic ion capnine (*m/z* = 350.2371). Furthermore, significant signals were detected for sulfobacin C (*m/z* = 558.9927; RT = 3.7 min), sulfobacin E (*m/z* = 574.9927; RT = 10.0 min), ketocapnine (*m/z* = 349.2253; RT = 10.9 min), capnine (*m/z* = 350.2372; RT = 10.6 min), sulfobacin F (*m/z* = 588.4589; RT = 15.5 min) and RIF 2 (*m/z* = 603.4539; RT = 16.9 min). Furthermore, several signals for unknown sulfobacins were detected, as shown in *Figure 50*.

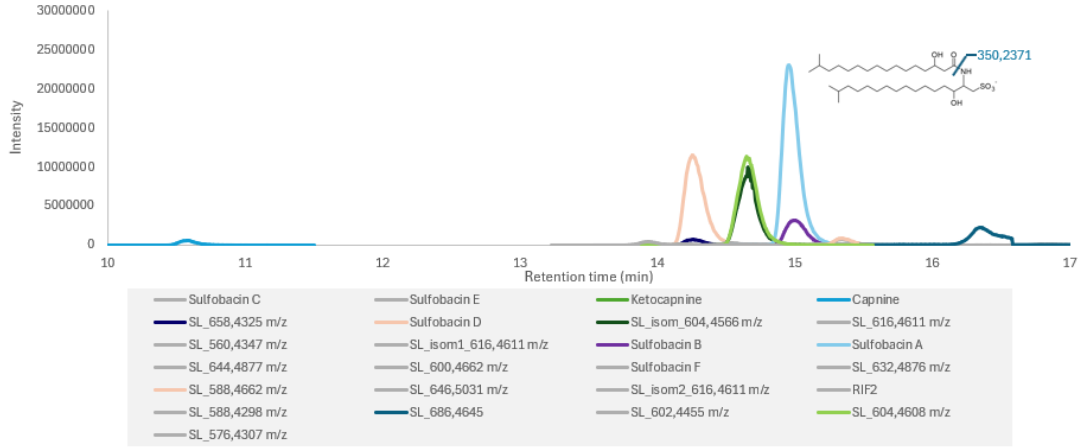

Figure 50: **Lipidomic analysis of *F. piscis LT0090*** detected 9 possible signals for known sulfobacins, as well as 16 signals for possible sulfobacins. MS/MS data was available for sulfobacin A (*m/z* = 618.4768), which comprised the fragment ion for capnine (*m/z* = 350.2371). Peak intensities were plotted in arbitrary units.

Addition of the precursor cysteate decreased observed signal intensities of possible sulfonolipids in *F. piscis LT0090*

Addition of cysteate (1 mg/ml) to the CYE medium altered the sulfonolipid production in the observed *Flavobacterium* strain (*Figure 51*). In general, lower signal intensities were observed for all sulfobacins previously identified in *Figure 50*.

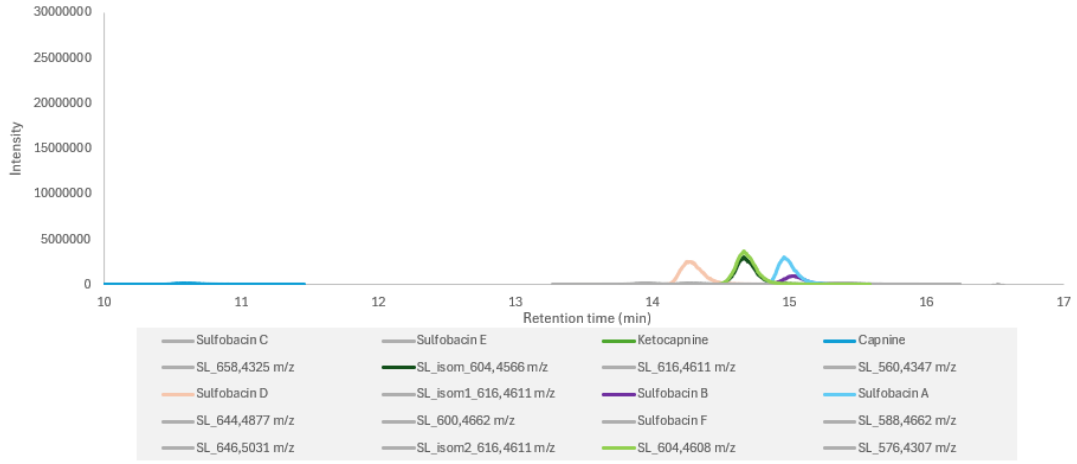

Figure 51: **Lipidomic analysis of *F. piscis LT0090*, substituted with 1 mg/ml cysteate** decreased all previously detected sulfobacin signals. Peak intensities were plotted in arbitrary units.

3.5.4 Sulfonolipid profile of *Flavobacterium sp. LT0091*

LC-MS analysis of the *Flavobacterium sp. LT0091* revealed low amounts of sulfobacin signals (*Figure 52*). Signals exceeding the threshold were sulfobacin C (*m/z* = 558.9927; RT = 3.6 min), sulfobacin E (*m/z* = 574.9927; RT 10.0), ketocapnine (*m/z* = 349.2253; RT = 10.9 min), sulfobacin D (*m/z* = 590.4451; RT = 14.4 min), sulfobacin B (*m/z* = 574.4501; RT = 15.0), sulfobacin F (*m/z* = 588.4589; RT = 15.5 min) and multiple unknown sulfobacins (*m/z* = 604.4566, 616.4611, 644.4877, 646.5031, 686.4645, 604.4608, 576.4307).

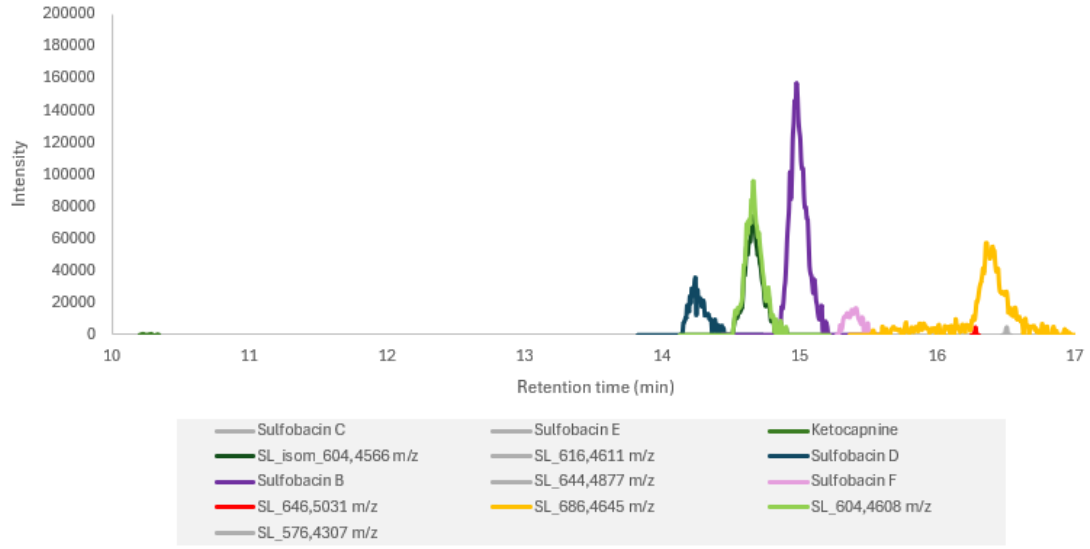

Figure 52: **Lipidomic analysis of *Flavobacterium sp. LT0091*** identified 13 possible signals of sulfobacins. Peak intensities were plotted in arbitrary units.

Addition of the precursor cysteate decreased sulfobacin signal intensity and abundance

Pre-experimental supplementation of 1 mg/ml cysteate to the CYE medium led to a decrease in the detected sulfobacin signals (*Figure 53*). Potential sulfobacin signals exceeding the detection threshold included sulfobacin C (*m/z* = 558.9927; RT = 3.6 min), sulfobacin E (*m/z* = 574.9927; RT 10.0), ketocapnine (*m/z* = 349.2253; RT = 10.9 min), unknown sulfobacin (*m/z* = 616.4611; RT = 14.7 min), unknown sulfobacin (*m/z* = 644.4877; RT = 16.3 min) and sulfobacin F (*m/z* = 588.4589; RT = 15.5 min).

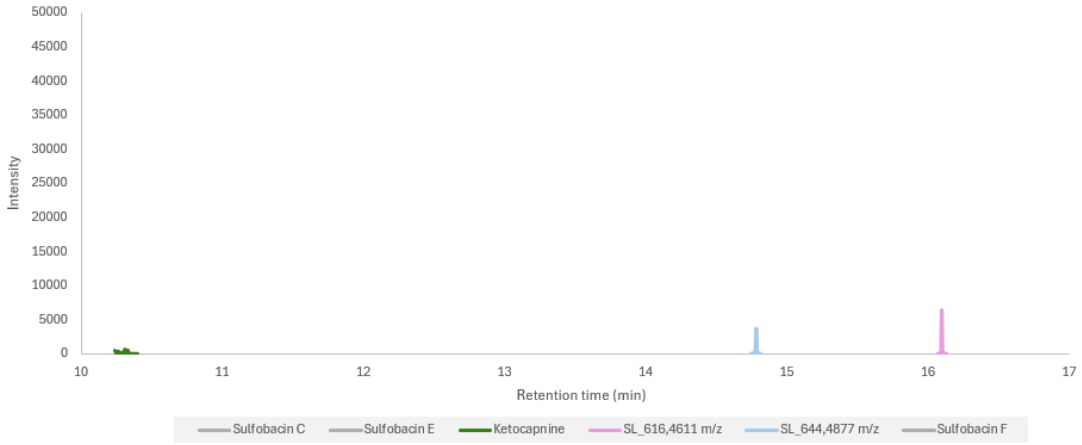

Figure 53: **Lipidomic analysis of *Flavobacterium sp. LT0091*, substituted with 1 mg/ml cysteate** decreased sulfobacin signal intensity and abundance. Peak intensities were plotted in arbitrary units.

4 Discussion

Since the discovery of sulfobacins in 1980, the amount of literature regarding these lipids has remained relatively limited. Beyond their essential role in bacterial gliding motility (Godchaux and Leadbetter, 1980), sulfobacins and their derivatives exhibit diverse bioactivities as signaling molecules in both choanoflagellates (Alegado et al., 2012; Woznica et al., 2016) and mammalian hosts (Older et al., 2024). A comprehensive understanding of their biosynthetic and regulatory pathways is therefore essential to unraveling their varied functions within the bacterial cell, as well as the interactions between sulfobacin producing bacteria and their multicellular partners.

4.1 Spatial organization and translocation mechanisms of the sulfobacin pathway

Bioinformatic topology analysis was employed to determine the subcellular localization of selected enzymes potentially involved in sulfobacin biosynthesis. Results from Phobius and DeepTMHMM indicate that both the cysteate acyl-ACP transferase (Fjoh_2419) and the putative sulfobacin synthase (Fjoh_2421) are soluble, globular proteins residing in the cytoplasm as they lack signal peptides. These findings are consistent with observations in related systems, where corresponding analogs from the bacterial sphingolipid biosynthetic pathway share the same subcellular arrangement (Uchendu et al., 2024). In many bacteria, the sphingolipid synthesis pathway involves a cytoplasmic ceramide synthase (bCerS). The putative sulfobacin analogue sulfobacin synthase (Fjoh_2421) exhibits the same subcellular organization, reflecting the typical topology of the microbial sphingolipid pathway rather than the membrane-associated processes found in eukaryotes (*Figure 54*). To further validate these findings, a topological analysis of the 3-ketocapnine reductase (CapC) is essential. While this enzyme was previously identified in *Ornithobacterium rhinotracheale*, it remains unidentified in other bacteria capable of sulfobacin biosynthesis (Y. Liu et al., 2022). Topological analysis of CapC (A0A3R5XUE6) revealed a high prediction for a soluble cytoplasmic protein. The bacterial sphingolipid analogue (CerR) is typically of transmembrane nature, suggesting that capnine and sulfobacin B synthesis - unlike sphinganine synthesis - is potentially residing in the cytoplasm. As a dedicated short chain reductase like CapC has not yet been identified in *F. johnsoniae*, current studies suggest the probability that this reduction step might be catalysed by a promiscuous reductase with broad substrate specifity (Y. Liu et al., 2022). This broad substrate specificity is further validated by

the LC-MS detection of capnine after the deletion of SulA, suggesting that these steps might also be taken over by analogous or unspecific enzymes.
Bioinformatic topology analysis for the putative sulfobacin monooxygenase Fjoh_1748 and Fjoh_4604 revealed a high multipass membrane probability for both proteins. This occupation of distinct subcellular niches is consistent with the finding in eukaryotes, where the dihydroceramide monooxygenase (Des2) posesses three membrane spanning domains (Enomoto et al., 2006). While the initial synthesis of sulfobacin B likely occurs in the cytoplasm, its hydrophobicity necessitates that subsequent modifications, such as the conversion to sulfobacin D, might needs to take place within the lipid bilayer (Aguilar and De Mendoza, 2006).

As sulfonolipids mostly reside in the outer cellular membrane, the subsequent transport still needs to be investigated (Pitta et al., 1989). Export routes, such as the Type IX Secretion System (T9SS) are unlikely for the translocation of sulfobacins. Though the sulfobacin dependent gliding ability and the type IX secretion system are intertwined, the T9SS is specialized for protein secretion (McBride, 2019). Additionally, bioinformatic analysis of the putative sulfobacin monooxygenases (Fjoh_1748 and Fjoh_4604) confirmed the absence of Sec-type signal peptides or C-terminal secretion signals required for T9SS-mediated export. Another option of transport is the utilization of mammalian cell entry (MCE) proteins. MCE complexes have been shown to transport lipids and other hydrophobic molecules from the inner membrane to the outer membrane and vice versa (Malinverni and Silhavy, 2009). However, no genes for MCE homologs were found near the genes fjoh_1748 and fjoh_4604. Furthermore, the negative charge of the sulfate group resembles the phosphate moieties of lipid A, thereby allowing for stable binding to the TLR4-MD-2 complex (Su et al., 2021). It can be hypothesized that sulfobacins may be transported by the cell in an analogous manner to that of LPS. This LPS transport (Lpt pathway) could mediate the transport of capnoids such as sulfobacin B and D, providing an efficient route for their translocation in the outer membrane (Sperandeo et al., 2017).

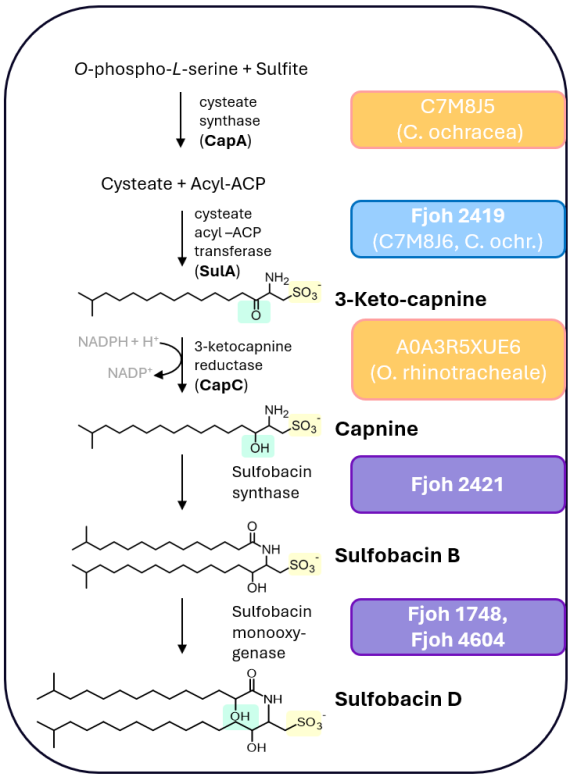

Figure 54: **The bacterial sulfobacin biosynthesis pathway:** This pathway is similar to the bacterial sphingolipid pathway. The putative sulfobacin synthase (Fjoh_2421) is likely located in the cytoplasm. Additional analysis of the 3-ketocapnine reductase (CapC) in other bacteria is needed for further validation. The orange boxes showcase bacteria, in which the genes for the enzymes were previously identified. The light blue box depicts the previously identified gene for SulA/ CapB in *F. johnsoniae* and *C. ochracea*. The purple boxes show the putative genes in *F. johnsoniae* for the enzymes involved in the downstream capnoid conversion.

Due to limitations in image processing and the diffraction limited resolution of the CLSM SP8 microscope, additional visualization of the proposed cytoplasmic SulA::mScarlet-I was inconclusive (Huang et al., 2009; Pawley, 2006). To bypass the diffraction limit, images were generated using the stimulated emission depletion (STED) microscope Stellaris 8 TAU-STED. However, significant photobleaching of the m-Scarlet-I fluorophore occurred under the high-intensity depletion laser (exceeding 10 MW/cm^2) (Bindels et al., 2017; Vicidomini et al., 2018) and attempts to stabilize the signal using the amine-based antifading reagent CitiFluor™ resulted in a decreased CytoLiner™ signal intensity, likely due to photoinduced electron transfer from the amines (Van Der Velde et al., 2016; Vogelsang et al., 2008).

4.2 Precursor-dependent bypass and thermal downregulation of sulfobacin biosynthesis

To investigate the regulation of SulA::mScarlet-I expression in response to precurser availability (1 mg/ml cysteate) and temperature variations, growth profiles were monitored alongside fluorescence microscopy. The expression levels were evaluated by quantifying the signal intensity of the cysteate acyl-ACP

transferase fusion protein during different growth phases.

During the course of this thesis, a *F. johnsoniae* Δ*2419* mutant became available, which allowed complementation of the tagged cysteate acyl-ACP transferase (SulA::mScarlet-I) using the replicating vector *pCP11*. This approach avoided the presence of two different gene copies within the cell, as the transconjugant lacked the chromosomal wildtype copy of SulA (fjoh_2419) (Snapp, 2009). Instead, the modified SulA::mScarlet-I was introduced via the replicating plasmid, resulting in the presence of multiple copies of the fusion gene within the cell. This increased gene dosage enabled the detection of the fusion protein under the CLSM SP8 microscope (Liang et al., 2000).

4.2.1 Impact of nutrient availability and exogenous precursors on SulA synthesis

Fluorescence intensities of individual cells increased as the culture reached the early stationary phase (10 hours). These elevated signals were interpreted as a direct increase in the expression of the SulA::mScarlet-I fusion protein. This observation aligns with the known regulation of proteins that are involved or associated with the type IX secretion system, which typically reach peak expression under nutrient-limited conditions (Kulkarni et al., 2017). Furthermore, studies by Stanier', 1946 showed that low nutrient concentrations trigger sulfonolipid-dependent gliding.

However, this nutrient-dependent regulation appears to be bypassed in the presence of an exogenous precursor. When exposing the *F. johnsoniae* Δ*2419, pCP11_fjoh_2419::mScarlet-I* strain to a high concentration of cysteate (1 mg/ml), the culture exhibited impaired growth compared to the control. It cannot be ruled out that this growth lag resulted from a variation in the initial inoculum density, despite the use of the same preculture for all experimental conditions. Despite this growth defect, the mScarlet-I fluorescence within individual cells increased notably during the exponential phase (6 hours). The early signal increase indicates a premature induction of SulA production. This finding indicates that cysteate abundance functions as a regulatory signal, overruling the metabolic control that was previously observed during exponential growth in nutrient-rich medium. The induced effect reaches a plateau after 10 hours, indicating that the cells likely have a metabolic saturation point upon entering the stationary phase (Liang et al., 2000). A decrease dependent on RNA-Polymerase-Omnibus-S (RpoS), a regulator of the general stress response, seems unlikely because the control cultures continued to show a significant increase in fluorescence intensity compared to the 6 hour mark. This intensity stagnation likely depicts a synthesis limitation further downstream in the pathway. While SulA activity is increased through cysteate abundance, the expression of subsequent enzymes may not increase proportionally (Battesti et al., 2011). A similar trend is reflected in the LC-MS data for *C. capnotolerans*, where the supplementation of cysteate induces an increased accumulation of capnine, while downstream sulfobacins do not increase proportionally. Consequently, this enzymatic overload of involved enzymes could trigger a negative feedback loop to prevent the overaccumulation of capnine and capnoids, thereby preventing effects like disrupted

membrane fluidity or cytotoxicity (Abbanat et al., 1986; Godchaux and Leadbe1ter, 1983).
This observation was not found for the complemented *F.johnsoniae* Δ*2419* knockout strain, as the replicating vector encoding SulA::mScarlet-I failed to restore sulfobacin biosynthesis and gliding motility. This loss of function is likely induced by steric hindrance, which could disrupt the assembly of a sulfobacin enzyme cluster or block the previously visualized pocket-like structure of SulA (Snapp, 2009). Additionally, utilizing the replicative plasmid *pCP11* could have resulted in pleiotropic effects due to the increased gene dosage compared to the wildtype (Braun et al., 2005; Zhu et al., 2017).
Expression of the fusion protein was additionally observed within the heterologous *E. coli* S17-1 λ pir host. The fluorescence demonstrates that the *F. johnsoniae* promoter is recognized during the transcription in *E. coli*.

4.2.2 Thermal constraints on SulA production

The expression of the cysteate acyl-ACP transferase not only reduced cell growth, but also resulted in lower fusion protein intensities when cultures were subjected to tested temperature extremes (14°C and 37°C). This suggests, that *de novo* sulfobacin biosynthesis is downregulated during thermal stress.
Given that sulfonolipids consitute up to 20% of the outer membrane (Pitta et al., 1989), an increase of unsaturated branched-chain fatty acids via the accumulation of specific capnoids would have been a plausible mechanism for cold adaptation. Such modifications typically increase the membrane fluidity in response to colder temperatures (Sohlenkamp and Geiger, 2016). The observed decrease in SulA::mScarlet-I expression indicates, that *F. johnsoniae* might conserve energy by reducing sulfobacin production in favor for more essential lipids (Russell and Cook, 1995). Alternatively, the temperatures of 14°C and 37°C may also be too extreme for the organism. At these temperatures, a global stress response, possibly mediated by RpoS-like regulators, might suppress sulfobacin-mediated adaptation strategies (Battesti et al., 2011).

4.3 Methodological evaluation of chromosomal tagging and expression constraints

In addition to the SulA::mScarlet-I fusion protein, the target proteins were intended to be examined using the *pYT313* based *in-frame* insertion of mScarlet-I. The suicide plasmid integration was confirmed for all four target genes and a successful *in-frame* insertion was accomplished for *fjoh_4604*, which validated the general experimental design (Mcbride and Kempf, 1996; Zhu et al., 2017).
Potential factors that influenced the high outcome of the wildtype genotype after the second recombination event include both biological and statistical constraints. Although the excision of a suicide plasmid theoretically yields a 50% probability for the mutant genotype (Reyrat et al., 1998; Quandt and Hynes, 1993), the actual recovery in this study seemed significantly lower. This shift is likely due to the metabolic

burden imposed by the 725 bp *mScarlet-I* tag. As this heterologous protein offers no advantage and potentially depletes the cellular amino acid pool, the resulting reduced fitness led to a decreased growth rate in the mutants (Bonomo and Gill, 2005; San Millan and MacLean, 2017). Consequently, during the non-selective growth phase, the restored wild-type cells outcompeted the slower growing mutants for nutrients and space (Vogwill and Maclean, 2015). This led to a higher abundance of wildtype bacteria, reducing the probability of screening a positive clone among the analyzed colonies (Ishikawa et al., 2018; Wu and Kaiser, 1996).

In the case of the confirmed *in-frame* insertion for *fjoh_4604*, the lack of signal likely stems from low native expression levels. As a single-copy fusion protein, the concentration of the proposed monooxygenase might fall below the detection threshold of fluorescence microscopy, a common challenge often avoided by using replicating plasmids like the *pCP11* plasmid (Hautefort and Hinton, 2000; Valdivia and Falkow, 1997). This detection limit could also explain the absence of fluorescence in recombinants after the first recombination event. Beyond the low expression levels, the resulting chromosomal architecture could induce polar effects within the operon, potentially disrupting the expression of the fusion protein and surrounding genes (Donnenberg and Kaper, 1991; Kalogeraki and Winans, 1997)

Furthermore, the high chance of Fjoh_4604 being a multipass membrane protein could also be a limiting factor for the intended C-terminal fusion. The enzyme integration into the inner membrane via the Sec or YidC pathways could be compromised by the mScarlet-I tag (Kiefer and Kuhn, 2007). The rapid, stable folding of mScarlet-I in the cytoplasm may sterically hinder translocation. This could lead to rapid proteolytic degradation or the formation of non-functional inclusion bodies (Bindels et al., 2017; Bukau et al., 2006).

4.4 Identification and characterization of the chemical diversity of sulfobacins in *Flavobacteriaceae* and *Weeksellaceae*

LC-MS/MS analysis was employed to characterize the sulfobacin-targeted lipid profile of several environmental *Flavobacteriaceae* strains (*Flavobacterium johnsoniae, Flavobacterium piscis*, and *Flavobacterium sp. LT0091*) and one aerobic, food related sulfobacin producer from the family *Weeksellaceae* (*Chryseobacterium capnotolerans*). By utilizing a transition list based on both established and potential sulfobacins (Hou et al., 2022) as well as gut-microbiome-derived data (Walker et al., 2017), several conserved sulfobacin candidates were identified.

Key findings include potential signals of ketocapnine, sulfobacin E, D, and F, alongside several previously uncharacterized sulfonolipids (*m/z* = 604,4608; 644,4877; 646,5031) in all tested species.

Furthermore, a significant overlap between the investigated strains and the sulfonolipids typically associated with the mammalian gut (*Alistipes* and *Odoribacter*) was observed (Walker et al., 2017). Specifically, signals for capnine and the potential sulfobacin *m/z* 588,4298 were detected in *F. johnsoniae,*

F. piscis, and *C. capnotolerans*, but were absent in *Flavobacterium sp. LT0091*. In contrast, sulfobacin B was identified in *F. johnsoniae, F. piscis*, and *Flavobacterium sp. LT0091*. The signal for *m/z* 602,4455 was detected in both *F. johnsoniae* and *F. piscis*, while the potential sulfobacin *m/z* = 616,4611 was present in all strains except *F. johnsoniae*.

The detection of *m/z* 588,602, 602,4455 and 616,4661 likely depicts the diversity of sulfobacins differing in methylene units. Furthermore, the identification of *m/z* 604,4608 suggests the presence of an additional hydroxylation to the detected signal *m/z* = 588,4298. Additionally, the pair *m/z* 644,4877 and 646,5031 possibly highlights variations in unsaturation within the capnoids.

Despite the absence of species-specific sulfobacins, *F. johnsoniae* and *C. capnotolerans*, both previously identified as sulfobacin producers (Godchaux and Leadbetter, 1980; von Heilborn et al., 2022), uniquely shared several signals (m/z 634,4670, 572,4349, 630,4761) and RIF-2. The unexpected presence of RIF-2 in F. johnsoniae warrants further investigation to exclude potential column carry-over.

The evolutionary conservation of these complex capnoids across environmental and gut-associated *Bacteroidota* species underscores the fundamental physiological advantage that transcends specific ecological niches (Abbanat et al., 1985; Sohlenkamp and Geiger, 2016).

It is important to note that the strains in this study were cultivated in complex media rather than chemically defined media. While these media support robust growth, they could introduce inherent variability, which could influence the detected capnoid diversity. Furthermore, the majority of the reported features were identified based primarily on accurate m/z values and alignment with expected retention times. Therefore, further investigation should include additional MS/MS data with the diagnostic fragments sulfate (*m/z* = 80,96) and capnine product ions (*m/z* = 333,21 and 350,24), as well as labeled sulfur (Godchaux and Leadbe1ter, 1983; Walker et al., 2017).

4.5 Cysteate supplementation modulates the sulfobacin profile in *Bacteroidota* strains

In order to investigate the influence of the precursor cysteate on the sulfobacin profiles of *C. capnotolerans, F. piscis*, and *F. sp. LT0091*, 1 mg/ml was added to the medium prior to cultivation.

Supplementation of the growth medium resulted in a shift in all investigated strains. In the gliding bacterium *C. capnotolerans*, the treatment induced a pronounced increase in the signal intensity for the precursor capnine (*m/z* = 350,2372) compared to standard conditions. This observation aligns with results previously reported for another species within the phylum *Bacteroidota*, *F. johnsoniae* (Vences-Guzmán et al., 2021).

Normal conditions led to the detection of 23 signals for potential sulfobacins, among them being sulfobacin A, D, E and F, as well as the sulfonolipid RIF-2, which has been shown to trigger multicellularity in

choanoflagellates (Woznica et al., 2016). Previous studies only identified sulfobacin A in *C. capnotolerans*, as well as two other sulfonolipids named cytolipin and flavolipin (von Heilborn et al., 2022).

Cysteate supplementation additionally lead to the detection of signals for sulfobacin B and C. A general increased signal strength facilitated structural verification via MS/MS, specifically identifying the diagnostic sulfonate fragment (*m/z* 80.9535) for capnine and the capnine product ion (*m/z* 350.2337) for sulfobacin A.

As previously stated, the increase in the capnine signal likely reflects a high degree of metabolic plasticity, allowing *C. capnotolerans* and other possible strains from the phylum *Bacteroidota* to adapt rapidly to fluctuating sulfur availability (Abbanat et al., 1986, Sohlenkamp and Geiger, 2016).

The additional detection of complex capnoids such as sulfobacin B and C after cysteate supplementation suggests that the primary biosynthetic route, potentially leading to sulfobacin A, likely reached a saturation limit. The accumulation of the precursor capnine may have surpassed a critical threshold, thereby facilitating the synthesis of non-essential sulfobacins like sulfobacin B or C (Y. M. Zhang and Rock, 2008). Furthermore, it should be noted that the use of a complex, non-standardized medium (tryptone soy broth) likely influenced the diversity of the detected sulfobacins.

In contrast to *C. capnotolerans*, precursor supplementation in *F. piscis* and *F. sp. LT0091* cultures led to a decrease in capnoid signal intensities. Despite the buffer content in the CYE medium, the addition of cysteate may have induced physiological stress. Such stressors can trigger a general stress response, potentially decreasing metabolic resources for non-essential lipid synthesis (Battesti et al., 2011). Furthermore, these species might maintain a membrane composition where sulfonolipid concentrations are strictly controlled (Sohlenkamp and Geiger, 2016; Y. M. Zhang and Rock, 2008).

While the genetic potential for capnine synthesis is widely distributed among *Bacteroidota* (Older et al., 2024), the low signal intensities observed for the gliding bacterium *F. sp. LT0091* suggests that this strain may be a low-producer under the tested conditions.

5 Conclusion and Outlook

This work provides valuable insights into the subcellular organization, structural diversity, and environmental regulation of the sulfobacin biosynthetic pathway in *Flavobacterium johnsoniae* and related *Bacteroidota*. While many studies have focused on common microbe derived lipids such as short chain fatty acids and phospholipids, this work suggests that sulfobacins might be equally important to bacterial physiology and inter-kingdom signaling (Stankeviciute et al., 2022; Older et al., 2024).

Structural Analogies and Spatial Organization: Bioinformatic topology analysis showed that the spatial organization of the sulfobacin pathway mirrors the bacterial sphingolipid pathway. The identification of the cysteate acyl-ACP transferase (SulA, Fjoh_2419) and the sulfobacin synthase (Fjoh_2421) as soluble cytoplasmic proteins and the prediction of the 3-ketocapnine reductase (CapC) as a cytoplasmic enzyme suggests, that the initial steps of sulfobacin synthesis occur in the cytoplasm. In contrast, the multipass membrane nature of the putative monooxygenases (Fjoh_1748 and Fjoh_4604) indicates that later modifications might transition to the lipid bilayer, possibly utilizing an Lpt transport mechanism for translocation to the outer membrane.

Strategic adaptation and expression constraints: The increase of fluorescence of the tagged SulA, observed during the stationary phase and cysteate supplementation (1 mg/ml), hints to a substrate induced regulatory mechanism. This might allow selected *Bacteroidota* to adjust their membrane composition to fluctuating environmental conditions, ensuring survival and motility during nutrient limitation (Sohlenkamp and Geiger, 2016). However, the failure of the SulA::mScarlet-I fusion to restore motility in the SulA knockout mutant suggests that the C-terminal tag might sterically block the enzyme's active site.

Conservation across environmental and gut-associated strains: A key finding of this work is the lipid profile overlap between environmental *Flavobacteriaceae*, food-related *Weeksellaceae*, and gut-associated *Bacteroidota* (*Alistipes* and *Odoribacter*). By identifying signals for capnine, sulfobacin B, and potential sulfonolipids (*m/z* 588,4298 and 616,4611) across multiple species, which demonstrates that capnoid biosynthesis is a fundamental physiological feature within the phylum *Bacteroidota*. The

detection of diverse methylene-unit variations, additional hydroxylations and variations in unsaturation depicts the chemical complexity of sulfobacins.

Breakthrough in *C. capnotolerans* lipidomics: While previous literature only identified sulfobacin A and specialized lipids like flavolipin (von Heilborn et al., 2022), this work provides the first evidence for a much broader sulfobacin abundance in *C. capnotolerans*, including sulfobacins B, C, D, E, and F, as well as the signaling molecule RIF-2. The presence of these complex capnoids upon cysteate supplementation show a high degree of metabolic plasticity. This suggests that once the primary biosynthetic pathway reaches saturation, excess capnine is used for the synthesis of different non-essential sulfobacin molecules.

Outlook:

Further investigation into the sulfobacin biosynthesis and its role in bacterial physiology is needed. First, the cytoplasmic nature of SulA (Fjoh_2419) should be confirmed through a similar experimental approach to Uchendu et al., 2024, where chloroform-saturated Tris buffer would lead to outer membrane permeabilization and a corresponding loss of fluorescence for membrane-associated proteins.

Furthermore, the current limitation of absolute identification due to a lack of MS/MS data should be addressed. Utilizing labeled sulfur would provide definitive proof of sulfobacin signals and facilitate the characterization of underexplored derivatives (Godchaux and Leadbe1ter, 1983; Walker et al., 2017). Given the first-time identification of a variety of sulfobacins and RIF-2 in *C. capnotolerans*, future studies should prioritize the functional characterization of these molecules.

In addition, as the selection of sulfobacin producers is currently biased toward soil and food related isolates, it is essential to broaden the investigation of bacteria in other environmental niches. This would further elucidate the understanding of sulfobacin diversity and their evolutionary role (Older et al., 2024; Sohlenkamp and Geiger, 2016).

Lastly, a lipidomic analysis using the *pCP11_fjoh_2419::mScarlet-I* plasmid in *E. coli* S17-1 λ pir could verify, that the C-terminal mScarlet-I fusion results in a misfolded, unfunctional enzyme. Since heterologous expression of *sulA* has previously been shown to induce capnine-like molecules in *E. coli* (Vences-Guzmán et al., 2021), this would provide final clarity on the loss of function observed.

Bibliography

Abbanat, D. R., Godchaux, W., & Leadbetter, E. R. (1988). *Surface-induced synthesis of new sulfonolipids in the gliding bacterium Cytophaga johnsonae* (tech. rep.).

Abbanat, D. R., Godchaux, W., Polychroniou, G., & Leadbetter, E. R. (1985). Biosynthesis of a sulfonolipid in gliding bacteria. *Biochemical and Biophysical Research Communications*, *130*(2), 873–878.

Abbanat, D. R., Leadbetter, E. R., Godchaux, W., & Escher, A. (1986). Sulphonolipids are molecular determinants of gliding motility. *Nature 1986 324:6095*, *324*(6095), 367–369.

Agarwal, S., Hunnicutt, D. W., & Mcbride, M. J. (1997). *Cloning and characterization of the Flavobacterium johnsoniae (Cytophaga johnsonae) gliding motility gene, gldA* (tech. rep.). www.pnas.org.

Aguilar, P. S., & De Mendoza, D. (2006, December). Control of fatty acid desaturation: A mechanism conserved from bacteria to humans.

Alegado, R. A., Brown, L. W., Cao, S., Dermenjian, R. K., Zuzow, R., Fairclough, S. R., Clardy, J., & King, N. (2012). A bacterial sulfonolipid triggers multicellular development in the closest living relatives of animals. *eLife*, *1*(1), e00013.

Battesti, A., Majdalani, N., & Gottesman, S. (2011). The RpoS-mediated general stress response in escherichia coli *.

Beard, J. A., & Click, B. H. (2020). The burden of cost in inflammatory bowel disease: a medical economic perspective. *Current opinion in gastroenterology*, *36*(4), 310–316.

Beemelmanns, C., Woznica, A., Alegado, R. A., Cantley, A. M., King, N., & Clardy, J. (2014). Synthesis of the rosette-inducing factor RIF-1 and analogs. *Journal of the American Chemical Society*, *136*(29), 10210–10213.

Bertani, G. (1951). Studies on lysogenesis. I. The mode of phage liberation by lysogenic Escherichia coli. *Journal of bacteriology*, *62*(3), 293–300.

Bindels, D. S., Haarbosch, L., Van Weeren, L., Postma, M., Wiese, K. E., Mastop, M., Aumonier, S., Gotthard, G., Royant, A., Hink, M. A., & Gadella, T. W. (2017). MScarlet: A bright monomeric red fluorescent protein for cellular imaging. *Nature Methods*, *14*(1), 53–56.

BLIGH, E. G., & DYER, W. J. (1959). A rapid method of total lipid extraction and purification. *Canadian journal of biochemistry and physiology*, *37*(8), 911–917.

Bonomo, J., & Gill, R. T. (2005). Amino acid content of recombinant proteins influences the metabolic burden response. *Biotechnology and Bioengineering*, *90*(1), 116–126.

Braun, T. F., Khubbar, M. K., Saffarini, D. A., & McBride, M. J. (2005). Flavobacterium johnsoniae gliding motility genes identified by mariner mutagenesis. *Journal of bacteriology*, *187*(20), 6943–6952.

Brown, E. M., Ke, X., Hitchcock, D., Jeanfavre, S., Avila-Pacheco, J., Nakata, T., Arthur, T. D., Fornelos, N., Heim, C., Franzosa, E. A., Watson, N., Huttenhower, C., Haiser, H. J., Dillow, G., Graham, D. B., Finlay, B. B., Kostic, A. D., Porter, J. A., Vlamakis, H., … Xavier, R. J. (2019). Bacteroides-Derived Sphingolipids Are Critical for Maintaining Intestinal Homeostasis and Symbiosis. *Cell Host and Microbe*, *25*(5), 668–680.

Buffie, C. G., Bucci, V., Stein, R. R., McKenney, P. T., Ling, L., Gobourne, A., No, D., Liu, H., Kinnebrew, M., Viale, A., Littmann, E., Van Den Brink, M. R., Jenq, R. R., Taur, Y., Sander, C., Cross, J. R., Toussaint, N. C., Xavier, J. B., & Pamer, E. G. (2014). Precision microbiome reconstitution restores bile acid mediated resistance to Clostridium difficile. *Nature 2014 517:7533*, *517*(7533), 205–208.

Bukau, B., Weissman, J., & Horwich, A. (2006). Molecular chaperones and protein quality control. *Cell*, *125*(3), 443–451.

Burisch, J., Jess, T., Martinato, M., & Lakatos, P. L. (2013). The burden of inflammatory bowel disease in Europe. *Journal of Crohn's & colitis*, *7*(4), 322–337.

Burisch, J., Vardi, H., Schwartz, D., Friger, M., Kiudelis, G., Kupčinskas, J., Fumery, M., Gower-Rousseau, C., Lakatos, L., Lakatos, P. L., D'Incà, R., Sartini, A., Valpiani, D., Giannotta, M., Arebi, N., Duricova, D., Bortlik, M., Chetcuti Zammit, S., Ellul, P., … Whitehead, E. (2020). Health-care costs of inflammatory bowel disease in a pan-European, community-based, inception cohort during 5 years of follow-up: a population-based study. *The lancet. Gastroenterology & hepatology*, *5*(5), 454–464.

Chaudhari, S. N., McCurry, M. D., & Devlin, A. S. (2021). Chains of evidence from correlations to causal molecules in microbiome-linked diseases. *Nature chemical biology*, *17*(10), 1046–1056.

Cummings, J. H., & Macfarlane, G. T. (1997). Role of intestinal bacteria in nutrient metabolism. *JPEN. Journal of parenteral and enteral nutrition*, *21*(6), 357–365.

Dagert, M., & Ehrlich, S. D. (1979). Prolonged incubation in calcium chloride improves the competence of Escherichia coli cells. *Gene*, *6*(1), 23–28.

Dai, H., Han, J., Wang, T., Yin, W. B., Chen, Y., & Liu, H. (2023). Recent advances in gut microbiota-associated natural products: structures, bioactivities, and mechanisms. *Natural product reports*, *40*(6), 1078–1093.

Daims, H., Lücker, S., & Wagner, M. (2006). daime, a novel image analysis program for microbial ecology and biofilm research. *Environmental microbiology*, *8*(2), 200–213.

Donnenberg, M. S., & Kaper, J. B. (1991). Construction of an eae deletion mutant of enteropathogenic Escherichia coli by using a positive-selection suicide vector. *Infection and immunity*, *59*(12), 4310–4317.

Durack, J., & Lynch, S. V. (2019). The gut microbiome: Relationships with disease and opportunities for therapy. *The Journal of experimental medicine*, *216*(1), 20–40.

Dziarski, R., Park, S. Y., Kashyap, D. R., Dowd, S. E., & Gupta, D. (2016). Pglyrp-Regulated Gut Microflora Prevotella falsenii, Parabacteroides distasonis and Bacteroides eggerthii Enhance and Alistipes finegoldii Attenuates Colitis in Mice. *PloS one*, *11*(1).

Eckroat, T. J., Greguske, C., & Hunnicutt, D. W. (2021). The Type 9 Secretion System Is Required for Flavobacterium johnsoniae Biofilm Formation. *Frontiers in microbiology*, *12*.

Enomoto, A., Omae, F., Miyazaki, M., Kozutsumi, Y., Yubisui, T., & Suzuki, A. (2006). Dihydroceramide:sphinganine C-4-hydroxylation requires Des2 hydroxylase and the membrane form of cytochrome b5. *Biochemical Journal*, *397*(2), 289–295.

Ferrières, L., Hémery, G., Nham, T., Guérout, A. M., Mazel, D., Beloin, C., & Ghigo, J. M. (2010). Silent Mischief: Bacteriophage Mu Insertions Contaminate Products of Escherichia coli Random Mutagenesis Performed Using Suicidal Transposon Delivery Plasmids Mobilized by Broad-Host-Range RP4 Conjugative Machinery. *Journal of Bacteriology*, *192*(24), 6418.

Flint, H. J., Scott, K. P., Duncan, S. H., Louis, P., & Forano, E. (2012). Microbial degradation of complex carbohydrates in the gut. *Gut microbes*, *3*(4).

Geiger, O., González-Silva, N., López-Lara, I. M., & Sohlenkamp, C. (2010). Amino acid-containing membrane lipids in bacteria. *Progress in Lipid Research*, *49*(1), 46–60.

Godchaux, W., & Leadbetter, E. R. (1980). Capnocytophaga spp. contain sulfonolipids that are novel in procaryotes. *Journal of bacteriology*, *144*(2), 592–602.

Godchaux, W., & Leadbe1ter, E. R. (1983). Unusual Sulfonolipids Are Charactenrstic of the Cytophaga-Flexibacter Group. *JOURNAL OF BACTERIOLOGY*, *1533*(3), 1238–1246. https://journals.asm.org/journal/jb

Haiser, H. J., & Turnbaugh, P. J. (2013). Developing a metagenomic view of xenobiotic metabolism. *Pharmacological research*, *69*(1), 21–31.

Hallgren, J., Tsirigos, K. D., Pedersen, M. D., Almagro Armenteros, J. J., Marcatili, P., Nielsen, H., Krogh, A., & Winther, O. (2022). DeepTMHMM predicts alpha and beta transmembrane proteins using deep neural networks.

Hanahan, D. (1983). Studies on transformation of Escherichia coli with plasmids. *Journal of molecular biology*, *166*(4), 557–580.

Hautefort, I., & Hinton, J. C. D. (2000). *Measurement of bacterial gene expression in vivo* (tech. rep.). The royal society. http://royalsocietypublishing.org/rstb/article-pdf/355/1397/601/85665/rstb.2000.0601.pdf

Hjertén, S. (1961). Agarose as an anticonvection agent in zone electrophoresis. *Biochimica et biophysica acta*, *53*(3), 514–517.

Hou, L., Tian, H. Y., Wang, L., Ferris, Z. E., Wang, J., Cai, M., Older, E. A., Raja, M. R. K., Xue, D., Sun, W., Nagarkatti, P., Nagarkatti, M., Chen, H., Fan, D., Tang, X., & Li, J. (2022). Identification and Biosynthesis of Pro-Inflammatory Sulfonolipids from an Opportunistic Pathogen Chryseobacterium gleum. *ACS Chemical Biology*, *17*(5), 1197–1206.

Huang, B., Bates, M., & Zhuang, X. (2009). Super resolution fluorescence microscopy. *Annual review of biochemistry*, *78*, 993.

Ishikawa, M., Yokoe, S., Kato, S., & Hori, K. (2018). Efficient counterselection for Methylococcus capsulatus (Bath) by using a mutated pheS gene. *Applied and Environmental Microbiology*, *84*(23).

Jumper, J., Evans, R., Pritzel, A., Green, T., Figurnov, M., Ronneberger, O., Tunyasuvunakool, K., Bates, R., Žídek, A., Potapenko, A., Bridgland, A., Meyer, C., Kohl, S. A., Ballard, A. J., Cowie, A., Romera-Paredes, B., Nikolov, S., Jain, R., Adler, J., … Hassabis, D. (2021). Highly accurate protein structure prediction with AlphaFold. *Nature 2021 596:7873*, *596*(7873), 583–589.

Kalogeraki, V. S., & Winans, S. C. (1997). *Suicide plasmids containing promoterless reporter genes can simultaneously disrupt and create fusions to target genes of diverse bacteria* (tech. rep.). Gene.

Kamiyama, T., Umino, T., Satoh, T., Sawairi, S., Shirane, M., Ohshima, S., & Yokose, K. (1995). Sulfobacins A and B, novel von Willebrand factor receptor antagonists. I. Production, isolation, characterization and biological activities. *The Journal of antibiotics*, *48*(9), 924–928.

Kaneshiro, E. S., Hunt, S. M., & Watanabe, Y. (2008). Bacteriovorax stolpii proliferation and predation without sphingophosphonolipids. *Biochemical and biophysical research communications*, *367*(1), 21–25.

Kaplan, G. G., & Ng, S. C. (2017). Understanding and Preventing the Global Increase of Inflammatory Bowel Disease. *Gastroenterology*, *152*(2), 313–321.

Kaplan, G. G., & Windsor, J. W. (2020). The four epidemiological stages in the global evolution of inflammatory bowel disease. *Nature Reviews Gastroenterology & Hepatology 2020 18:1*, *18*(1), 56–66.

Kato, M., Watanabe, K., Tanaka-Bandoh, K., Watanabe, K., & Ueno, K. (1995). Sphingolipid composition in Bacteroides species. *Anaerobe*, *1*(2), 135–139.

Kawazoe, R., Okuyama, H., Reichardt, W., & Sasaki1, S. (1991). *Phospholipids and a Novel Glycine-Containing Lipoamino Acid in Cytophaga johnsonae Stanier Strain C21* (tech. rep. No. 17).

Kharade, S. S., & McBride, M. J. (2014). Flavobacterium johnsoniae chitinase ChiA is required for chitin utilization and is secreted by the type IX secretion system. *Journal of bacteriology*, *196*(5), 961–970.

Kharade, S. S., & McBride, M. J. (2015). Flavobacterium johnsoniae PorV is required for secretion of a subset of proteins targeted to the type IX secretion system. *Journal of bacteriology*, *197*(1), 147–158.

Kiefer, D., & Kuhn, A. (2007). YidC as an essential and multifunctional component in membrane protein assembly. *International review of cytology*, *259*, 113–138.

Kohayashi, i., Mikami, S., Shigemori, I., Shimonishia, Y., Izutah, S., & Yoshidab, S. (1995). Flavocristamides A and B, New DNA Polymerase a Inhibitors from a Marine Bacterium Flavobacterium sp. *Tetrahedron*, *51*(38), 10487–10490.

Kongpracha, P., Wiriyasermkul, P., Isozumi, N., Moriyama, S., Kanai, Y., & Nagamori, S. (2022). Simple But Efficacious Enrichment of Integral Membrane Proteins and Their Interactions for In-Depth Membrane Proteomics. *Molecular & Cellular Proteomics*, *21*(5), 100206.

Kulkarni, S. S., Johnston, J. J., Zhu, Y., Hying, Z. T., & McBride, M. J. (2019). The Carboxy-Terminal Region of Flavobacterium johnsoniae SprB Facilitates Its Secretion by the Type IX Secretion System and Propulsion by the Gliding Motility Machinery. *Journal of bacteriology*, *201*(19).

Kulkarni, S. S., Zhu, Y., Brendel, C. J., & McBride, M. J. (2017). Diverse C-terminal sequences involved in Flavobacterium johnsoniae protein secretion. *Journal of Bacteriology*, *199*(12).

Kumar, A., Yassin, N., Marley, A., Bellato, V., Foppa, C., Pellino, G., Myrelid, P., Millan, M., Gros, B., Avellaneda, N., Catalan-Serra, I., El-Hussuna, A., Cunha Neves, J. A., Roseira, J., Cunha, M. F., Verstockt, B., Bettenworth, D., Mege, D., & Brookes, M. J. (2023). Crossing barriers: the burden of inflammatory bowel disease across Western Europe. *Therapeutic advances in gastroenterology*, *16*.

Lauber, F., Deme, J. C., Lea, S. M., & Berks, B. C. (2018). Type 9 secretion system structures reveal a new protein transport mechanism. *Nature 2018 564:7734*, *564*(7734), 77–82.

Lauber, F., Deme, J. C., Liu, X., Kjær, A., Miller, H. L., Alcock, F., Lea, S. M., & Berks, B. C. (2024). Structural insights into the mechanism of protein transport by the Type 9 Secretion System translocon. *Nature Microbiology 2024 9:4*, *9*(4), 1089–1102.

Lavelle, A., & Sokol, H. (2020). Gut microbiota-derived metabolites as key actors in inflammatory bowel disease.

Lederberg, J., & Tatum, E. L. (1946). Gene recombination in Escherichia coli. *Nature*, *158*(4016), 558.

Liang, S. T., Xu, Y. C., Dennis, P., & Bremer, H. (2000). mRNA composition and control of bacterial gene expression. *Journal of Bacteriology*, *182*(11), 3037–3044.

Lima, S. F., Gogokhia, L., Viladomiu, M., Chou, L., Putzel, G., Jin, W. B., Pires, S., Guo, C. J., Gerardin, Y., Crawford, C. V., Jacob, V., Scherl, E., Brown, S. E., Hambor, J., & Longman, R. S. (2022). Transferable

Immunoglobulin A-Coated Odoribacter splanchnicus in Responders to Fecal Microbiota Transplantation for Ulcerative Colitis Limits Colonic Inflammation. *Gastroenterology*, *162*(1), 166–178.

Liu, J., McBride, M. J., & Subramaniam, S. (2007). Cell surface filaments of the gliding bacterium Flavobacterium johnsoniae revealed by cryo-electron tomography. *Journal of Bacteriology*, *189*(20), 7503–7506.

Liu, Y., Wei, Y., Tong, Teh, M., Liu, D., Zhou, Y., Zhao, S., Ang, L., Zhao, H., & Zhang, Y. (2022). Identification and Characterization of the Biosynthetic Pathway of the Sulfonolipid Capnine. *ACS Chemical Biology*.

Maeda, J., Nishida, M., Takikawa, H., Yoshida, H., Azuma, T., Yoshida, M., & Mizushina, Y. (2010). Inhibitory effects of sulfobacin B on DNA polymerase and inflammation. *International journal of molecular medicine*, *26*(5), 751–758.

Malinverni, J. C., & Silhavy, T. J. (2009). *An ABC transport system that maintains lipid asymmetry in the Gram-negative outer membrane* (tech. rep.). PNAS. www.pnas.org/cgi/content/full/

Mark, B. M., & Zhu, Y. (2013). Gliding motility and Por secretion system genes are widespread among members of the phylum bacteroidetes. *Journal of bacteriology*, *195*(2), 270–278.

Mcbride, M. J., & Kempf, M. J. (1996). *Development of Techniques for the Genetic Manipulation of the Gliding Bacterium Cytophaga johnsonae* (tech. rep. No. 3).

McBride, M. J. (2019). Bacteroidetes Gliding Motility and the Type IX Secretion System. *Microbiology Spectrum*, *7*(1), 0002–2018.

McBride, M. J., & Nakane, D. (2015). Flavobacterium gliding motility and the type IX secretion system.

McBride, M. J., Xie, G., Martens, E. C., Lapidus, A., Henrissat, B., Rhodes, R. G., Goltsman, E., Wang, W., Xu, J., Hunnicutt, D. W., Staroscik, A. M., Hoover, T. R., Cheng, Y. Q., & Stein, J. L. (2009). Novel features of the polysaccharide-digesting gliding bacterium Flavobacterium johnsoniae as revealed by genome sequence analysis. *Applied and Environmental Microbiology*, *75*(21), 6864–6875.

Nelson, S. S., Bollampalli, S., & McBride, M. J. (2008). SprB is a cell surface component of the Flavobacterium johnsoniae gliding motility machinery. *Journal of Bacteriology*, *190*(8), 2851–2857.

Neyrinck, A. M., Schüppel, V. L., Lockett, T., Haller, D., & Delzenne, N. M. (2016). Microbiome and metabolic disorders related to obesity: Which lessons to learn from experimental models? *Trends in Food Science and Technology*, *57*, 256–264.

Older, E. A., Mitchell, M. K., Campbell, A., Lian, X., Madden, M., Wang, Y., van de Wal, L. E., Zaw, T., VanderVeen, B. N., Tatum, R., Murphy, E. A., Chen, Y. H., Fan, D., Ellermann, M., & Li, J. (2025). Human gut commensal Alistipes timonensis modulates the host lipidome and delivers anti-inflammatory outer membrane vesicles to suppress colitis in an Il10-deficient mouse model. *Gut microbes*, *17*(1).

Older, E. A., Zhang, J., Ferris, Z. E., Xue, D., Zhong, Z., Mitchell, M. K., Madden, M., Wang, Y., Chen, H., Nagarkatti, P., Nagarkatti, M., Fan, D., Ellermann, M., Li, Y. X., & Li, J. (2024). Biosynthetic enzyme anal-

ysis identifies a protective role for TLR4-acting gut microbial sulfonolipids in inflammatory bowel disease. *Nature communications*, *15*(1), 9371.

Omran, A. R. (2005). The Epidemiologic Transition: A Theory of the Epidemiology of Population Change. *The Milbank Quarterly*, *83*(4), 731.

Pawley, J. B. (2006). Handbook of biological confocal microscopy: Third edition. *Handbook of Biological Confocal Microscopy: Third Edition*, 1–985.

Pekkle Lam, H. Y., Lai, M. J., Wu, W. J., Chin, Y. H., Chao, H. J., Chen, L. K., Peng, S. Y., & Chang, K. C. (2023). Isolation and characterization of bacteriophages with activities against multi-drug-resistant Acinetobacter nosocomialis causing bloodstream infection in vivo. *Journal of Microbiology, Immunology and Infection*, *56*(5), 1026–1035.

Pitta, T. P., Leadbetter, E. R., & Godchaux, W. (1989). Increase of ornithine amino lipid content in a sulfonolipid-deficient mutant of Cytophaga johnsonae. *Journal of bacteriology*, *171*(2), 952–957.

Quandt, J., & Hynes, M. F. (1993). Versatile suicide vectors which allow direct selection for gene replacement in gram-negative bacteria. *Gene*, *127*(1), 15–21.

Radka, C. D., Frank, M. W., Rock, C. O., & Yao, J. (2020). Fatty acid activation and utilization by Alistipes finegoldii, a representative Bacteroidetes resident of the human gut microbiome. *Molecular microbiology*, *113*(4), 807–825.

Raetz, C. R. H., Reynolds, C. M., Stephen Trent, M., & Bishop, R. E. (2007). Lipid A Modification Systems in Gram-Negative Bacteria. *Annu Rev Biochem*, *32*, 44.

Raetz, C. R., & Whitfield, C. (2002). Lipopolysaccharide endotoxins.

Reyrat, J.-M., Pelicic, V., Gicquel, B., & Rappuoli, R. (1998). Counterselectable markers: untapped tools for bacterial genetics and pathogenesis. *Infection and immunity*, *66*(9), 4011–4017.

Russell, J. B., & Cook, G. M. (1995). *Energetics of Bacterial Growth: Balance of Anabolic and Catabolic Reactions* (tech. rep. No. 1).

San Millan, A., & MacLean, R. C. (2017). Fitness Costs of Plasmids: a Limit to Plasmid Transmission. *Microbiology spectrum*, *5*(5).

Shrivastava, A., Johnston, J. J., Van Baaren, J. M., & McBride, M. J. (2013). Flavobacterium johnsoniae GldK, GldL, GldM, and SprA are required for secretion of the cell surface gliding motility adhesins sprb and remA. *Journal of Bacteriology*, *195*(14), 3201–3212.

Shrivastava, A., Lele, P. P., & Berg Correspondence, H. C. (2015). A Rotary Motor Drives Flavobacterium Gliding. *Current Biology*, *25*, 338–341.

Shrivastava, A., Rhodes, R. G., Pochiraju, S., Nakane, D., & McBride, M. J. (2012). Flavobacterium johnsoniae RemA is a mobile cell surface lectin involved in gliding. *Journal of bacteriology*, *194*(14), 3678–3688.

Shrivastava, A., Roland, T., & Berg, H. C. (2016). The Screw-Like Movement of a Gliding Bacterium Is Powered by Spiral Motion of Cell-Surface Adhesins. *Biophysical Journal*.

Singer, S. J., & Nicolson, G. L. (1972). The fluid mosaic model of the structure of cell membranes. *Science (New York, N.Y.)*, *175*(4023), 720–731.

Smeyne, R. J., Schilling, K., Robertson, L., Luk, D., Oberdick, J., Curran, T., & Morgan, J. I. (1992). fos-lacZ transgenic mice: mapping sites of gene induction in the central nervous system. *Neuron*, *8*(1), 13–23.

Smith, H. O., & Welcox, K. W. (1970). A restriction enzyme from Hemophilus influenzae. I. Purification and general properties. *Journal of molecular biology*, *51*(2), 379–391.

Snapp, E. L. (2009). Fluorescent Proteins: A Cell Biologist's User Guide. *Trends in cell biology*, *19*(11), 649.

Sohlenkamp, C., & Geiger, O. (2016). Bacterial membrane lipids: diversity in structures and pathways. *FEMS microbiology reviews*, *40*(1), 133–159.

Sperandeo, P., Martorana, A. M., & Polissi, A. (2017, November). The lipopolysaccharide transport (Lpt) machinery: A nonconventional transporter for lipopolysaccharide assembly at the outer membrane of Gram-negative bacteria.

Stanier', R. Y. (1946). *STUDIES ON NONFRUITING MYXOBACTERIA I. CYTOPHAGA JOHNSONAE, N. SP., A CHITIN-DECOMPOSING MYXOBACTERIUM* (tech. rep.). https://journals.asm.org/journal/jb

Stankeviciute, G., Guan, Z., Goldfine, H., & Klein, E. A. (2019). Caulobacter crescentus Adapts to Phosphate Starvation by Synthesizing Anionic Glycoglycerolipids and a Novel Glycosphingolipid. *mBio*, *10*(2).

Stankeviciute, G., Tang, P., Ashley, B., Chamberlain, J. D., Hansen, M. E., Coleman, A., D'Emilia, R., Fu, L., Mohan, E. C., Nguyen, H., Guan, Z., Campopiano, D. J., & Klein, E. A. (2022). Convergent evolution of bacterial ceramide synthesis. *Nature Chemical Biology*, *18*(3), 305–312.

Su, L., Athamna, M., Wang, Y., Wang, J., Freudenberg, M., Yue, T., Wang, J., Marie Moresco, E. Y., He, H., Zor, T., & Beutler, B. (2021). Sulfatides are endogenous ligands for the TLR4-MD-2 complex. *PNAS*.

Uchendu, C. G., Guan, Z., & Klein, E. A. (2024). Spatial organization of bacterial sphingolipid synthesis enzymes.

Valdivia, R. H., & Falkow, S. (1997). Fluorescence-based isolation of bacterial genes expressed within host cells. *Science (New York, N.Y.)*, *277*(5334), 2007–2011.

van Meer, G., Voelker, D. R., & Feigenson, G. W. (2008). *Membrane lipids: where they are and how they behave* (tech. rep.). www.nature.com/reviews/molcellbio

Van Der Velde, J. H., Oelerich, J., Huang, J., Smit, J. H., Aminian Jazi, A., Galiani, S., Kolmakov, K., Guoridis, G., Eggeling, C., Herrmann, A., Roelfes, G., & Cordes, T. (2016). A simple and versatile design concept for fluorophore derivatives with intramolecular photostabilization. *Nature Communications 2016 7:1*, *7*(1), 10144–.

Vences-Guzmán, M. Á., Peña-Miller, R., Hidalgo-Aguilar, N. A., Vences-Guzmán, M. L., Guan, Z., & Sohlenkamp, C. (2021). Identification of the Flavobacterium johnsoniae cysteate-fatty acyl transferase required for capnine synthesis and for efficient gliding motility. *Environmental Microbiology*, *23*(5), 2448–2460.

Vicidomini, G., Bianchini, P., & Diaspro, A. (2018). STED super-resolved microscopy. *Nature Methods 2018 15:3*, *15*(3), 173–182.

Vogelsang, J., Kasper, R., Steinhauer, C., Person, B., Heilemann, M., Sauer, M., Tinnefeld, P., Vogelsang, J., Steinhauer, C., Person, B., Tinnefeld, P., Kasper, R., Heilemann, M., & Sauer Angew Laserphysik, M. (2008). Fluorescence Spectroscopy A Reducing and Oxidizing System Minimizes Photobleaching and Blinking of Fluorescent Dyes**. *Angew. Chem. Int. Ed*, *47*, 5465–5469.

Vogwill, T., & Maclean, R. C. (2015). The genetic basis of the fitness costs of antimicrobial resistance: a meta-analysis approach. *Evolutionary applications*, *8*(3), 284–295.

von Heilborn, D. H., Nover, L. L., Weber, M., Hölzl, G., Gisch, N., Waldhans, C., Mittler, M., Kreyenschmidt, J., Woehle, C., Hüttel, B., & Lipski, A. (2022). Polar lipid characterization and description of Chryseobacterium capnotolerans sp. nov., isolated from high CO2-containing atmosphere and emended descriptions of the genus Chryseobacterium, and the species C. balustinum, C. daecheongense, C. formosense, C. gleum, C. indologenes, C. joostei, C. scophthalmum and C. ureilyticum. *International Journal of Systematic and Evolutionary Microbiology*, *72*(5).

Walker, A., Pfitzner, B., Harir, M., Schaubeck, M., Calasan, J., Heinzmann, S. S., Turaev, D., Rattei, T., Endesfelder, D., Castell, W. Z., Haller, D., Schmid, M., Hartmann, A., & Schmitt-Kopplin, P. (2017). Sulfonolipids as novel metabolite markers of Alistipes and Odoribacter affected by high-fat diets. *Scientific Reports 2017 7:1*, *7*(1), 1–10.

Woznica, A., Cantley, A. M., Beemelmanns, C., Freinkman, E., Clardy, J., & King, N. (2016). Bacterial lipids activate, synergize, and inhibit a developmental switch in choanoflagellates. *Proceedings of the National Academy of Sciences of the United States of America*, *113*(28), 7894–7899.

Wu, S. S., & Kaiser, D. (1996). Markerless deletions of pil genes in Myxococcus xanthus generated by counterselection with the Bacillus subtilis sacB gene. *Journal of bacteriology*, *178*(19), 5817–5821.

Yard, B. A., Carter, L. G., Johnson, K. A., Overton, I. M., Dorward, M., Liu, H., McMahon, S. A., Oke, M., Puech, D., Barton, G. J., Naismith, J. H., & Campopiano, D. J. (2007). The structure of serine palmitoyltransferase; gateway to sphingolipid biosynthesis. *Journal of molecular biology*, *370*(5), 870–886.

Zhang, X., & Mosser, D. M. (2008). Macrophage activation by endogenous danger signals. *The Journal of pathology*, *214*(2), 161–178.

Zhang, Y. M., & Rock, C. O. (2008). Membrane lipid homeostasis in bacteria. *Nature reviews. Microbiology*, *6*(3), 222–233.

Zhu, Y., Thomas, F., Larocque, R., Li, N., Duffieux, D., Cladière, L., Souchaud, F., Michel, G., & McBride, M. J. (2017). Genetic analyses unravel the crucial role of a horizontally acquired alginate lyase for brown algal biomass degradation by Zobellia galactanivorans. *Environmental microbiology*, *19*(6), 2164–2181.